

**HARNESSING PROTEIN TRANSPORT PRINCIPLES FOR ENGINEERING
APPLICATIONS: A COMPUTATIONAL STUDY**

by

Eric Christopher Freeman

BSE, Geneva College, 2006

MS, University of Pittsburgh, 2009

Submitted to the Graduate Faculty of
the Swanson School of Engineering in partial fulfillment
of the requirements for the degree of
Doctor of Philosophy

University of Pittsburgh

2012

UNIVERSITY OF PITTSBURGH
SWANSON SCHOOL OF ENGINEERING

This dissertation was presented

by

Eric Freeman

It was defended on

December 13, 2011

and approved by

William W. Clark, PhD, Associate Professor, Department of Mechanical Engineering and
Material Science

Wilson S. Meng, PhD, Associate Professor, Graduate School of Pharmaceutical Sciences

Patrick Smolinski, PhD, Associate Professor, Department of Mechanical Engineering and
Material Science

Vishnu B. Sundaresan, PhD, Assistant Professor, Department of Mechanical and Nuclear
Engineering

Jeffery S. Vipperman, PhD, Associate Professor, Department of Mechanical Engineering and
Material Science

Dissertation Director: Lisa Mauck Weiland, PhD, Associate Professor, Department of
Mechanical Engineering and Material Science

Copyright © by Eric Freeman

2012

HARNESSING PROTEIN TRANSPORT PRINCIPLES FOR ENGINEERING APPLICATIONS: A COMPUTATIONAL STUDY

Eric Freeman, PhD

University of Pittsburgh, 2012

The biological world contains elegant solutions to complex engineering problems. Through reproducing these observed biological behaviors it may be possible to improve upon current technologies. In addition, the biological world is, at its core, built upon cellular mechanics. The combination of these observations prompts an exploration of cellular mechanics for engineering purposes

This dissertation focuses on the construction of a computational model for predicting the behavior of biologically inspired systems of protein transporters, and linking the observed behaviors to desired attributes such as blocked force, free strain, purification, and vaccine delivery. The goal of the dissertation is to utilize these example cases as inspirations for development of cellular systems for engineering purposes. Through this approach it is possible to offer insights into the benefits and drawbacks associated with the usage of cellular mechanics, and to provide a framework for how these cellular mechanisms may be applied. The intent is to define a generalized modeling framework which may be applied to an extraordinary range of engineering design goals.

Three distinctly different application cases are demonstrated via the bioderived model which serves as the basis of this dissertation. First the bioderived model is shown to be effective for characterizing the naturally occurring case of endocytosis. It is subsequently applied to the distinctly different cases of water purification and actuation to illustrate versatility.

TABLE OF CONTENTS

TABLE OF CONTENTS.....	v
LIST OF TABLES.....	ix
LIST OF FIGURES.....	x
PREFACE.....	xiv
1.0 INTRODUCTION AND LITERATURE REVIEW.....	1
1.1 OVERVIEW.....	1
1.2 CELLULAR BACKGROUND.....	2
1.2.1 Lipid Bilayer Definitions.....	3
1.2.2 Introduction to Transport Pathways.....	5
1.2.3 Current Engineering Applications Involving Cellular Systems.....	9
1.3 MATHEMATICAL MODELING CONSTRUCT.....	13
1.3.1 General Equations.....	14
1.3.2 Model Overview.....	36
1.3.3 Summary.....	37
2.0 ENDOSOME STUDIES.....	38
2.1 ENDOSOMAL TRANSPORT.....	39
2.2 EXISTING ENDOSOME MODELS.....	40

2.3	SELECTED TRANSPORT APPROACH	42
2.4	IDENTIFICATION AND CALIBRATION OF EQUATIONS FOR ENDOSOME SIMULATION	42
2.5	ENDOSOME TRANSPORT VALIDATION CRITERIA	47
2.5.1	Endosome Transport Validation Step 1: Acidification Profile	47
2.5.2	Endosome Transport Validation Step 2 – Na ⁺ K ⁺ ATPase impact	48
2.5.3	Endosome Transport Validation Step 3 – Resting Membrane Potential	49
2.6	ENHANCING ENDOSOME BURST THROUGH PROTON SPONGES.....	49
2.6.1	Proton Sponge Background	50
2.6.2	Additional Equations for Proton Sponge + Endosome Simulation	51
2.6.3	Validation Step 1: Sponge Validation.....	56
2.6.4	Validation Step 2 – Endosome + Sponge Interaction	59
2.6.5	Endosome-Sponge Interaction Summarized.....	62
2.6.6	Endosome Expansion Extension.....	63
2.6.7	Dendrimer Study Summary	67
2.7	ENDOSOME CONCLUSIONS.....	68
3.0	WATER PURIFICATION STUDIES	70
3.1	WATER PURIFICATION CONCEPTS.....	71
3.1.1	Protein Transporter Selection	73
3.2	BIOCHAR INTRODUCTION.....	76
3.2.1	Biochar Creation	77
3.2.2	Biochar Quantification.....	81
3.3	EQUATIONS FOR WATER PURIFICATION	84

3.3.1	Transport Equations for System 1.....	86
3.3.2	Transport Equations for System 2.....	87
3.3.3	Transport Equations for System 3.....	88
3.4	WATER PURIFICATION CALIBRATION/VALIDATION.....	89
3.5	WATER PURIFICATION RESULTS.....	91
3.5.1	Nutrient Removal for System 1	91
3.5.2	Nutrient Removal for System 2	92
3.5.3	Nutrient Removal for System 3	95
3.6	WATER PURIFICATION CONCLUSIONS	100
4.0	REVERSIBLE OSMOTIC ACTUATION STUDIES.....	102
4.1	INSPIRATION.....	103
4.2	PROPOSED SYSTEM.....	104
4.3	EQUATIONS FOR OSMOTIC ACTUATION	107
4.4	MODEL CALIBRATION/VALIDATION.....	110
4.5	OSMOTIC ACTUATION RESULTS	113
4.5.1	Relating v_{drive} to generated membrane potentials.....	114
4.5.2	Baseline Actuation Performance.....	115
4.5.3	Input Potential Dependence	117
4.5.4	Role of Membrane Capacitance.....	122
4.6	DISCUSSION	124
4.7	OSMOTIC ACTUATION CONCLUSIONS.....	126
5.0	CONCLUSIONS.....	127
5.1	ENDOSOME SUMMARY	128

5.2	WATER PURIFICATION SUMMARY	128
5.3	OSMOTIC ACTUATION SUMMARY	129
6.0	CONTRIBUTIONS	131
7.0	PUBLICATIONS.....	133
7.1	REFERRED JOURNAL PAPERS.....	133
7.2	NON-REFEREED CONFERENCE PAPERS WITH PRESENTATION.....	134
7.3	NON-REFEREED CONFERENCE PAPERS WITH POSTER.....	134
	APPENDIX A.....	135
	APPENDIX B	138
	APPENDIX C	155
	APPENDIX D.....	162
	BIBLIOGRAPHY.....	174

LIST OF TABLES

Table 1. Butcher Array for 5th order Explicit Runge-Kutta [50].....	35
Table 2. Endosome Input Values	46
Table 3. Proton Sponge Inputs	57
Table 4. Sponge-Endosome Comparisons	62
Table 5. Purification Transport Configurations	86
Table 6. Water Purification Inputs	90
Table 7. Osmotic Actuator Baseline Inputs	112

LIST OF FIGURES

Figure 1.1. Bilayer configuration in the presence of an aqueous media.	3
Figure 1.2. Variance in the lipid tilt and orientation demonstration[10].	4
Figure 1.3. Bilayer mechanical testing across a pore[11].	4
Figure 1.4. Example of protein transporters. From left to right: cotransporters/exchangers, pumps, and voltage gated channels.	7
Figure 1.5. Experimental nastic actuation apparatus with a barrel-shaped inclusion with transport membranes across a porous substrate connecting the inclusion to the external reservoir. Flow across the transport membranes will cause deformation of the diaphragm stretched across the top of the inclusion.....	10
Figure 1.6. Example of using nastic-inspired materials for bulk deformation. Spherical inclusions are selectively triggered causing expansion/contraction, through which bulk deformation may be achieved.	10
Figure 1.7. Illustration of using ligand-gated channels in sensing applications.	11
Figure 1.8. Illustration of a hair sensing system - oscillations generate measureable electric current through varying the capacitance of the bilayer.[5].	12
Figure 1.9. The membrane approximated as a capacitance circuit through Hodgkin-Huxley.....	15
Figure 1.10. $[S]^+$ ion pump sketch.....	17
Figure 1.11. Predicted pump behavior with varying ATP and ion gradients.....	19
Figure 1.12. $2[S]^+ [X]^+$ ion exchanger sketch.....	20
Figure 1.13. Predicted cotransporter/exchanger currents with varying ion gradients.	21
Figure 1.14. Voltage gated $[S]^+$ ion channel sketch.....	22

Figure 1.15. Predicted voltage gated ion channel current with a 60 mV gating voltage (marked in red) and varied ion gradients.....	26
Figure 1.16. Predicted ion diffusion current with varied ion gradients.....	28
Figure 1.17. Predicted internal pressure p_r as a function of the membrane stretch λ with $\gamma = 0.067$, $\mu_0 = 2.5 \mu\text{N/m}$, $t_0 = 5.2 \text{ nm}$, and $r_0 = 0.5 \mu\text{m}$ (cellular inputs). The marked region corresponds to the maximum stretch observed in the endosome studies.	32
Figure 1.18. Butcher array notation.....	34
Figure 1.19. General modeling process represented in 4 steps.	36
Figure 1.20. Core components of the biomembrane model.	37
Figure 2.1. Sketch of the endocytosis process.....	39
Figure 2.2. Sketch of the combination of H^+ ATPases, Na^+ K^+ ATPases and Cl^- H^+ diffusion considered for modeling of endosomal pH.	40
Figure 2.3. Predicted endosome acidification with (top line) and without (bottom line) Na^+ K^+ ATPase.....	47
Figure 2.4. Illustration of the proton sponge hypothesis in 3 steps.	50
Figure 2.5. Proton sponge sketch.	52
Figure 2.6. Sketch of the simplifications used to represent the dendrimers as a series of shells with nearest neighbor calculations.....	55
Figure 2.7. Predicted sponge titration vs. experimental data. The data in the upper right corner is experimental data from Jin[72], and the larger figure contains the sponge model predictions.....	58
Figure 2.8. Predicted pH vs. experimental pH data for PAMAM and POL.....	59
Figure 2.9. Predicted Cl^- accumulation vs. experimental Cl^- accumulation for PAMAM and POL.	60
Figure 2.10. Predicted change in volume vs. experimental change in volume for PAMAM and POL.....	61
Figure 2.11. Predicted change in volume comparisons for sponges of interest. The dashed red line indicates expected region of burst.....	65

Figure 2.12. Predicted change in volumes for changes in sponge radii.....	66
Figure 2.13. Predicted internal pH with respect to change in volume for unmodified PAM-DET.	67
Figure 3.1. Envisioned removal scheme.....	72
Figure 3.2. Phosphate/proton exchanger coupled with a nitrate/proton cotransporter (system 1).....	73
Figure 3.3. Standard nutrient removal protein system seen in plant root cells.....	74
Figure 3.4. Photosystem coupled with phosphate/proton and nitrate/proton cotransporters (system 2).....	75
Figure 3.5. System 2 coupled with voltage gated calcium channels (system 3).....	75
Figure 3.6. System used for creating biochar in the laboratory.....	77
Figure 3.7. Flaming pyrolysis in TLUD sketch [95].....	78
Figure 3.8. Measured terminal temperature of pyrolysis.....	79
Figure 3.9. Changes in char surface area with respect to the terminal pyrolysis temperature[95].....	80
Figure 3.10. Measured change in char mass during pyrolysis.....	81
Figure 3.11. System used for measuring nitrate concentrations in the laboratory.....	83
Figure 3.12. Measured nitrate removal by the char with respect to the external concentration of the nitrate.....	83
Figure 3.13. Predicted nutrient removal for system 1.....	92
Figure 3.14. Predicted nitrate removal for system 2. The dashed line represents the external concentration.....	93
Figure 3.15. Predicted phosphate removal for system 2. The dashed line represents the external concentration.....	93
Figure 3.16. Predicted nitrate removal with varying capacitance for system 2.....	95
Figure 3.17. Predicted nitrate removal for system 3.....	96
Figure 3.18. Predicted phosphate removal for system 3.....	96

Figure 3.19. Illustration of nutrient vs. membrane potential development with and without calcium voltage gated channels.	97
Figure 3.20. Predicted nitrate removal for system 3 with and without 100g of biochar.	98
Figure 3.21. Predicted phosphate removal for system 3 with and without 100g of biochar.	99
Figure 3.22. Predicted nitrate removal for system 3 with 100g of biochar and varied v_{pmf}	100
Figure 4.1. The proposed osmotic actuation system. Driving membranes are labeled 1, 2, and 3, while chambers are labeled I and II.	105
Figure 4.2. Encapsulated cells with connecting transport membranes. Membranes 1 and 3 allow for potassium transport to the reservoirs, membrane 2 contains the driving input and allows for calcium transport between the two motor cells I and II.	106
Figure 4.3. Converting Central Displacement to % Areal Free Strain	113
Figure 4.4. The input potential is distributed across the three transport membranes.	114
Figure 4.5. Predicted free central diaphragm displacement for osmotic actuation.	116
Figure 4.6. Predicted blocked stress for osmotic actuation.	116
Figure 4.7. Predicted central diaphragm displacement with reduced calcium (5 mM).	117
Figure 4.8. Predicted central diaphragm displacement with varied v_{drive} . With v_{drive} set to 1000 mV, the generated membrane potentials surpass the individual membrane threshold of 200 mV which will result in system failure.	118
Figure 4.9. Predicted central diaphragm displacement with removed input v_{drive} at $\frac{1}{2}$ time and $\frac{1}{4}$ time.	120
Figure 4.10. Predicted central diaphragm displacement with varied input $v_{drive}(t)$	121
Figure 4.11. Predicted central diaphragm displacement with varied membrane capacitance C	123
Figure 4.12. Illustration of capacitance's relation to signaling – membrane potential development inversely related to membrane capacitance, increasing the membrane capacitance reduces signal development, reducing action potential generation. The upper image corresponds to baseline capacitance case in figure 4.10, and the lower image corresponds to increased capacitance case.	123
Figure 4.13. Illustration of a possible bimorph application of the dual chamber apparatus for large scale deflections.	125

PREFACE

There are many people involved in the creation of this dissertation. First I'd like to thank my advisor Dr. Weiland for her tireless patience and guidance over the past years. It's been many years since I first arrived at the University of Pittsburgh, shaggy haired and uncertain of the future. Without her help I wouldn't be submitting this dissertation today. I'd also like to thank the many professors along the way who have encouraged me in my studies and presented new ideas and concepts to stimulate and develop my interests. This of course includes my committee members, who have set aside time from their busy schedules to help refine and improve this research. Additional thanks go to all of the researchers and students who I've met along the way who have expressed interest in the application of cellular mechanics in engineering, and shared their own views and interests with me. Their insights and recommendations have helped immensely

I must also thank my friends and family. My family, both old and new, for supporting me in my endeavors and always having my best interests at heart. My friends, for their encouragement and the many good times we've shared.

And finally I'd like to thank my wife Natalie for always having my back. Your blessing and support mean the world to me.

1.0 INTRODUCTION AND LITERATURE REVIEW

1.1 OVERVIEW

At their core, biological systems are largely enabled by their foundation; cellular structures. Biology is built upon these cells, and these cells with their remarkable diversity and range of function imbue their larger system with specific qualities. These cells may be viewed as independent entities or machines, capable of a great variety of tasks based on cellular structure and contents[1] . For example, cells are capable of responding to forces[2], passing electrical signals[3-5], and converting electrochemical energy[6]. Scientific advances have allowed for the isolation and reproduction of these cells, allowing researchers to tailor cells for specific goals and purposes[7].

The intent of this dissertation is to illustrate the potential impact of cellular approaches on engineering. Through cellular tailoring it may be possible to recreate abilities such as rapid signaling, sensing, actuation, and purification. In future years these cells may be mass produced and constructed in series, allowing for artificial construction of organs such as the heart[8].

The dissertation will be structured as follows. First a literature review will be detailed providing background for current cellular approaches and their possible applications. Next the motivation for a computational model will be established, and the details of the model will be discussed. After this the dissertation may be split into three sections detailing illustrative applications: Vaccine Delivery, Water Purification, and Enhanced Osmotic Actuation. The

intent of presenting these vastly different application cases is to illustrate the extraordinary range of design opportunity enabled by formalizing the core governing equations of cellular active response. Each of these sections will include a brief literature review, providing the additional background information and equations used for these specific simulations. Results will then be discussed and summarized, and conclusions will be drawn.

1.2 CELLULAR BACKGROUND

Before proceeding, some basic definitions must be established. As the dissertation is tailored for a traditional mechanical engineering audience it must be assumed that the nature of protein transporters and their functions are not well known or established.

The core components responsible for the desired cellular activities studied in this dissertation are the protein transporters. These are naturally occurring proteins responsible for performing the tasks necessary for cell functionality. These protein transporters require the presence of a natural “scaffold”, or a bilayer lipid membrane. This membrane is what imbues the cell with the ability to maintain a concentration gradient and a membrane potential, and effectively operates as a barrier between the extracellular and intracellular regions. Both of these components will be covered in detail in the following sections.

1.2.1 Lipid Bilayer Definitions

The bilayer lipid membrane (figure 1.1) is a naturally occurring membrane that surrounds the cell and is necessary for cellular function. The membrane is comprised of a phospholipid matrix which serves as a substrate for the embedded transport proteins. The phospholipids contain two parts: a hydrophilic head and a hydrophobic tail. When placed in an aqueous solution, this causes the phospholipids to naturally form a bilayer structure with the hydrophilic heads facing outwards[9]. This bilayer membrane serves as a barrier around the cell, which maintains a separation of charge and concentration between the two sides.

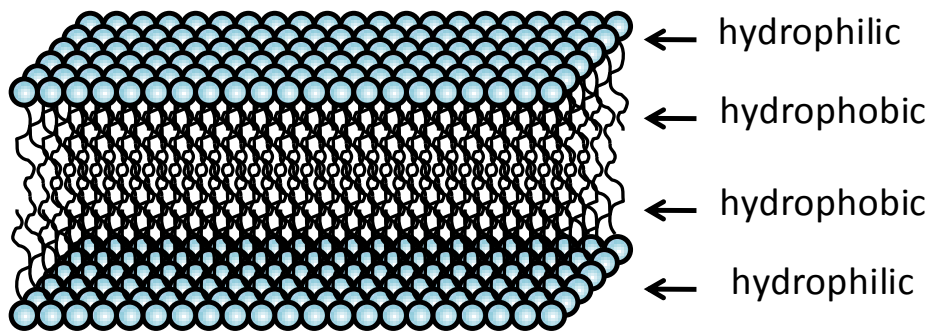


Figure 1.1. Bilayer configuration in the presence of an aqueous media.

The mechanical characteristics of the lipid membrane are currently being established, and computational models have been constructed to examine the nature of membrane deformation. DeVita and Stewart for instance have modeled the membrane as a liquid crystal, which offers insight to the nature of the membrane[10]. When stress or displacements are applied to the lipid membranes, the lipid molecules are observed to tilt away from the actual orientation of the curvature. Through this process the lipid molecules are able to glide along each other and provide the membrane with flexibility and mobility[10].

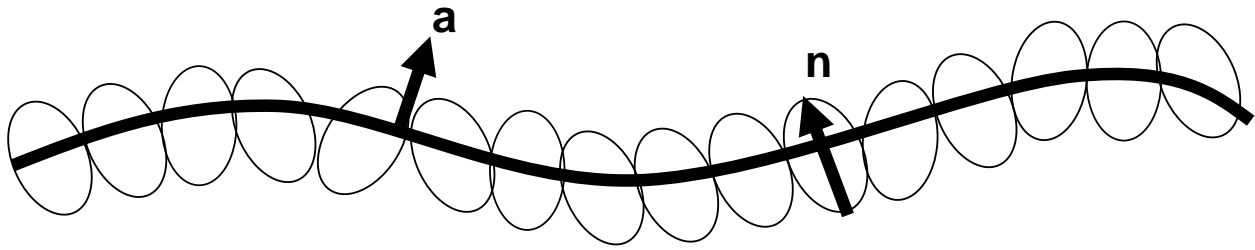


Figure 1.2. Variance in the lipid tilt and orientation demonstration[10].

Experimental characterization of the membrane has also been performed through the research by Hopkinson [11] and Needham and Dunn[12], focusing on the material properties and durability. These characteristics are important as the lipid membrane serves as the scaffold for the protein transporters, and understanding its durability and lifespan is crucial for engineering purposes. It was found that with an applied internal pressure across a pore (figure 1.3); the critical pressure was highly dependent on the pore dimensions, with a maximum internal pressure of 66 kPa[11]. Similar observations have been made on membrane stability with relation to pore size; increased pore sizes greatly reduce the lifespan of the membrane[13].

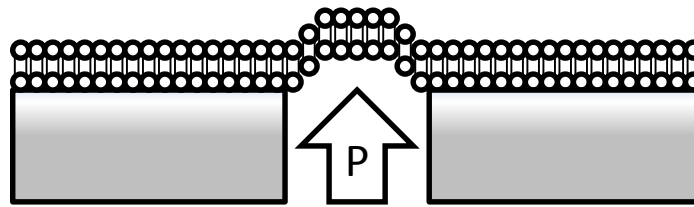


Figure 1.3. Bilayer mechanical testing across a pore[11].

1.2.1.1 Increasing Membrane Durability

While methods have been employed to increase the membrane's durability, it still is very fragile and must be reinforced further if these protein transporter solutions are to see widespread engineering use. For illustration, lipid bilayers used in sensing applications currently exhibit a

maximum lifespan of around two weeks with further research being performed to extend the lifespan[13].

It is possible to use synthetic bilayers that employ polymers rather than phospholipids; however these artificial substrates are often not a suitable substrate for many transport proteins leading to a rejection of the substrate by the protein[7]. Until further advances are made in polymer science for use as protein substrates, methods must focus on strengthening natural phospholipid bilayers.

There are multiple types of phospholipid that offer various degrees of stability and durability. For example organisms from Archaea (a group of single cell organisms typically found in extreme environments) are dominant in extreme environments and have membranes formed from bipolar lipids (bolalipids). These lipids span the entire width of the membrane due to their structure, and confer increased structural stability[14]. These bolalipids are currently difficult to obtain, but research efforts are focusing on their artificial synthesis[15].

Membrane durability may also be enhanced through the use a hydrogel as a support structure for the bilayer membrane. Hydrogels offer support while simultaneously retaining aqueous flow to and from the membrane. Encapsulating the bilayer membrane in the hydrogel offers structural stability, and membrane stability has been observed for up to three weeks using this method[16].

1.2.2 Introduction to Transport Pathways

Ions may be moved across the relatively impermeable lipid bilayer through transport pathways, which are largely comprised of protein transporters. While there are many varieties of cellular transporters, they may be divided into several basic groups. In addition to passive diffusion,

there are three primary classes of protein transporters that will be considered for the model; pumps, cotransporters/exchangers, and channels[17].

Pumps use energy from hydrolysis of the chemical fuel ATP to move an ionic species against its electrochemical gradient (Figure 1.4, center); pumps are sometimes referred to as ATPase. These pumps are the driving force behind establishing concentration gradients – they do not move species towards equilibrium but rather utilize energy to alter the state of the system. In Figure 1.4 the curved arrow schematically illustrates the chemical breakdown of ATP into phosphate and ADP. This provides the energy to selectively transport its target species *S* across the membrane against its electrochemical gradient. In the illustrated case the target species are protons; the pump is working to establish a pH gradient through the motion of protons across the membrane.

Cotransporters/exchangers use the energy from the downhill motion of one ionic species to move another uphill against its electrochemical gradient (Figure 1.4, left). A cotransporter moves both species in the same direction into or out of the cell. An exchanger moves the selected species in opposite directions. Either species can be the driving species, dependent on the structure of the specific transporter[17]. In nature these transporters generally work together with the pumps. In the illustrated case, the exchanger is moving the transported protons back across the membrane, and using the energy gained to create a potassium concentration gradient.

Channels allow specific species to move along their downhill electrochemical gradients (Figure 1.4, right). Channels are also voltage gated, and are thus dependent on the overall membrane potential of the system. If the membrane potential reaches a certain value, the channels will open and allow passive transport of selected species to move the membrane

potential back towards equilibrium[18]. In the illustrated case, the channels will open when the membrane potential crosses the gating threshold, and allow for the rapid transport of potassium back out of the cell interior, resetting the concentration gradients.

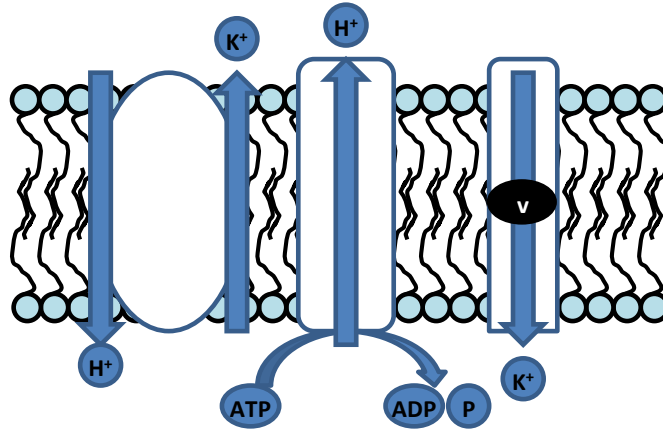


Figure 1.4. Example of protein transporters. From left to right: cotransporters/exchangers, pumps, and voltage gated channels.

Finally passive transport through diffusion must be considered. The biologically occurring bilayer membrane is porous to small species. Passive diffusion without transport assistance may occur dependent on the concentration gradients and the membrane potential.

Collectively, transporters and diffusion processes create an evolution of state of the enclosed region with respect to the surroundings. Cells are classified as dead when the proteins cease to function, as the interior of the cell will gradually evolve to match the surrounding conditions through diffusion currents.

1.2.2.1 Protein Transporters Impact on Bilayer Properties

The lipid bilayer is essential for membrane-protein functionality, and properties such as lipid composition and thickness have a strong impact on protein activity[19]. The proteins are

observed to self-insert into the lipid bilayer, and provide a gateway across the membrane's thickness (figure 1.5). Lipid molecules are not commonly found in the crystal structures of the proteins, and the ones that are located are tightly bound to the protein. These retained lipids are often essential for protein functionality.

Research has been conducted on the impact of adding protein transporters to the bilayer membrane. Intuitively the overall electrical and mechanical properties are changed considerably when the mechanically discontinuous and electrically active proteins are introduced to a bilayer membrane. For instance when proteins are introduced, the conduction properties of the proteins largely control the response of the membrane potential[20]. Through this observation the assumption may be made that any change in the membrane potential is due to ion transport. It is this behavior that leads to the simplifying Hodgkin-Huxley approximation for describing the system response[21].

Similarly proteins have been observed to result in a swell in membrane thickness around the protein-lipid interface[19], as the protein moves towards regions of lipids that favor a hexagonal phase. Further the position of proteins in the lipid bilayer may be calculated as a function of the lipid composition[22]. Thus the mechanical and electrical properties can vary significantly, not only from case to case, but also from point to point within a single case. In many ways this is analogous to local property variation observed in multiphase engineering materials. In those instances, assumption of continuous properties is reasonable so long as the investigation itself is at a sufficiently large length scale. In this dissertation it is the collective response that is of interest, and thus continuum mechanical and electrical properties will similarly be assumed.

1.2.3 Current Engineering Applications Involving Cellular Systems

One of the earliest engineering goals regarding cellular systems was the simulation of nastic actuation, inspired by the ability of plants to contort and bend through controlled transport of fluid and charge across their cellular membranes. An experimental configuration was constructed by Sundaresan and Leo[23, 24]. A barrel shaped inclusion was constructed (figure 1.5). Pores were created at one end of the barrel, and the opposing end was covered in an elastic membrane to allow deformation. Lipid membranes were constructed across the pores, and sucrose/proton cotransporters were embedded in the membrane. The membrane was placed in a fluid reservoir containing sucrose and a pre-set pH gradient. The pH gradient triggers the embedded cotransporters, which allows for the active transport of protons and sucrose/water into the inclusion, demonstrating actuation.

Follow-on studies were subsequently performed by Sundaresan and Matthews[24, 25]. In summary, it was found that the transport configuration demonstrated work by deforming the upper diaphragm through active diffusion of water upwards into the inclusion. The overall deformation achieved experimentally was a central displacement of 62.3 μm with a diaphragm radius of 9.75 mm[24]. The level of displacement was highly dependent on the Sucrose concentration gradient, providing impetus for the SUT4 cotransporters.

Initial nastic actuation was promising; however the experimental configuration was limited to the barrel apparatus seen in figure 1.5. To appreciate the potential of nastic actuation, consider a scenario where the inclusion is spherical in shape, and mimics natural cells. This would allow the insertion of the vesicles into a polymer matrix, which would lead to bulk deformation as seen in figure 1.6.

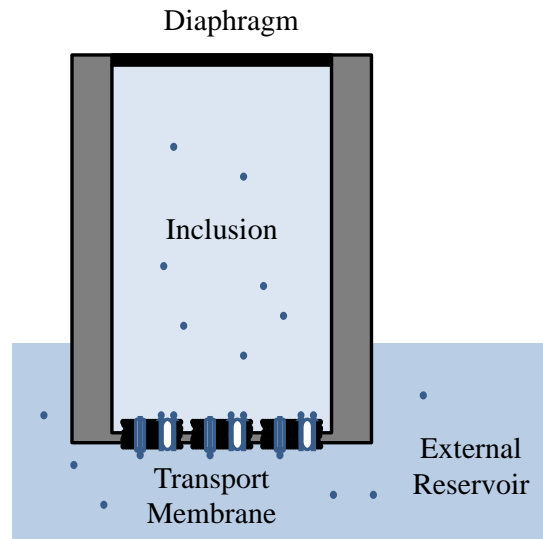


Figure 1.5. Experimental nastic actuation apparatus with a barrel-shaped inclusion with transport membranes across a porous substrate connecting the inclusion to the external reservoir. Flow across the transport membranes will cause deformation of the diaphragm stretched across the top of the inclusion.

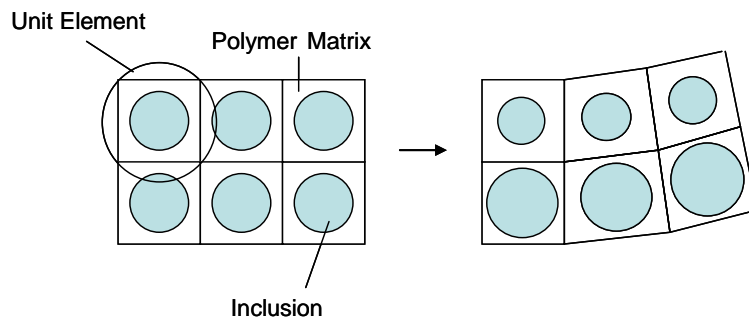


Figure 1.6. Example of using nastic-inspired materials for bulk deformation. Spherical inclusions are selectively triggered causing expansion/contraction, through which bulk deformation may be achieved.

An additional development explored by Sundaresan is the development of a battery system. The research is still in preliminary phases, but the ability of the cell to maintain a membrane potential and release the potential through rectifying currents may be an ideal method for energy storage[26]. This may be useful as micro-batteries.

Another engineering application of these systems is sensing[13, 27]. Through ligand or voltage gated channels, the presence of a charge or a specific concentration may be measured through the current detected across the bilayer. The driving mechanism behind this is the channel itself, which is triggered by either the development of a membrane potential due to general concentration imbalances (voltage gated), or the presence of a specific ion (ligand gated). For illustration, a bilayer may be constructed maintaining a specific concentration gradient. Through the inclusion of a ligand-gated channel, specifically tuned to sense the desired secondary ion and allowing for the transport of the primary ion responsible for the concentration gradient, a sensing device may be constructed. This is illustrated in figure 1.7.

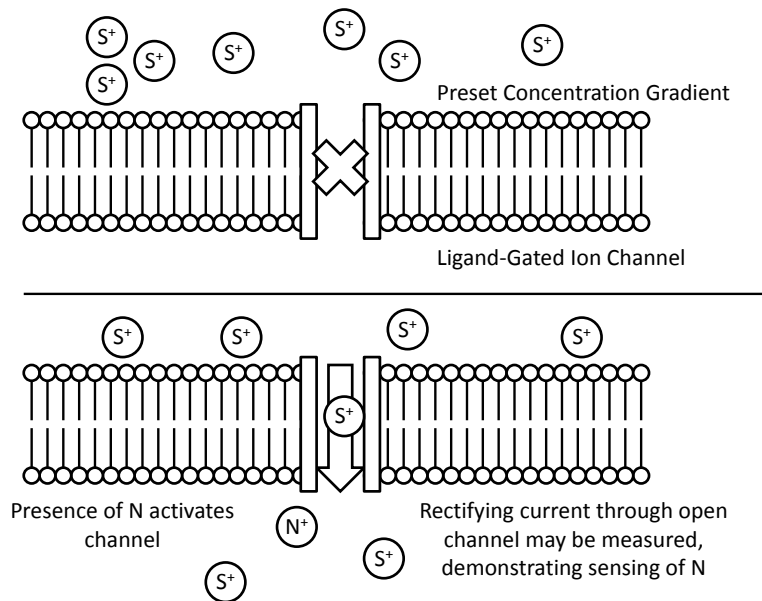


Figure 1.7. Illustration of using ligand-gated channels in sensing applications.

Possible applications of these sensing systems include the ability to sense dangerous concentrations in a surrounding medium at the microscale or at very low levels. This would be combined with either the triggering of an alarm by the measured electric current across the

bilayer, or the surrounding concentration would be nullified by the controlled automatic release of a neutralizing agent stored within the bilayer inclusion.

A method for sensing flows has been proposed and studied by Leo and Sarles, mimicking mechanotransduction in hearing cells[5]. This application utilizes the same bilayer membrane seen in the other cases, but utilizes a mechanical deformation to trigger electrical current and measure the oscillation of the sensing hair. An illustration of this behavior may be seen in figure 1.8.

Future goals for this application involve mimicking the ability of the human ear to automatically tailor cellular proportions to amplify or diminish the incoming signal, allowing for a wide range of sensing frequencies. This may be accomplished through the application of a system of cellular inclusions with proteins altering the electrical properties of the connective bilayers.

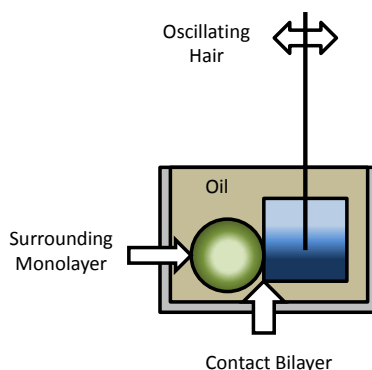


Figure 1.8. Illustration of a hair sensing system - oscillations generate measurable electric current through varying the capacitance of the bilayer.[5].

Another example of mechanotransduction has been experimentally observed through indentation of neurites[3, 4]. The deformation of the neurites' cellular structure causes a measurable firing of an action potential, used in cellular signaling. While the exact mechanics

behind the generation of the action potential due to deformation are still unclear, it has been determined to be a feature of the cytoskeleton rather than the protein transporters themselves. Mimicking the natural sensing network through cellular approaches may enhance the development of artificial limbs, in addition to traditional sensing applications.

Finally, and as will be discussed in some detail in later chapters, these systems of transporters may be used in osmotic actuation and filtration studies. Osmotic actuation is inspired by observations of plant guard cells, which use selective transport of calcium and potassium to raise and lower the osmotic pressure in the cells, effectively opening and shutting pores for water retention[28]. These mechanics may be used in guiding osmotic actuation design through cellular mechanics.

Filtration is observed in plant roots[29], where cellular mechanics facilitates the uptake of nutrients nitrates and phosphates against high concentration gradients. Similar mechanisms may be employed for the filtration of these nutrients out of river water, or for the reclamation of a desired ion from a surrounding medium.

In summary, while application of cellular structures for engineering purposes is still infant in its development, the foregoing discussion helps to illustrate the extraordinary range of potential impact.

1.3 MATHEMATICAL MODELING CONSTRUCT

The research presented here focuses on defining the core governing equations describing the behavior of protein transporters and offering a template for their simultaneous solution. The resulting computational model was designed for flexibility, with the ability to rapidly mix and

match transport types along with varying external and internal conditions. Through this the model may be applied to any cellular system and may also be modified to mesh the transport model with additional equations, linking the cellular activity with secondary systems of interest such as dendrimer titration or osmotic expansion.

Through this approach the dissertation allows for the classification of a new class of smart material – biologically inspired membranes. Built upon biomimetic principles, these materials offer advanced solutions to a variety of engineering applications. These envisioned materials will be highly tailorable, inheriting cellular abilities from their unique structures and contents. This dissertation offers multiple case studies as an illustration of their potential, but the range of applications is much broader as seen in the current applications section.

1.3.1 General Equations

Each of the studies presented utilizes a similar core of equations. The feasibility of developing a generalized approach to modeling transient response of an extraordinarily broad range of design application rests in the reality that each of these applications draws from the same, new class of materials, and is therefore accompanied by its core governing equations. Just as in other applications of a class of material, the core governing equations are calibrated for a given application. For instance, many polymers may be characterized by NeoHookean governing equations, while thermal or electrical stimulus equations may also be imposed for specific cases. The same is true here. The core governing equations and their derivations are fixed, and presented here; calibration of these as well as additional case-specific equations will be discussed in their respective chapters.

1.3.1.1 Circuit Approximations

The membrane itself was approximated as a capacitance circuit via the Hodgkin Huxley model[21]. This assumption requires that the protein transporters are relatively dense in order to simplify the circuit so that all currents are represented through ion transport, and is generally appropriate for this research[20]. Since the applications considered here were driven by protein transport, the membrane was approximated as a circuit between the intracellular and extracellular space, as seen in figure 1.9.

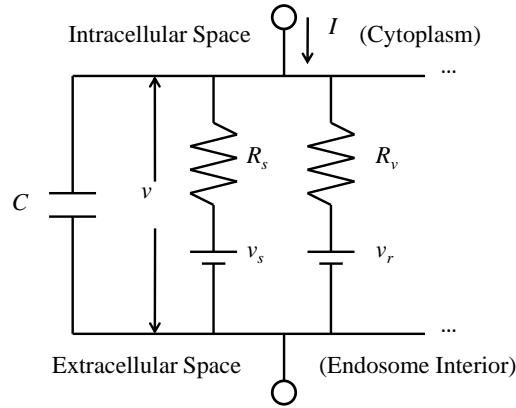


Figure 1.9. The membrane approximated as a capacitance circuit through Hodgkin-Huxley.

Through this the membrane potential v was determined by summing the currents across each transporter[21].

$$\frac{dv}{dt} = -\frac{1}{C} \left(\sum i_{transport} \right) \quad (1.1)$$

where C is the membrane capacitance.

1.3.1.2 Concentration Changes

As noted above, the currents through the transporters affect the membrane potential, and necessarily also evolution of the concentration gradient.

The currents across the proteins represent the flow of ions. This was then translated into a change in concentration through Faraday's constant.

$$\frac{d[S]}{dt} = \frac{\sum i_s}{Vol * F} \quad (1.2)$$

[*S*] is the mM concentration of the selected species *S*, *Vol* is the current volume of the membrane enclosed region, and *F* is Faraday's constant.

1.3.1.3 Nernst Potentials

Evolution of the ion concentration gradient(s) across the membrane necessarily results in evolution of their respective Nernst equilibrium potentials. The evolution of the Nernst equilibrium potentials was tracked via instantaneous assessment of the concentration gradient[30]

$$v_s = \frac{kT}{ze} \ln \left(\frac{[S]_e}{[S]_i} \right) \quad (1.3)$$

where *k* is Boltzmann's constant, *T* is the temperature, *e* is the charge per atom, *z* is the valence, and [*S*] is the concentration of species *S* on the external and internal sides of the membrane in mM. As concentration gradients accumulate this potential term increases, offsetting the currents across the protein transporters. These concentration-driven potential terms act in concert with the membrane potential equation.

1.3.1.4 Transport Equations

Equations 1.1 through 1.3 provide a framework for relating protein activity towards the generation of membrane potentials and concentration gradients. The resulting potential terms

(equations 1.1 and 1.3) are then linked to the transport across the proteins through the following equations.

1.3.1.4.1 Protein Pumps

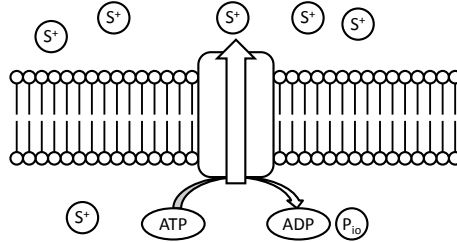
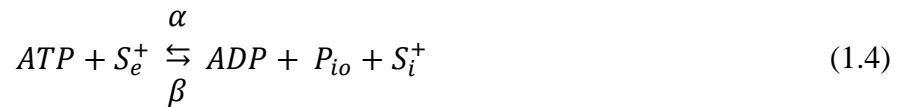


Figure 1.10. $[S]^+$ ion pump sketch.

As discussed previously, protein pumps utilize the hydrolysis of ATP to transport a selected species across the membrane. For example, consider an S^+ -specific proton pump. The reaction may be modeled as:



where ATP is broken down into ADP + Phosphates (P_{io}), and a single S^+ ion is moved from the external to the internal regions as denoted by the subscripts e and i . The energy associated with the motion of the ion S may be written as

$$\Delta G_S = e(v - v_S) \quad (1.5)$$

where the Gibbs energy G is associated with the motion of species S^+ , v is the membrane potential, and v_S is the Nernst equilibrium potential for S^+ . The total energy required for this reaction may be written as:

$$\Delta G = \Delta G_{ATP} + \Delta G_S = e(v_{ATP} + v - v_S) \quad (1.6)$$

where $v_{ATP} = \Delta G_{ATP}/e$, and is commonly calculated as $21k_B T/e$ [31].

For the pump activity itself, saturation effects are expected. The total pump activity is limited by the maximum flow, therefore the sum of the forward and backward reaction rates of equation 1.4 were set to be a constant (λ) representing this total possible speed.

$$\alpha + \beta = \lambda \quad (1.7)$$

At equilibrium, the forward and reverse reactions must occur at the same frequency, yielding:

$$\frac{\alpha}{\beta} = \exp\left(-\frac{\Delta G}{k_B T}\right) \quad (1.8)$$

Solving these two equations yielded:

$$\alpha = \frac{\lambda \exp\left(-\frac{\Delta G}{k_B T}\right)}{1 + \exp\left(-\frac{\Delta G}{k_B T}\right)} \quad (1.9a)$$

$$\beta = \frac{\lambda}{1 + \exp\left(-\frac{\Delta G}{k_B T}\right)} \quad (1.9b)$$

Taking the difference of these reaction rates yielded (where λ is the total rate):

$$\alpha - \beta = \lambda \tanh\left(-\frac{\Delta G}{2k_B T}\right) \quad (1.10)$$

Which was then be directly related to the pump flow as:

$$i_{pump} = Me(\alpha - \beta) \quad (1.11a)$$

$$i_{pump} = Me\lambda * \tanh\left(\frac{e(-v - v_{ATP} + v_S)}{2k_B T}\right) \quad (1.11b)$$

where M is the number of pumps (assuming independent pump operation). A similar approach may be employed for any other pump proteins dependent on the transported ions.

For an illustration on how this equation operates, observe figure 1.11. The central line represents the expected flow with no ATP present and no concentration gradient. The total flow is zero at the center, then increases as the membrane potential becomes increasingly negative (inward-rectifying flow). When ATP is introduced, the curve shifts to the right. The pump is allowed to continue operating and establish a membrane potential. This activity will then cause the formation of a concentration gradient, which will resist the inwards flux and reduce the pump's potential.

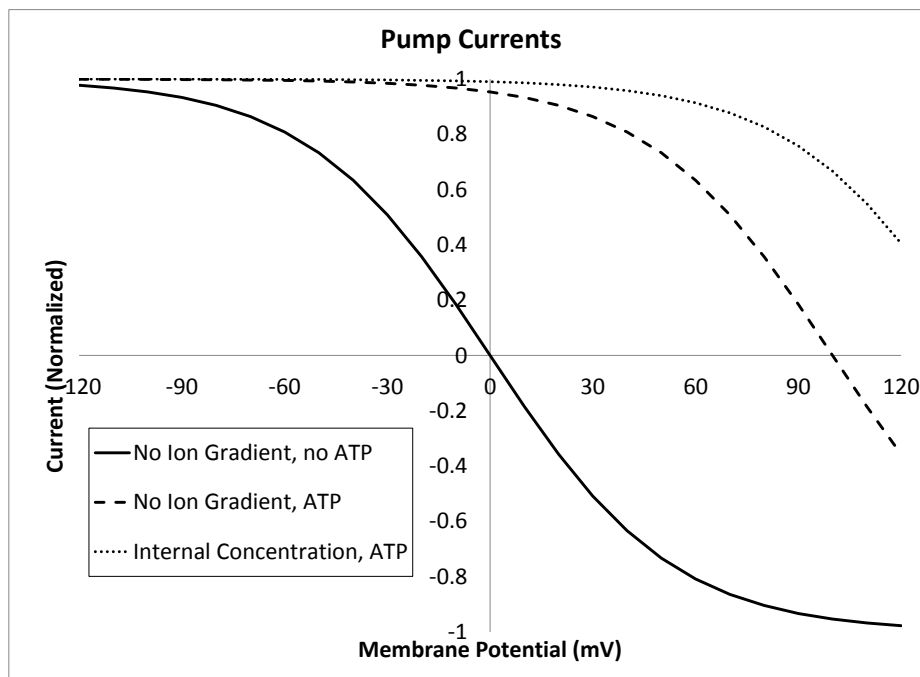


Figure 1.11. Predicted pump behavior with varying ATP and ion gradients.

1.3.1.4.2 Cotransporters/Exchangers

A similar derivation was applied for calculating current through the cotransporters/ exchangers. For this derivation, an exchanger which swaps 2 S^+ in one direction for every 1 X^+ in the opposite direction will be offered for illustration as seen in figure 1.12.

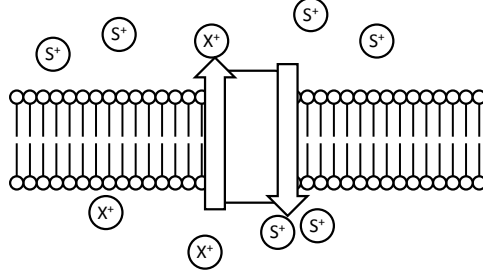


Figure 1.12. $2[S]^+ [X]^+$ ion exchanger sketch.

This reaction may be represented through:



The flow through this transporter is governed entirely by the membrane potentials and electrochemical gradients for S^+ and X^+ . The energy produced when 2 intracellular S^+ ions are moved outside of the cell is used to move one extracellular X^+ into the cell. The energy from this may be represented as:

$$\Delta G_X = e(v - v_X) \quad (1.13a)$$

$$\Delta G_S = -2e(v - v_S) \quad (1.13b)$$

where the total free energy change in the reaction is:

$$\Delta G = \Delta G_X + \Delta G_S = e(-v + 2v_S - v_X) \quad (1.14)$$

For cotransporters and exchangers, saturation effects were not expected and ΔG will vary around zero[32].

$$\alpha = \lambda [S]_i^2 [X]_e^1 \exp\left(-\frac{ev}{2k_B T}\right) \quad (1.15a)$$

$$\beta = \lambda [S]_e^2 [X]_i^1 \exp\left(\frac{ev}{2k_B T}\right) \quad (1.15b)$$

From these reaction rates, the flow through the exchanger was calculated as:

$$i_{exchanger} = -Ne(\alpha - \beta) \tag{1.16a}$$

$$i_{exchanger} = 2Ne\lambda \sqrt{[S]_e^2 [S]_i^2 [X]_e^1 [X]_i^1} \sinh\left(\frac{e(v - 2v_S + v_X)}{2k_B T}\right) \tag{1.16b}$$

where N is the number of exchangers.

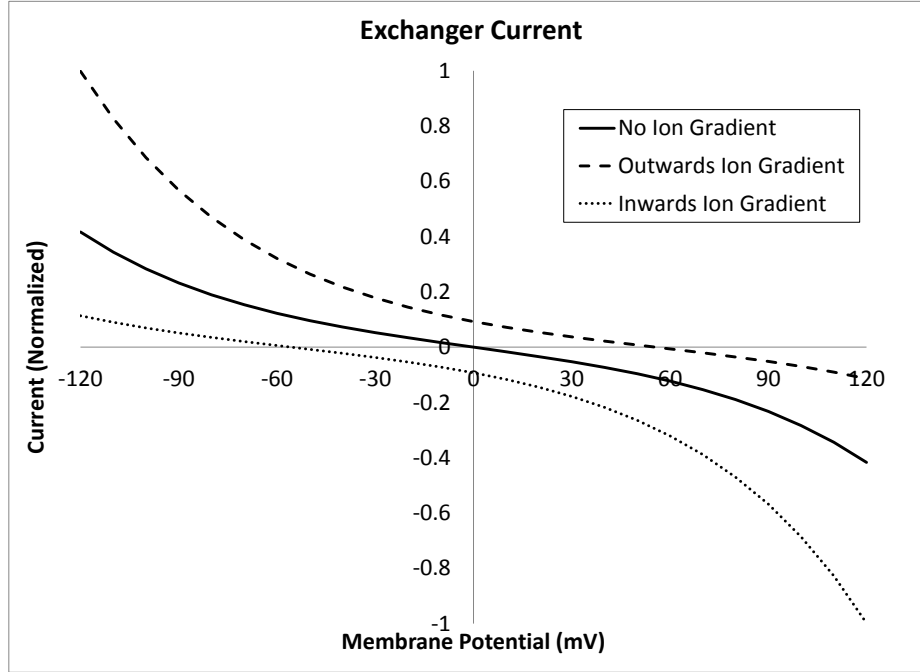


Figure 1.13. Predicted cotransporter/exchanger currents with varying ion gradients.

A similar approach may be used for creating equations for cotransporters. For current behavior, refer to figure 1.13. The central line assumes equal concentrations on both sides. The upper line assumes that the concentrations favor reaction β (reverse reaction), and ion S^+ is entering the cellular interior. The lower line assumes that the concentrations favor α , and the ion X^+ is exiting the cell. It should be noted that the proposed reaction is electrogenic; the net reaction will generate a membrane potential. If the transfer of charge was balanced with a 1 to 1 ratio, the membrane potential would have no effect on the transport.

1.3.1.4.3 Voltage Gated Ion Channels

Voltage Gated Ion Channels are ion-selective channels with a voltage-gating behavior. These channels allow for passive diffusion of the selected ion S^+ , but will remain gated when the membrane potential is below a certain threshold (or gating voltage). These ion channels are commonly used in conjunction with action potentials[18], and allow for rapid diffusion of their selected ions when triggered by the action potentials.

The voltage gated ion channel considered in this derivation is S^+ selective, as seen in figure 1.14.

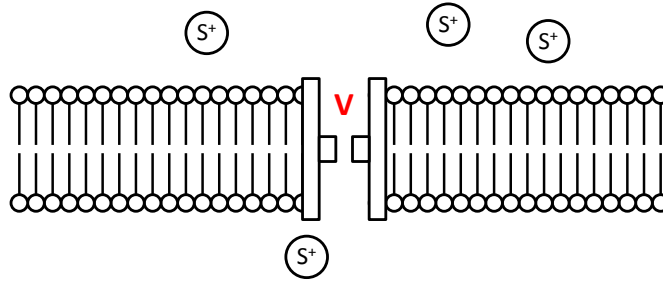


Figure 1.14. Voltage gated $[S]^+$ ion channel sketch.

The ionic channels were assumed to exist in two states – completely open (O) or completely closed (C), and they fluctuated between these states in a simple Markov process [33] described by first order kinetics[34].



α is the chance of a channel to open, and β is the chance to close. From this, the total ratio of channels (open to close) was represented through:

$$\frac{dx}{dt} = \alpha(1 - x) - \beta x \equiv \frac{x_{\infty} - x}{\tau} \quad (1.18a)$$

$$x_{\infty} = \frac{\alpha}{\alpha + \beta} \quad (1.18b)$$

$$\tau = \frac{1}{\alpha + \beta} \quad (1.18c)$$

Here x_∞ represents the steady state fraction of open channels, and τ represents the relaxation time. It was assumed that the difference in energy between the open and closed positions is:

$$\Delta G = G_{open} - G_{closed} = q(v_x - v) \quad (1.19)$$

where q is the gating charge (typically $4e$) such that qv represents the change in potential energy due to redistribution of charge during the transition, and qv_x represents the difference in in mechanical conformational energy of the channel opening. At equilibrium, $dx/dt = 0$ and the ratio of the channels in the open or closed states is:

$$\frac{x_\infty}{1 - x_\infty} = \frac{\alpha}{\beta} \quad (1.20)$$

This ratio is also given by the Boltzmann distribution[35]:

$$\frac{x_\infty}{1 - x_\infty} = \exp\left(-\frac{\Delta G}{k_B T}\right) \quad (1.21)$$

Combining the previous three equations with $q = +4e$ (standard gating charge) results in:

$$x_\infty = \left[1 + \exp\left(\frac{4e(v_x - v)}{k_B T}\right)\right]^{-1} \quad (1.22a)$$

This may also be rewritten as:

$$x_\infty = \frac{1}{2} \left[1 + \tanh\left(\frac{2e(v - v_x)}{k_B T}\right)\right] \quad (1.22b)$$

This represents the current probability of a channel being open at steady state, and is dependent on the difference between the current membrane potential v and the gating voltage v_x . It is

possible to include time dependent behavior as well through the following equation, where τ is the relaxation time:

$$\frac{dx}{dt} = \frac{1}{\tau} \cosh\left(\frac{2e(v - v_x)}{k_B T}\right) \left(\frac{1}{2} \left(1 + \tanh\left(\frac{2e(v - v_x)}{k_B T}\right)\right) - x\right) \quad (1.23)$$

The ion current derivation for the voltage gated channels took a different approach from the transporter current, but resulted in a similar equation through several simplifying assumptions. First d was defined as the channel length, with $-d/2$ and $d/2$ acting as the coordinates at either end of the channel, and $A(x)$ was defined as the surface area of the pore itself, varying along the length of the channel. $\phi = \phi(x)$ was defined as the x component of the flux ϕ ; the other components were assumed to be negligible. By stationary flow the current i must be constant through all cross sections, or independent of x . Therefore the flux is inversely proportional to the cross-sectional area, where:

$$i_{channel} = ze\phi A = constant \quad (1.24)$$

This equation was then combined with the Nernst-Planck equation for the total flux of ions due to diffusion and electric forces:

$$\phi = ukT * \exp\left(-\frac{zeU}{k_B T}\right) \nabla \left[[S] \exp\left(\frac{zeU}{k_B T}\right) \right] \quad (1.25)$$

where u is the ion mobility, U is the electric potential. ϕ from equation 24 was inserted into this equation and the result was multiplied by $\exp(ze(U-U_o)/kT)$, introducing a constant voltage U_o such that:

$$U\left(-\frac{d}{2}\right) = U_o + \frac{v}{2} \quad U\left(\frac{d}{2}\right) = U_o - \frac{v}{2} \quad (1.26)$$

This combination yielded the equation:

$$\frac{i_{channel}}{A} \exp\left(\frac{ze(U - U_o)}{k_B T}\right) = -zeukT \frac{d}{dx} \left[[S] \exp\left(\frac{ze(U - U_o)}{k_B T}\right) \right] \quad (1.27)$$

Integrating from one end of the pore to the other ($x = d/2$ to $x = -d/2$) resulted in:

$$i_{channel} = \frac{zeukT}{I} \left[[S]_e \exp\left(-\frac{zev}{2k_B T}\right) - [S]_i \exp\left(\frac{zev}{2k_B T}\right) \right] \quad (1.28)$$

where:

$$I = \int_{-d/2}^{d/2} \frac{1}{A} \exp\left(\frac{ze(U - U_o)}{k_B T}\right) dx \quad (1.29)$$

The factor $\sqrt{[S]_e [S]_i}$ was extracted from this equation, and the ratio of the concentrations was written in the same form as the Nernst equilibrium potentials (equation 1.3). This resulted in:

$$i_{channel} = \frac{2zeukT}{I} \sqrt{[S]_e [S]_i} \sinh\left(\frac{ze(v - v_s)}{2k_B T}\right) \quad (1.30)$$

The pore geometry was assumed to have a constant cross section A_o with a constricting pore A_{pore} as seen in figure 1.15, which allowed I to be written as:

$$I \approx \frac{\epsilon d}{A_{pore}} \quad (1.31)$$

where d is the length of the channel and ϵd is the length of the pore. This assumed that the contribution from the pore dominated the integral I , where A_{pore}/A_o is of the order ϵ^2 .

Combining this with the voltage gating coefficient x resulted in the final equation for channel flow.

$$i_{channel} = x * 2zekT \sqrt{[S]_e^1 [S]_i^1} \frac{A_{pore}}{\epsilon d} \sinh\left(\frac{e(v - v_s)}{2k_B T}\right) \quad (1.32)$$

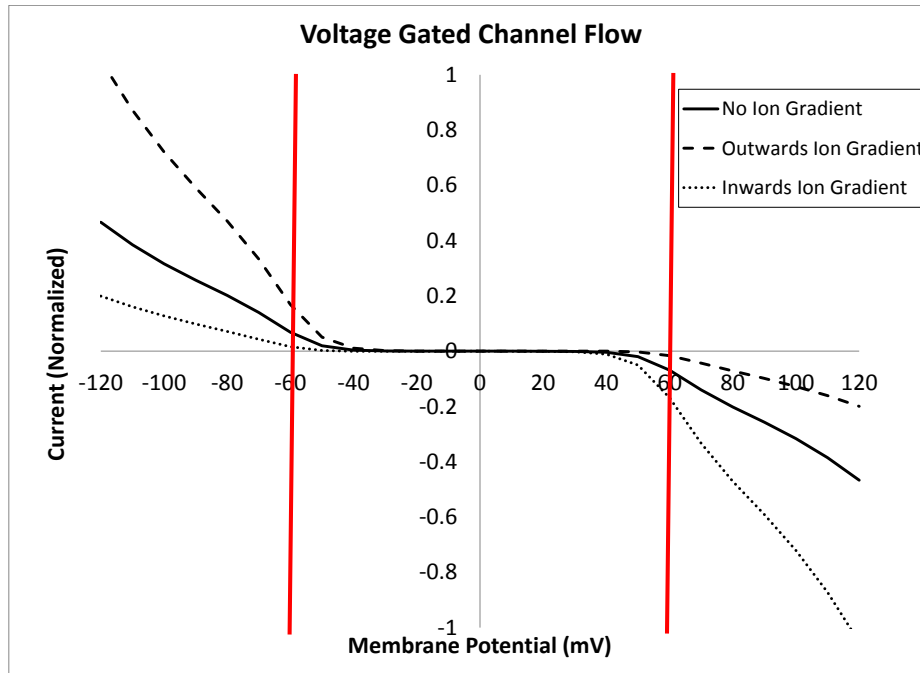


Figure 1.15. Predicted voltage gated ion channel current with a 60 mV gating voltage (marked in red) and varied ion gradients.

For visualization, refer to figure 1.15. In this case, equation 22b (steady state) has been employed for the gating behavior, with $v_x = 60$ mV as demarked by the red vertical lines. The channels have been inserted in both directions across the membrane, allowing for gating at both +/- 60 mV; channels may also operate as one-way conduits. The center line has no pre-set ion concentration gradients. The additional two cases have ion concentration gradients of 5/1, and the impact on channel flow may be observed.

1.3.1.4.4 Ion Diffusion

The final mode of transport considered here was through membrane permeability. This was modeled through the Nernst-Planck equation, which represents the flux due to a combination of an electric field and concentration gradients. In one dimensional form, the flux of ion S^+ per unit area of membrane is given as[36, 37]:

$$J_S = \left[D_S \frac{d[S(x)]}{dx} + u_S z_S F [S(x)] \frac{dv}{dx} \right] \quad (1.33)$$

where D_S is the diffusion constant for ion S , u_S is the mobility of the ion S^+ , $[S(x)]$ is the concentration of S^+ with respect to x , and v is the membrane potential. This assumed no convective flow and that the flow was not affected by other flows or forces. The concentrations at both surfaces of the membrane were assumed to be the total concentration multiplied by a common partition coefficient β . The equation was then integrated with respect to x to yield the Goldman-Hodgkin-Katz equation[38-40]:

$$i_{diff} = -AP_S F \left(\frac{zFv}{RT} \right) \left[\frac{[S]_i - [S]_e e^{\left(\frac{-zFv}{RT} \right)}}{1 - e^{\left(\frac{-zFv}{RT} \right)}} \right] \quad (1.34)$$

where A is the surface area, F is Faraday's constant, and P_S is the permeability of the membrane to the species S .

The behavior of this equation may be seen in figure 1.16. For diffusion without a preset ion gradient, the current appears to vary near-linearly with the membrane potential v . The addition of an ion gradient shifts the curve away from the original, and reducing the diffusion accordingly. In this case, the addition of a 5 to 1 external to internal concentration results in a resting membrane potential of 43 mV. This is equivalent to the Nernst equilibrium potential for

the ion gradient (43 mV), revealing that the derived diffusion currents behave in a similar fashion to the previously discussed protein transport currents.

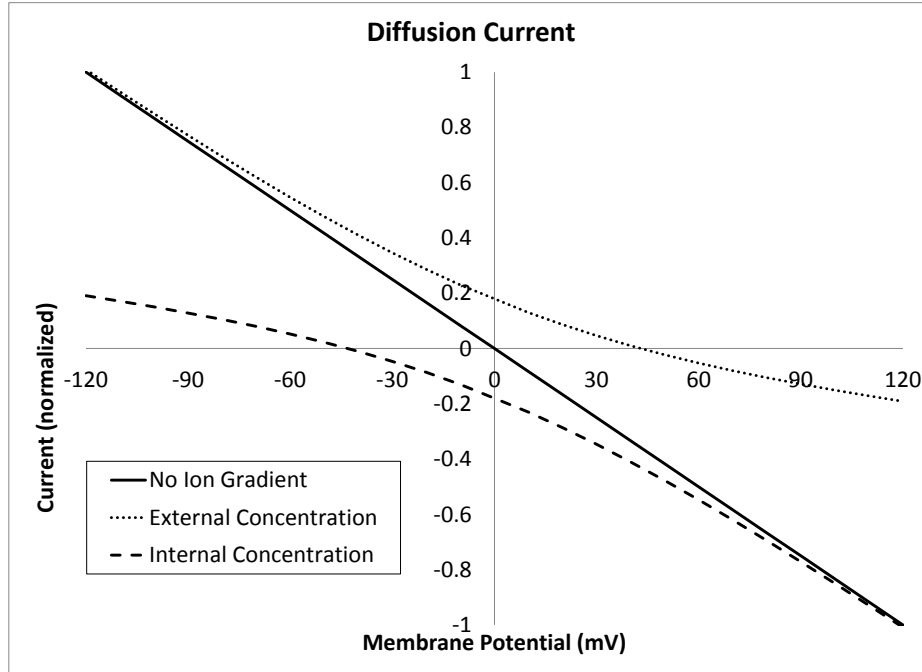


Figure 1.16. Predicted ion diffusion current with varied ion gradients.

1.3.1.5 Changes in Volume

A unique feature of the model is the ability to predict changes in volume and shape due to external forces and the development of osmotic pressures. These equations are featured in both the endosomal burst and the osmotic actuation chapters, and are derived from classic elastic energy methods[41, 42].

Both cases rely on the generation of an osmotic pressure, as seen in equation 1.35. Osmotic pressure is generated as a function of concentration gradients, and this osmotic pressure was determined from the van't Hoff equation[43],

$$\pi = RT\theta \sum ([S]_i - [S]_e) - C \quad (1.35)$$

where θ is the osmotic reflection coefficient which varies from 0 to 1. Osmotic pressure was initialized to zero through the application of the constant C ; thus any increase in osmotic pressure is due to transport across the membrane.

This osmotic pressure generates osmotic transport across the membrane, increasing or decreasing the volume of the vesicle. The total change in vesicle volume was determined by[44]:

$$\frac{dV}{dt} = KA \left(\sum_s \pi_s - p_r \right) + \sum_s \bar{V}_s \frac{d}{dt} (n_s)_i \quad (1.36)$$

where K is the hydraulic diffusivity of the membrane, A is the surface area, and V_s is the volume of each species transported. The net volume change was broken into two terms. The first term is the volume change due to osmotic transport, and the second is the volume change due to species transport. Generally the first term will be much greater than the second. The diffusivity of the membrane was determined from the osmotic permeability of the membrane given as[45]:

$$K = \frac{P_{os} V_w}{RT} \quad (1.37)$$

where P_{os} is the permeability and V_w is the molar volume of water.

1.3.1.6 Elastic Energy

An important feature of the presented model is the ability to link the predicted deformation (equation 1.36) to an elastic deformation of the surrounding material. Among the core equations, the representation of elastic energy is most subject to varied methods. However, some accommodation of elastic energy is required. As such it is retained as a core equation.

For the nastic actuation study discussed in section 1.2.3, ABAQUS was used to calculate the resisting deformation, modeling the surrounding material as a hyperelastic material through Mooney-Rivlin equations[27, 46]. For the cases considered here more traditional geometries are used which allow for standard elasticity equations. Even so, more than one approach is considered for capturing elastic energy. Put simply, these equations must be modified to yield a resisting pressure based on a total change in volume ΔV as appropriate to the application of interest

In the endosome simulations presented in chapter 2, the surrounding membrane was approximated as a hollow sphere surrounding the cell contents. From the mechanical energy principle:

$$\Delta\Sigma = \Sigma_{t2} - \Sigma_{t1} \quad (1.38)$$

where Σ represents the energy in the system denoted at times $t1$ and $t2$, it was shown that the work done by surface tractions t_n acting over a continuum simple path l between two equilibrium states without a body force was balanced by the change in the total strain energy[41]:

$$\int_l \Delta\Sigma dV = \int_l \int_{dl} t_n da \cdot dx \quad (1.39)$$

The cell was then modeled as an isotropic spherical membrane with an undeformed radius r_0 and thickness $t_0 \ll r_0$ initially. The spherical shape was assumed to remain constant due to a hydrostatic internal pressure p_r , and the sphere was assumed to deform uniformly. The uniform isotropic stretch is given by $\lambda = r/r_0$, the transverse normal stretch is given by $\lambda_3 = t/t_0$, and the pressure p_r at the initial state is zero. It was also assumed that the stored energy Σ

may be written solely as a function of the stretch λ , with $\Sigma = 0$ at $\lambda = 1$. From these two assumptions, equation 1.39 was rewritten as:

$$4\pi r_0^2 t_0 \Sigma(\lambda) = 4\pi r_0^3 \int_1^\lambda \lambda^2 p_r(\lambda) d\lambda \quad (1.40)$$

which was simplified to:

$$p_r(\lambda) = \frac{t_0}{r_0 \lambda^2} \frac{d\Sigma(\lambda)}{d\lambda} \quad (1.41)$$

For an incompressible material, this may be written as:

$$p_r(\lambda) = \frac{2t_0}{\lambda r_0} \left[1 - \frac{1}{\lambda^6} \right] (\beta_1 - \lambda^2 \beta_{-1}) \quad (1.42)$$

where β_1 and β_{-1} are constants related to the material properties. This was then combined with a constitutive equation for biological tissue[47].

$$\Sigma = \frac{\mu_0}{2\gamma} [e^{\gamma(l_1-3)} - 1] \quad (1.43)$$

This resulted in the final form for the pressure resisting the deformation:

$$p_r(\lambda) = \frac{2\mu_0 t_0}{r_0 \lambda} \left[1 - \frac{1}{\lambda^6} \right] e^{\gamma(2\lambda^2 - \lambda^{-4} - 3)} \quad (1.44)$$

The internal pressure was calculated as a function of the membrane shear modulus of elasticity μ , the instantaneous deformation, and a material characteristic γ . γ was assumed to be 0.067, which corresponds to the point at which $dp_r/d\lambda \geq 0$ for all λ [41]. This ensures that the values remain stable throughout the simulation while allowing the greatest degree of deformation. The resulting pressure vs. stretch predictions may be seen in figure 1.17. As the membrane deforms, the resulting pressure increase starts to drop until a plateau is reached. The plateau point also represents the maximum stretch observed during the simulations.

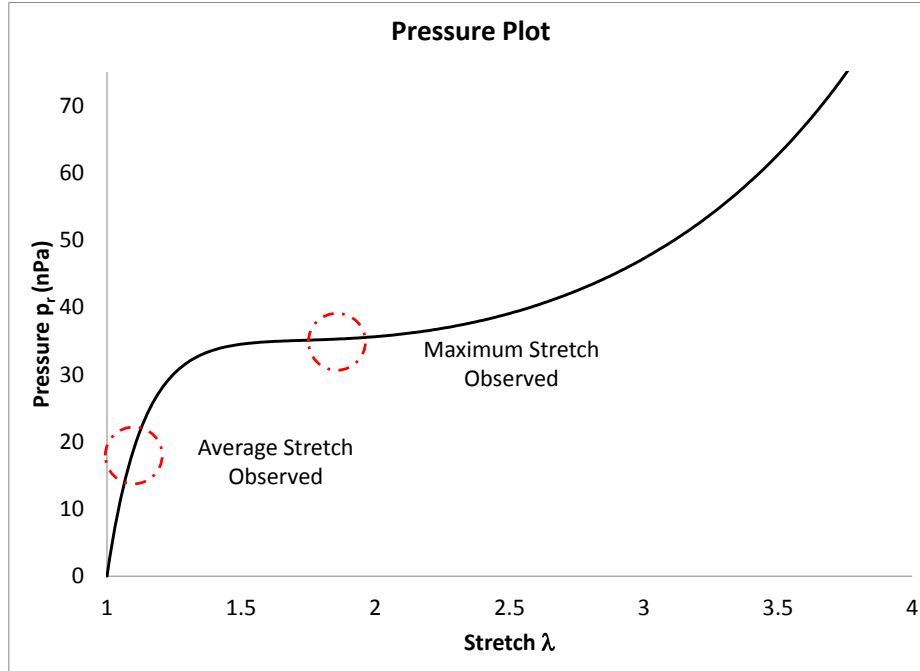


Figure 1.17. Predicted internal pressure p_r as a function of the membrane stretch λ with $\gamma = 0.067$, $\mu_0 = 2.5 \mu\text{N/m}$, $t_0 = 5.2 \text{ nm}$, and $r_0 = 0.5 \mu\text{m}$ (cellular inputs). The marked region corresponds to the maximum stretch observed in the endosome studies.

In the osmotic actuation case of chapter 4, the deformation was instead focused on the expansion of a circular rubber diaphragm. The equation for this deformation was derived from the work of Timoshenko and Woinowsky-Krieger[42].

The displacement u was modeled as:

$$u = \frac{p_r r^4}{64D} \quad (1.45)$$

where D is the plate bending stiffness:

$$D = \frac{Et^3}{12(1 - \nu^2)} \quad (1.46)$$

E is the modulus of elasticity for the diaphragm, t is the diaphragm thickness, and ν is Poisson's ratio for the diaphragm. The total displaced volume under the cap was calculated by integrating equation 1.45, which resulted in:

$$\Delta V = 2\pi \int_0^r r \cdot u dr = \frac{p_r \pi r^6 (1 - \nu^2)}{16Et^3} \quad (1.47)$$

Since the desired form is the resulting pressure from the deformation ΔV , this was rewritten as:

$$p_r = \frac{16Et^3 \Delta V}{\pi r^6 (1 - \nu^2)} \quad (1.48)$$

This form accounts for linear displacement. As the diaphragm deforms, the response will transition from linear response to non-linear response[25, 48]. The diaphragm profile was determined by:

$$u = \frac{p_r}{2} \left\{ \frac{2}{\beta^3} \left[\frac{I_0(\beta\xi) - I_0(\beta)}{I_1(\beta)} \right] + \frac{1 - \xi^2}{\beta^2} \right\} \quad (1.49)$$

where I_i are modified Bessel functions of the first kind, β is the membrane stress, and ξ is the non-dimensional parameter for radial position. However, the programming language selected (VB.net) does not support these modified Bessel functions and no math libraries currently exist, so linear elasticity is assumed for the diaphragm deformation case.

1.3.1.7 System Solution

The overarching goal of this dissertation is to define the core governing equations for a new class of active materials. Inherent to this goal is defining a pathway towards their simultaneous solution. While the specific simultaneous solution approach could be varied, it is understood that the foregoing represents a stiff set of simultaneous equations; it is unlikely that analytical

approaches will be viable. Thus a classic numerical methods approach, Runge-Kutta, is offered as a viable path toward application.

Runge-Kutta methods may be expressed in a general form as seen in equation 1.50 [49] where i progresses from 1 to 5 (5th order).

$$\mathbf{k}_i = \mathbf{f} \left(t_n + c_i h \mathbf{y}_n + h \sum_{j=1}^5 a_{ij} \mathbf{k}_j \right) \quad (1.50)$$

In this equation h is the step size (or timestep), f is the differential equation, and k is the function evaluation at each stage. The values at the next step were calculated through a summation of all 5 evaluations.

$$\mathbf{y}_{n+1} = \mathbf{y}_n + h \sum_{j=1}^5 b_j \mathbf{k}_j \quad (1.51a)$$

$$\hat{\mathbf{y}}_{n+1} = \hat{\mathbf{y}}_n + h \sum_{j=1}^5 \hat{b}_j \mathbf{k}_j \quad (1.51b)$$

A_{ij} and b_j represent coefficients for the integration, which may be represented in the Butcher array in table 1. The layout is summarized as follows, where c_i is the fraction of the current timestep where row A_{ij} is employed.

c	A
	\mathbf{b}^T
	$\hat{\mathbf{b}}^T$

Figure 1.18. Butcher array notation.

For this particular case, the butcher array employed may be seen in table 1.

Table 1. Butcher Array for 5th order Explicit Runge-Kutta [50]

0							
$\frac{1}{5}$	$\frac{1}{5}$						
$\frac{3}{10}$	$\frac{3}{40}$	$\frac{9}{40}$					
$\frac{4}{5}$	$\frac{44}{45}$	$-\frac{56}{15}$	$\frac{32}{9}$				
$\frac{8}{9}$	$\frac{19372}{6561}$	$-\frac{25360}{2187}$	$\frac{64448}{6561}$	$-\frac{212}{729}$			
1	$\frac{9017}{3168}$	$-\frac{355}{33}$	$\frac{46732}{5247}$	$\frac{49}{176}$	$-\frac{5103}{18656}$		
1	$\frac{35}{384}$	0	$\frac{500}{1113}$	$\frac{125}{192}$	$-\frac{2187}{6784}$	$\frac{11}{84}$	
y_1	$\frac{35}{384}$	0	$\frac{500}{1113}$	$\frac{125}{192}$	$-\frac{2187}{6784}$	$\frac{11}{84}$	0
\hat{y}_1	$\frac{5179}{57600}$	0	$\frac{7571}{16695}$	$\frac{393}{640}$	$-\frac{92097}{339200}$	$\frac{187}{2100}$	$\frac{1}{40}$

The system of equations was stiff, and predictor-correct methods were employed to maintain stability. The timescale was adjusted based on the current rate of change, to ensure that error remains minor and that the system does not become unstable. Basic sanity-checks are also employed at each step, checking for negative concentrations or invalid currents. If the next step's error value was too high or it failed a sanity check, the timestep was halved and the step was repeated.

The data from the simulations was printed to a space-delimited text file. Data includes current step number, simulation time, internal concentrations, membrane potential, and

transporter currents. This data allowed the analysis of the change in internal conditions as the simulation progressed. Through this transporter interaction were observed and the feasibilities of the proposed systems were assessed.

1.3.2 Model Overview

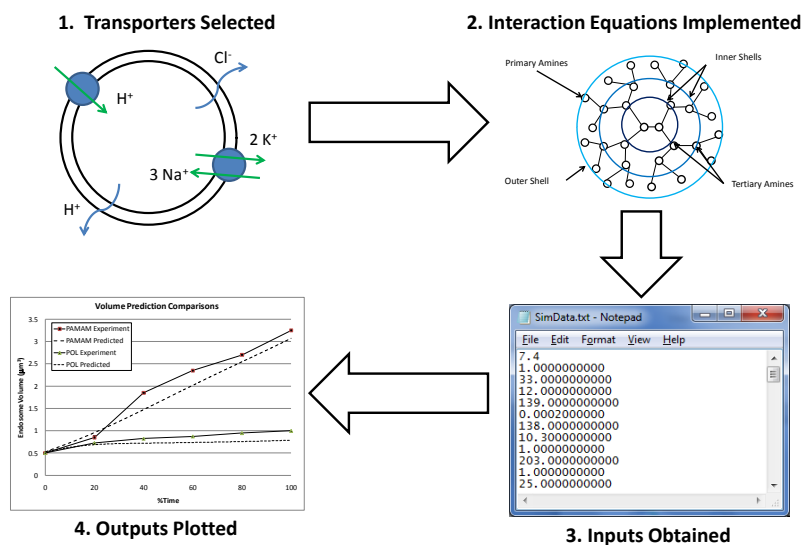


Figure 1.19. General modeling process represented in 4 steps.

The preceding sections have offered detailed discussion of each of the key components required to assess engineered systems based on cellular structures. While the number of parameters can be significant, the presented solution may be represented in just four steps (figure 1.19). First, the core equations are determined for the case of interest. Second, interaction equations may be implemented to account for additional behavior, such as the interaction with additional chemical species (Figure 1.19 illustrates a case where the core cellular system equations are coupled to interaction with a dendrimer that behaves as a “proton sponge”). Inputs are obtained from experiment and/or lower length scale models as appropriate and model outputs are printed to a space-delimited text file for observation.

1.3.3 Summary

The overall scope of the dissertation may be summed up as follows. A new class of active materials, biomimetic membranes (or biomembranes), is suggested. A mathematical model is constructed with the ability to link cellular activity to system performance. Figure 1.20 illustratively summarizes the material constituents that are considered core to the development of biomimetic membranes.

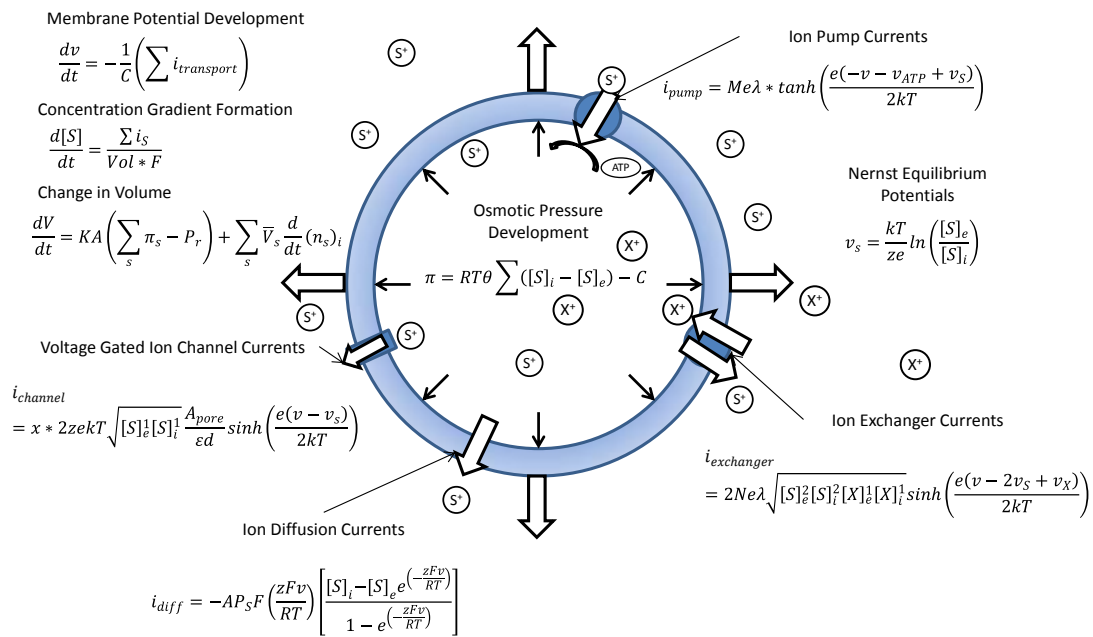


Figure 1.20. Core components of the biomembrane model.

The creation of this model allows for predictive modeling of a new highly tailorable class of smart materials; biomimetic membranes. In the following chapters the claimed versatility of this new class of engineering materials will be defended through adaptation of this system to distinctly different applications: vaccine delivery, water purification, and hydraulic actuation.

2.0 ENDOSOME STUDIES

DNA vaccination is a technique for introducing a nucleic acid to a cell nucleus in order to immunize the cell against diseases. These vaccines are still in the experimental stages, and show great promise for treatment of diseases and tumors. However, there are several barriers to successful vaccine delivery.

Vaccine or gene delivery through non-viral means is limited by instability of the vaccine in blood circulation and extracellular fluids, as well as sequestration of the vaccine/gene in cellular organelles such as endosomes[51-54]. Biological activities of these DNA vaccines are dependent upon their escape from these cellular organelles to allow for accumulation in the cytosol and/or nucleus in which molecular targets are located. A common entry pathway of exogenous particulates into cells is through endocytosis. This process encompasses multiple mechanisms, with the common initial step of encasing the nucleic acids within small lipid vesicles, or endosomes. In this process the cell extends and engulfs the surroundings (figure 2.1), including a vaccine when present, for intake; the DNA is then enclosed in a vesicle known as an endosome[52]. With the foreign species (DNA) encased, this endosome is then transported to the interior of the cell where undergoes maturation and eventually fuses with a lysosome wherein degradation of nucleic acids occurs. While the endosome provides a mode of transport for uptake, it also acts to destroy and break down its contents via a pH driven process before releasing it into the cell[31, 55, 56]. This acidification process breaks down the contents (down

to a pH of 5), and may severely degrade the DNA vaccine in the process. Therefore for effective DNA vaccine delivery this degradation stage of endocytosis process be circumvented.

It has been postulated that inducing endosome burst (lysis) may be an effective way to affect the release of endocytosed vaccine DNA prior to the onset of degradation[57]. If correct, manipulation of its tenets may be a useful tool for improving efficiency of nucleic acid delivery.

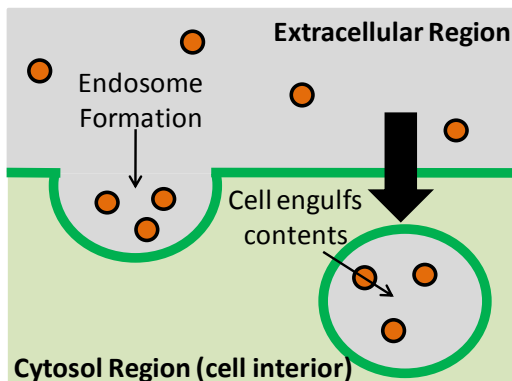


Figure 2.1. Sketch of the endocytosis process.

This chapter will be structured as follows. After a brief literature review of endocytosis, the system of equations utilized in the endosome case study will be presented. Calibration data along with sources will be listed, and validation steps will be detailed. Once the calibration and validation steps are completed, the model will then be used to explore various specific methods for enhancing the desired endosomal burst to enable effective DNA-vaccine delivery.

2.1 ENDOSOMAL TRANSPORT

The biomembrane approach may prove useful for exploring various methods for inducing endosome burst. Endosomes are at their core cellular structures with systems of protein transporters, and the detailed method of simulation from chapter 1 will prove useful. Several

transport pathways have been identified within the endosome, which may be seen in figure 2.2. The acidification of the endosome itself is driven by a combination of proton pumps (H^+ ATPase) and proton diffusion[55]. As the endosome acidifies and the membrane potential increases due to the pump flows, diffusion will increase. This increase in diffusion is expected to eventually match the flow through the proton pumps [55, 58] causing a pH plateau. The proton diffusion plays a key role in moderating the endosome acidification. The diffusion rate increases with membrane potential and the concentration gradient.

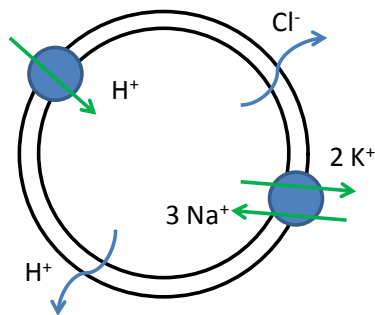


Figure 2.2. Sketch of the combination of H^+ ATPases, $Na^+ K^+$ ATPases and $Cl^- H^+$ diffusion considered for modeling of endosomal pH.

The development of a membrane potential is regulated by chloride (Cl^-) diffusion and a sodium-potassium pump ($Na^+ K^+$ ATPase). These transporters work in parallel to affect the evolution of the endosome interior.

2.2 EXISTING ENDOSOME MODELS

Simulation of the endosome process has been performed previously with varying approaches. A model that studies the final pH equilibrium of an endosome has been created by Rybak et al[59]. These authors note that several transporters traditionally exist in the endosome membrane: H^+

ATPase, $\text{Na}^+ \text{K}^+$ ATPase, and Cl^- Channels. This model provided a method for varying the transporters present and observing their effects on the final equilibrium state of the endosome. However, this approach did not allow for transient analysis of the endocytosis process. After manipulating transporter activity in their model, Rybak et al. ultimately report that the internal pH is largely dependent on the number of H^+ ATPase present and the diffusion of ions through the endosome membrane.

Grabe and Oster [31] have also studied the acidification of endosomes. Their studies indicate that the endosome membrane is also permeable to $\text{H}^+ \text{Cl}^- \text{K}^+$ diffusion and that $\text{Na}^+ \text{K}^+$ channels are also present. However, it is not clear that the transport kinetics of these channels were simulated in the paper, rather this transport mechanism appears to have been replaced by diffusion terms. This model allowed for transient simulation of the endosome process with the ability to vary the transporters present, but did not focus on using the model to assist in triggering endosome burst.

Both the Rybak et al.[59], and the Grabe and Oster [31] studies yield insights into the acidification process; studies such as these are important for understanding the evolution of acidification as it relates to vaccine degradation. However these approaches did not consider the role of membrane mechanical properties and how this consideration might be employed to avert degradation in the first place. The following study focuses on linking the protein transporter activity towards the development of an osmotic pressure through which endosome rupture may be achieved.

2.3 SELECTED TRANSPORT APPROACH

The model for this study was built on the equations presented in chapter 1, and transport proteins were selected based on the literature review. These transporters include flow across Na^+/K^+ ATPase (pumps), H^+ ATPase (pumps), as well as H^+ , Cl^- , and water diffusion. In addition the membrane properties including elasticity and rupture were considered. Concentrations of each of the species present (water, Na^+ , K^+ , H^+ , Cl^-) were tracked in the simulation resulting in predictions of the internal pH, internal pressure, and volume change. Because the goal is to achieve burst prior to the onset of vaccine degradation, only the behavior of an early endosome, in the initial stages of acidification, was considered.

In this study the diffusion coefficients were assumed to remain constant at the experimental values[60, 61]. The diffusion coefficients may increase slightly as the membrane stretches; however there is insufficient information to predict this exact behavior.

The ultimate goal of this type of study is to exploit mechanisms that lead to expansion in cells. The model discussed in this paper is unique in its time dependent tracking, component flexibility, and ability to track the change in volume, internal concentrations, and membrane potential over time.

2.4 IDENTIFICATION AND CALIBRATION OF EQUATIONS FOR ENDOSOME SIMULATION

In accordance with the Hodgkin Huxley model[21], the membrane was treated as a capacitance circuit separating the intracellular and extracellular space. The membrane potential v was

determined by summing the currents $i_{transport}$ across each the membrane and dividing by the membrane capacitance C (based on equation 1.1).

$$\frac{dv}{dt} = -\frac{1}{C} \left(\sum i_{transport} \right) \quad (2.1)$$

The Nernst equilibrium potentials were calculated each timestep as a function of Boltzmann's constant k_B , the temperature T , the valence z , the basic charge e , and the ratio of the external and internal concentrations $[S]_e$ and $[S]_i$ (based on equation 1.3):

$$v_s = \frac{k_B T}{ze} \ln \left(\frac{[S]_e}{[S]_i} \right) \quad (2.2)$$

This equation was repeated for each of the species present in the endosome, including $[H]^+$, $[Cl]^-$, $[Na]^+$, $[Ca]^{2+}$, and $[K]^+$.

Pumps were implemented for both protons and sodium/potassium. These were modeled as functions of the number of transporters M_H and M_{NaK} , the basic charge e , Boltzmann's constant k_B , rate constants λ_{NaK} and λ_H , and the difference between the energy from ATP v_{ATP} , the membrane potential v , and the Nernst equilibrium potentials v_H , v_{Na} , and v_K (based on equation 1.11):

$$i_{Hpump} = M_H e \lambda_H * \tanh \left(\frac{e(-v - v_{ATP} + v_H)}{2k_B T} \right) \quad (2.3)$$

$$i_{NaKpump} = M_{NaK} e \lambda_{NaK} * \tanh \left(\frac{e(-v - v_{ATP} + 3v_{Na} - 2v_K)}{2k_B T} \right) \quad (2.4)$$

The proton pump is responsible for the gradual acidification of the endosome. As the endosome moves toward the cell interior, the proton pumps will continuously move protons against their electrochemical gradient into the endosome using the energy gained from the hydrolysis of ATP.

The sodium potassium pumps move sodium and potassium against their electrochemical gradients into and out of the endosome using the hydrolysis of ATP. Three sodium molecules are pumped in as two potassium molecules are pumped out; this transport is assumed to be simultaneous. Therefore sodium flow cannot occur without potassium flow, and vice versa.

The final mode of transport considered here was through membrane permeability. The membrane was taken to be permeable to H^+ and Cl^- ions[60, 61]. The diffusion flows were then calculated as functions of the transport surface area A , the permeabilities P_H and P_{Cl} , Faraday's constant F , the membrane potential v , the concentrations of $[H]^+$ and $[Cl]^-$, the Universal Gas Constant R , and the temperature T (based on equation 1.34):

$$i_{HDiff} = -AP_{H^+}F \left(\frac{Fv}{RT} \right) \left[\frac{[H]_i - [H]_e e^{\left(\frac{-Fv}{RT}\right)}}{1 - e^{\left(\frac{-Fv}{RT}\right)}} \right] \quad (2.5)$$

$$i_{ClDiff} = -AP_{Cl^-}F \left(\frac{-Fv}{RT} \right) \left[\frac{[Cl]_i - [Cl]_e e^{\left(\frac{Fv}{RT}\right)}}{1 - e^{\left(\frac{Fv}{RT}\right)}} \right] \quad (2.6)$$

With these equations the change in internal species concentrations was calculated as functions of the currents i_s , the internal volume Vol , and Faraday's constant F (based on equation 1.2).

$$\frac{d[S]}{dt} = \frac{\sum i_s}{Vol * F} \quad (2.7)$$

This was done for each of the active concentrations. The acidification of the endosome (pH) is a primary concern, and was taken into account through a modified version of equation 1.2.

$$\frac{dpH}{dt} = \frac{\sum i_{H^+}}{Vol * F * C_{buff}} \quad (2.8)$$

Here C_{buff} is an experimentally defined property of the aqueous solution, and has units of [mM/pH unit] .

Changes in concentrations generate osmotic pressure. This osmotic pressure was determined from the van't Hoff equation, where R is the gas constant, T is the temperature, θ is the osmotic reflection coefficient (0 to 1), and C is a constant employed to set the initial osmotic pressure to zero (based on equation 1.35).

$$\pi = RT\theta \sum ([S]_i - [S]_e) - C \quad (2.9)$$

This osmotic pressure generation results in osmotic transport across the membrane, increasing or decreasing the volume of the endosome. The total change in vesicle volume was calculated as a function of the hydraulic conductivity K , the difference between the osmotic pressure π and the generated resistance pressure p_r , and the summation of the volumes V_s of the transported species (based on equation 1.36):

$$\frac{dV}{dt} = KA \left(\sum_s \pi_s - p_r \right) + \sum_s \bar{v}_s \frac{d}{dt} (n_s)_i \quad (2.10)$$

In this case study, the osmotic pressure increase (first summation term on the right hand side) is the primary agent for endosome expansion, while the active transport is negligible (second summation term). The osmotic expansion is matched by a resistance to the deformation generated by the surrounding membrane. Here the membrane was approximated as a hyperelastic biological material[41], where the internal pressure was calculated as a function of the shear modulus μ_0 , the radius r_0 , and material property γ (set to 0.067) (based on equation 1.44):

$$p_r(\lambda) = \frac{2\mu_0 t_0}{r_0 \lambda} \left[1 - \frac{1}{\lambda^6} \right] e^{r(2\lambda^2 - \lambda^{-4} - 3)} \quad \lambda = \frac{r}{r_0} \quad (2.11)$$

The endosome model input parameters have been derived from literature as described by Table 2. Inputs which may be modified are marked as variable, while all other inputs are held constant.

Table 2. Endosome Input Values

Variable	Symbol	Value	Source
External pH	pH_e	7.4 mM	[62]
Internal pH	pH_i	7.4 mM	[62]
External Cl^-	$[\text{Cl}]_e$	4 mM	[62]]
Internal Cl^-	$[\text{Cl}]_i$	116 mM	[62]
Mod Cl^-	$[\text{Cl}]_m$	35 mM	[63]
External Na^+	$[\text{Na}]_e$	12 mM	[62]
Internal Na^+	$[\text{Na}]_i$	145 mM	[62]
External K^+	$[\text{K}]_e$	139 mM	[62]
Internal K^+	$[\text{K}]_i$	4 mM	[62]
Osmotic Coefficient	θ	0.73	[31]
NaK Flow	λ_{NaKe}	30 pA	[31]
# of $\text{Na}^+ \text{K}^+$ ATPase	M_{NaK}	100	Variable
H Flow	λ_{He}	100 pA	[31]
# of H^+ ATPase	M_H	100	Variable
Ini Membrane Potential	v_0	90 mV	[18]
Membrane Thickness	h	5.2 nm	Standard
Temperature	T	321 K	Body Temp
Capacitance	C	0.1 $\mu\text{F}/\text{cm}^2$	Standard
Shear Modulus	μ_0	2.5 μN	[64]
Water Permeability	P_{H_2O}	0.052 cm/sec	[65]
Proton Permeability	P_H	0.67E-3 cm/sec	[61]
Chloride Permeability	P_{Cl}	1.2E-5 cm/sec	[60]
Endosome Radius	r	0.5 μm	[63]
Sonawane Sponge Density	p_S	7.85E-02 pg/endosome	Calibration [63]
Extended Sponge Density	p_E	1.8 mg/ml	Calibration

The initial composition at the interior was assumed to be similar to the composition of the cell exterior, and vice-versa. This assumption derived from the recognition that the formation of the endosome arises from the cell extending and engulfing a portion of its surroundings.

2.5 ENDOSOME TRANSPORT VALIDATION CRITERIA

There were three criteria of interest that will be examined to ensure that the endosome transport model predictions are correct. The first criterion is the nature of the acidification. The second is the function of the $\text{Na}^+ \text{K}^+$ ATPase. The third is the resting membrane potential.

2.5.1 Endosome Transport Validation Step 1: Acidification Profile

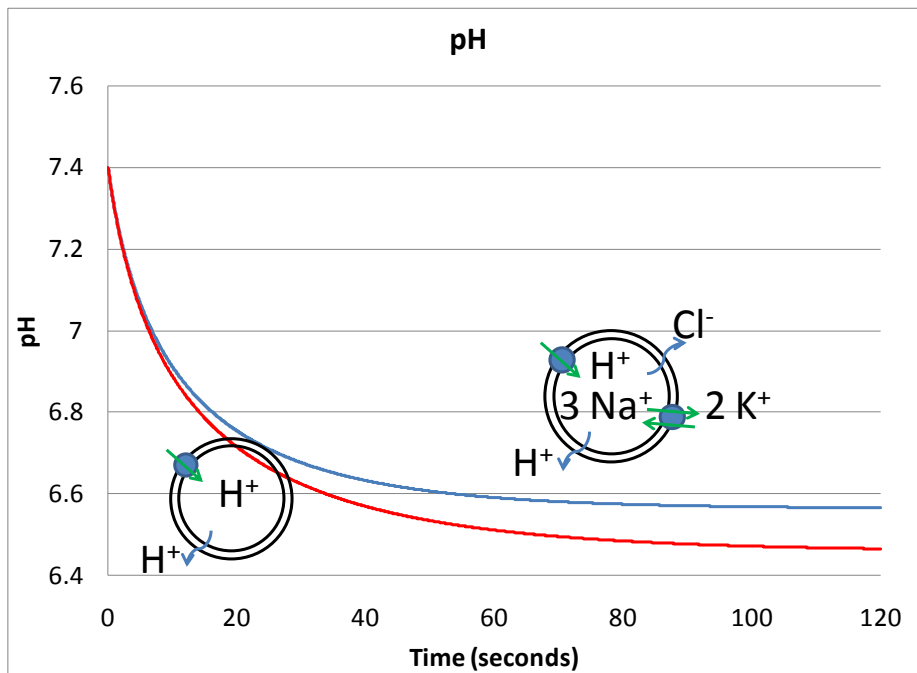


Figure 2.3. Predicted endosome acidification with (top line) and without (bottom line) $\text{Na}^+ \text{K}^+$ ATPase.

Employing the input parameters of Table 2, the evolution of acidification of the endosome was plotted (figure 2.3, upper line). The acidification itself is a function of the membrane potential generation, the proton pump activity, and the proton diffusion. It is observed that the acidification are similar to the experimental results[31, 66], including a predicted internal pH plateau of around 6.5.

Initially the internal pH changes rapidly but this involves the generation of a membrane potential and of a Nernst equilibrium potential for the protons. Both of these terms directly increased the proton diffusion. Endosomes have been found to be highly permeable to proton flow, and around the pH value of 6.5 the diffusion leak current matches the proton pump current, resulting in an equilibrium point or plateau[55].

This demonstrates that the H^+ ATPase and the H^+ diffusion predictions in the presence of an evolving membrane potential and ATP hydrolysis are physically reasonable.

2.5.2 Endosome Transport Validation Step 2 – $Na^+ K^+$ ATPase impact

The plateau effect just described is a function of the membrane potential, the concentration gradients, and the diffusion currents. While the proton pump is a primary source of membrane potential generation, the impact of other transporters must be considered. The $Na^+ K^+$ ATPase simulated here is electrogenic; its operation will generate a membrane potential. Since the $Na^+ K^+$ ATPase works to transport three positively charged ions in for two positively charged ions out, this will generate a positive membrane potential. This positive membrane potential development will negatively affect proton pump flow (equations 2.3, 2.4) while simultaneously increasing diffusion flow (equations 2.5, 2.6).

Therefore the presence of the $\text{Na}^+ \text{K}^+$ ATPase is expected to reduce the acidification of the endosome[55, 56]. This was verified by disabling the $\text{Na}^+ \text{K}^+$ ATPases and comparing the acidification curves (figure 2.3, lower line). The reasoning for this step was to provide additional confidence in ability of the proteins to work together and impact system conditions appropriately.

2.5.3 Endosome Transport Validation Step 3 – Resting Membrane Potential

In addition, the model consistently predicts an evolution of the membrane potential toward 90 mV resting (or equilibrium) potential; -90 mV is commonly found in cells as the resting potential[18], and is due to the concentration gradients and currents (especially Cl^- diffusion) across the cell wall. The endosome membrane potential predicted here is positive because the cytoplasm has been taken as the exterior of the endosome, swapping the measured direction. The natural occurrence of this resting membrane potential in the absence of any attempts to enforce the condition lends confidence in the accurate simulation of a cell system.

2.6 ENHANCING ENDOSOME BURST THROUGH PROTON SPONGES

With the endosome model now calibrated and validated the next goal is examining methods for enhancing vaccine delivery. It has been postulated that endosome lysis (or burst) may be induced shortly after endocytosis to allow the release of the enclosed vaccine before significant acidification occurs.

In particular, the “Proton Sponge Effect”[51, 53, 54, 63, 67, 68] states that the presence of a weakly basic molecule may cause an endosome to burst, and is illustrated in figure 2.4. In particular, the proton sponge would be introduced alongside a nucleic acid to affect release of the nucleic acid prior to the onset fusion with lysosomes. As seen in step 1, it is argued that sponges, which typically are polyamines, work as a buffer by absorbing free protons in endosomes. Absorbed protons are not allowed to escape the endosome through diffusion, thus no longer contribute to the internal pH or the Nernst equilibrium potential of the protons. As the absorbed protons accumulate, they gradually increase the membrane potential past the equilibrium. Since this equilibrium potential is primarily established by chloride diffusion[18], chloride will then begin to diffuse through channels into the endosome in an attempt to restore the equilibrium potential (step 2). This raises the osmotic pressure further. These two events will continue to raise the osmotic pressure and expand the vesicle until it passes the critical area strain, rupturing the membrane and releasing the contents (step 3).

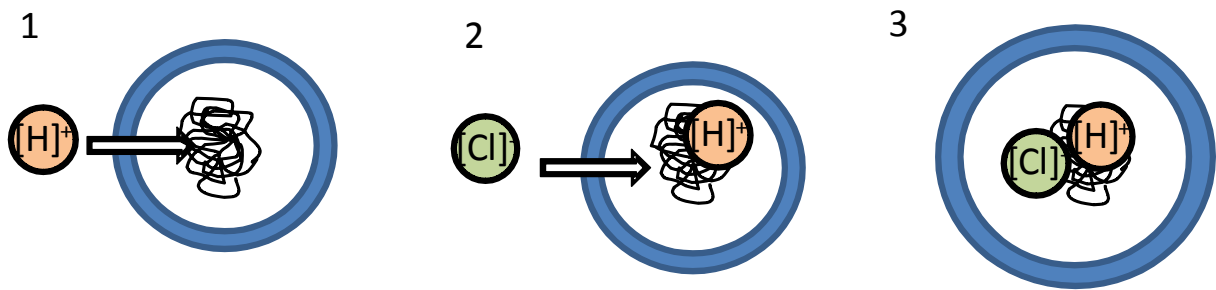


Figure 2.4. Illustration of the proton sponge hypothesis in 3 steps.

2.6.1 Proton Sponge Background

Experimental observations supportive of the proton sponge effect were reported by Sonawane et al.[63]. They used hamster ovary cells to track and observe conditions such as concentrations,

pH and endosome volume over time and compare the impacts of using several different polyamines (second generation PAMAM, PEI, and POL). They observed that PAMAM and PEI decreased acidification while simultaneously increasing $[Cl^-]$ accumulation, causing endosomal swelling. Similar observations have been made of polyethylenimine (PEI) complexed with DNA by Godbey et al.[69], and Forrest and Pack[70].

On the other hand, Funhoff et al. found no evidence of endosome burst for certain polyamines, suggesting involvement of other undetermined factors[71]. The hypothesis is aptly named, as the contributing factors and behaviors are still disputed. Therefore, mechanistic models describing the effect with predictive power are needed. The model will therefore be modified to accommodate proton sponge predictions as a step toward exploring the validity/usefulness of the proton sponge hypothesis toward enhancing DNA vaccine delivery.

2.6.2 Additional Equations for Proton Sponge + Endosome Simulation

In order to explore the implications of introducing a proton sponge to an endosome, governing equations for the sponge are required. This section therefore defines the necessary equations for dendrimers (sponges).

Dendrimers, illustrated in Figure 2.5, were introduced to the model through a combination of protonation site interactions and the Henderson Hasselbalch equations. These polyamines contain primary and tertiary amines, both of which are sites where protons may be taken up by the sponge. In the extracellular environment (pH \sim 7.4), the primary amines (pKa \sim 9) located on the surface of the polymer are protonated while the tertiary amines remain largely as free base. The superior transfection efficiency of dendrimers compared to polymers containing solely primary amines, has been attributed to the abundance of tertiary amines.

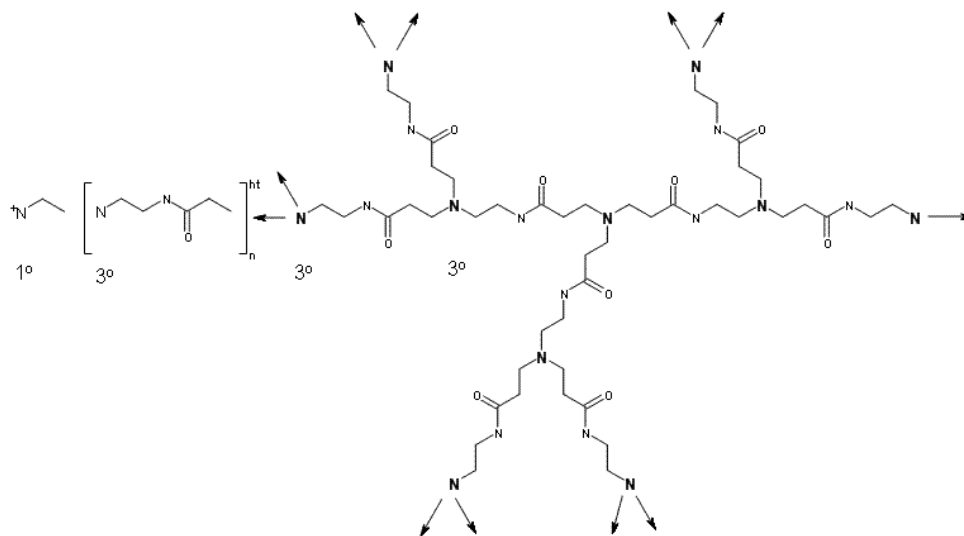


Figure 2.5. Proton sponge sketch.

Because dendrimers occupy definable volumes, the tertiary amines can be differentiated as “interior” and “exterior” protonation sites with approximated pKa of 4-6 and 6-7, respectively. It has been proposed that protonation of the exterior tertiary amines is crucial for endosome buffering and subsequent bursting[72], due to overlap of its pKa with pH in early endosomes. The interior tertiary amines remain un-protonated in the life span of an early endosome.

Once a proton sponge is engulfed in an endosome, protons entering the endosome are taken up by the enclosed polyamine. This reaction was modeled through the Henderson-Hasselbalch approach[73], where the rate of uptake was a function of the polymer pKa and the internal pH of the endosome. Free protons were tracked and attached through equation 2.12.

$$\frac{d[H^+]_{sponge}}{dt} = k_{prot}[X]_{free} - k_{loss}[X]_{prot} \quad (2.12)$$

where $[X]_{free}$ is the number of available protonation sites and the k values were the reaction rates for protonation and dissociation. The constants k_{prot} and k_{loss} were taken directly from Henderson-Hasselbalch, where k is the rate of the reaction.

$$k_{prot} = k * \frac{10^{pKa-pH}}{1 + 10^{pKa-pH}} \quad (2.13a)$$

$$k_{loss} = k * \frac{10^{pH-pKa}}{1 + 10^{pH-pKa}} \quad (2.13b)$$

While this is suitable for a sponge with a single protonation site, these equations do not account for site-interactions. Dendrimers contain many protonation sites with varying pKas, and as these sites protonate the positively charged sites will directly affect surrounding pKas. This behavior has been accounted for through a site-interaction model from Borkovec and Koper[74].

The change in pKa for a specified site was related to the initial pKa and the interaction coefficients with neighboring sites. This was modeled through equation 2.14[74].

$$pK_i = pK_{i0} - \sum_{i \neq j} \varepsilon_{ij} \langle x \rangle_j \quad (2.14)$$

pK_i is the current pKa of the protonation site, pK_{i0} is the original pKa value prior to protonation, and the summation term loops over all nearby neighbors and their chance of protonation.

Because the Borkovec and Koper model is able to track the proton concentration changes this method is ideal for determining changes in the sponge pKas as acidification occurs. Their approach is therefore adopted here. The interaction coefficients ε_{ij} of equation 2.14 were calculated as functions of the interatomic energy function W divided by the Boltzmann constant k_B and the temperature T .

$$\varepsilon_{ij} = \frac{W(r_{ij})}{k_B T \ln 10} \quad (2.15)$$

The interatomic energy function was calculated as a function of the distance between neighboring protonation sites r , the permittivity of the medium $\varepsilon_0 D_w$, and the Debye length κ :

$$W(r) = \frac{e^2}{4\pi\varepsilon_0 D_w} \cdot \frac{e^{-\kappa r}}{r} \quad (2.16)$$

The Debye length in an electrolyte was calculated as a function of the permittivity and the ionic strength I .

$$\kappa^{-1} = \sqrt{\frac{D_w \varepsilon_0 k_B T}{2N_A e^2 I}} \quad (2.17)$$

The ionic strength was calculated through the current internal concentrations of charged species through equation 2.18.

$$I = \frac{1}{2} \sum [X]_i z_i^2 \quad (2.18)$$

Through this method, dendrimer pKas considered here could be constantly updated as a function of their level of protonation.

The dendrimer governing equations, 2.12-2.18, were implemented with three main assumptions. First, the overall structure was assumed to be spherical in shape. This allowed the polymer to be divided into multiple shells as depicted in figure 2.6. The outer shell contains the exterior amines, which are typically fully protonated at extracellular pH levels. The internal shells contain the titrable amines, which aid in buffering the endosome. Second, each of these shells was then simplified to represent a single pKa value to model all titrable amines in the region. The volumes of each shell were calculated along with the average distances between sites inside the shell and distances between the center of neighboring shells. This simplified the number of protonation sites to one or two sites per shell dependent on the specific uptake

characteristics of the dendrimer considered. Since the potentials are distance dependent and decrease rapidly as the sites move further away from each other, only nearest neighbors were considered for calculating site interactions.

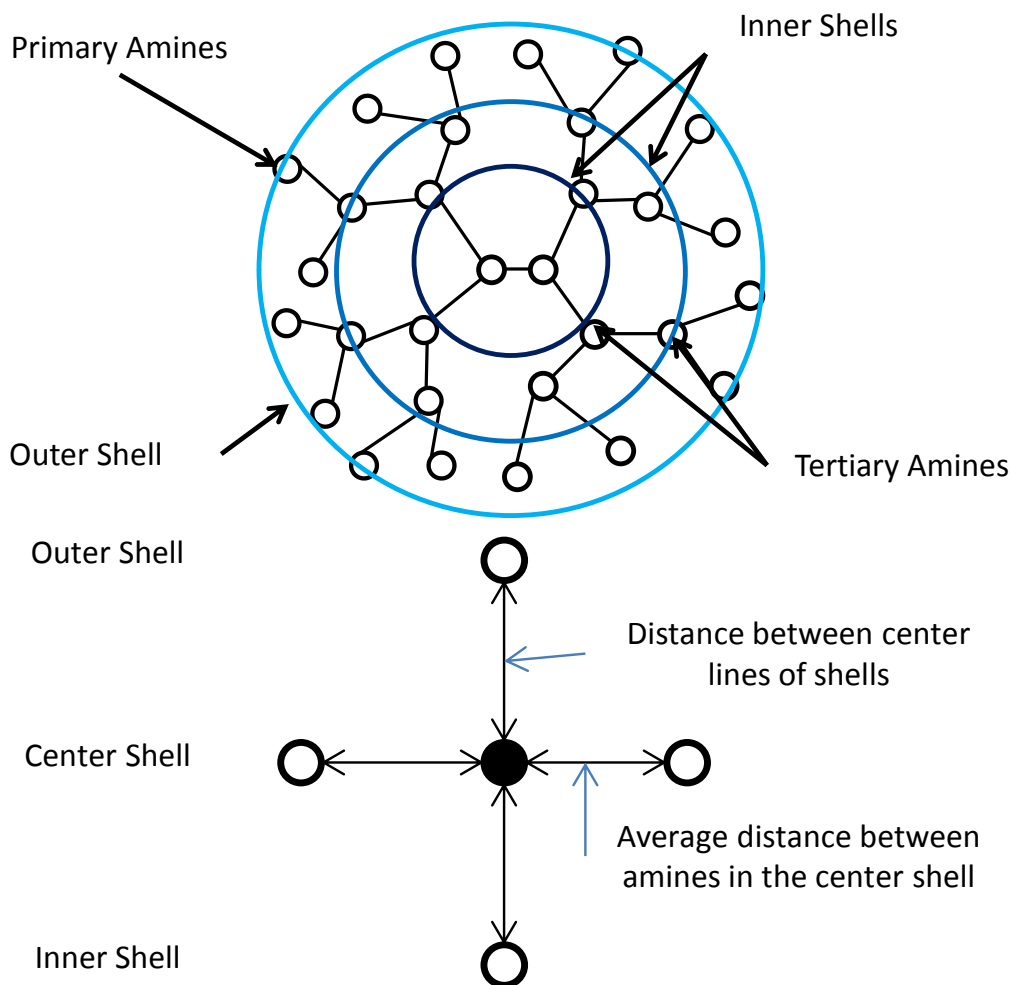


Figure 2.6. Sketch of the simplifications used to represent the dendrimers as a series of shells with nearest neighbor calculations.

Finally, it has been shown that dendrimers expand in volume when protonated. For instance, molecular dynamics simulations of protonating PAMAM molecules show that the expected change in radius from low protonation to full protonation is roughly 50% [75]. Accordingly, the radius was scaled as a function of protonation level and the original sponge radius throughout the simulation. This permitted for an estimation of the dendrimer's changes in

geometry as it protonates. The combination of these equations allowed for the simulation of a combination of titratable amines. This provided the framework for testing the buffering effect in endosomes.

2.6.3 Validation Step 1: Sponge Validation

Before the model may be employed to determine the viability of the various sponges discussed previously, the equations must be validated through comparison to experimental data. The endosome behavior itself has been previously validated, leaving the sponge buffering behavior and sponge-endosome interaction as points of interest. Sponge buffering behavior was validated through comparison with Jin et al.'s experimental studies on sponge buffering[72]. Sponge-Endosome interactions were validated through comparison to Sonawane's' studies on chloride flux and volume expansion[63].

As shown in figure 2.4, the expected outcome relies on three steps: Buffering, Cl⁻ accumulation, and Osmotic Swelling. Each of these steps was examined and validated using data from the literature for comparison. Since the literature typically does not contain all of the required information, data from multiple publications was combined.

Several sponges were considered during this process. A full list may be seen in table 3, including information on the reason for their re-creation in the model. In a few cases complete information on the sponge utilized in the literature was not available, and values were extrapolated from other data sets. As a general overview of the process, the first step for buffering capacity validation was completed through comparison to the experiments of Jin et al[72]. The validated sponge behavior was then carried over to the endosome model where data

from Sonawane was used to explore the incoming chloride flux and the resulting osmotic swelling.

Table 3. Proton Sponge Inputs

Polymer	Modeling Purpose	Calibration Source	pKa's	MW	Primary Amines	Tertiary Amines	Diameter
PAMAM G4	Mass Calibration, Sponge Validation	[72]	9.2, 6.7	14214	52	128	40
PAM-DET	Double-Protonation Validation	[72]	9.2, 6.7, 6.0	16428	52	178	45
PAM-OH	Fluid Buffering Calibration, Sponge Validation	[72]*	*6.7	12000	0	78	35
PolyLysine	Endosome-Sponge Validation	[63, 72]	10.53	N/A	N/A	N/A	N/A
PAMAM	Endosome-Sponge Validation	[63, 72]	9.2, 6.7	7107*	26*	64*	20*
pDAMA5	Comparison against Funhoff Predictions	[71]	9.5, 5.5	5000	17	42	105

*Extrapolated from text, exact values not listed

The first validation case considered was based on dendrimers tested by Jin et al. [72]. Jin et al. constructed a dendrimer, PAM-DET, in which the exterior amines doubly protonate at around endosomal pH, with a pKa of 6.0[72]. The titration results of this novel dendrimer were compared to results for two other sponges, PAM-OH and PAMAM G4. Jin determined that the double-protonation around the endosomal pH enhanced the buffering capabilities of PAM-DET, which increases the sponges' viability for enhancing DNA vaccine delivery.

The model conditions were set to account only for incoming protons to simulate a simple buffering phenomenon – protons were introduced to the system at a gradual and constant rate and the relation between the internal pH and the total incoming protons are tracked. The rate of introduction was slow enough to ensure quasi-equilibrium, resulting in a time-independent pH-proton relationship. During model calibration through comparison to Jin's experimental results

it was recognized that both the dendrimer and the surrounding fluid can behave as buffers, so the effects were isolated. The buffering capacity of the fluid was estimated from the initial slope of the PAM-OH case (indicated on figure 2.7), as PAM-OH itself displays no inherent buffering at high pH values due to the lack of primary amines. The total mass of the dendrimers was then calibrated through varying the mass of PAM-DET until the intercept at an internal pH value of four was roughly equivalent. All cases utilized the same mass of dendrimer (grams/mm³).

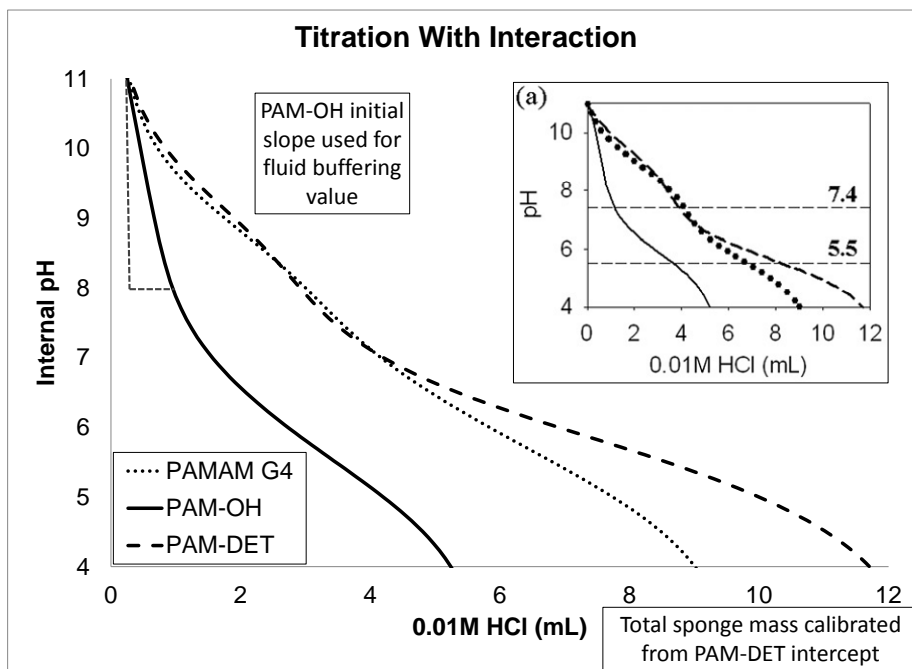


Figure 2.7. Predicted sponge titration vs. experimental data. The data in the upper right corner is experimental data from Jin[72], and the larger figure contains the sponge model predictions.

As illustrated in Figure 2.7 the predicted buffering behavior of the dendrimers captures all of the information obtained from the experiment. In particular, without the modifications to account for the double-protonation of the primary amines, the predicted buffering increase from PAMAM G4 to PAM-DET is diminished. Inclusion of double protonation in the model (equations) establishes model validation for this effect while its exclusion suggests that the

postulated double-protonation effect discussed by Jin et al. [72] is responsible for the increase in buffering capacity, and the resulting increase in transfection efficiency.

2.6.4 Validation Step 2 – Endosome + Sponge Interaction

With the sponge system working correctly, the next step was to assess how the sponges work with the existing endosome model. This was accomplished through comparison to information taken from Sonawane et al. [63]. A few notes must be made on these comparisons. First, the timescale employed by Sonawane is 75 minutes, which is considerably longer than the lifespan of a naturally occurring early endosome. Secondly, the conditions present in these experiments do not exactly mirror conditions found in the body, and alterations to the inputs were made.

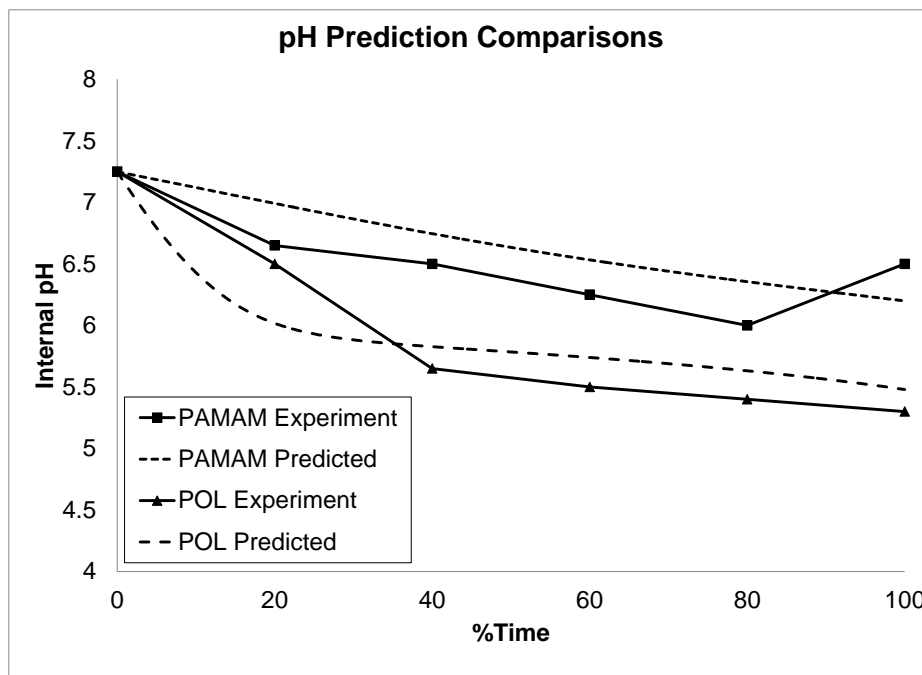


Figure 2.8. Predicted pH vs. experimental pH data for PAMAM and POL.

Using the modified chloride concentration value reported by Sonawane et al. [63] as seen in table 2, calculations were performed to simulate time-dependent changes of protonation of

polyamines, pH, chloride accumulation, and volume expansion in endosomes simultaneously. This simulation considers two polyamines: PAMAM (second generation) and poly-l-lysine (POL). With pKa near 10, POL is not expected to protonate at endosomal pH and only minimal change in volume is expected. The resulting pH changes over time were compared to experimental data (Figure 2.8).

As seen in figure 2.8, the pH levels initially decrease, then move towards a gradual plateau. The plateau in this case is lower than traditional endosome studies, due to the increased length of the simulation and varied external Cl^- concentrations, but the general behavior is similar. The PAMAM case demonstrates lower acidification due to the increased buffering ability of the PAMAM dendrimer in comparison to the POL case.

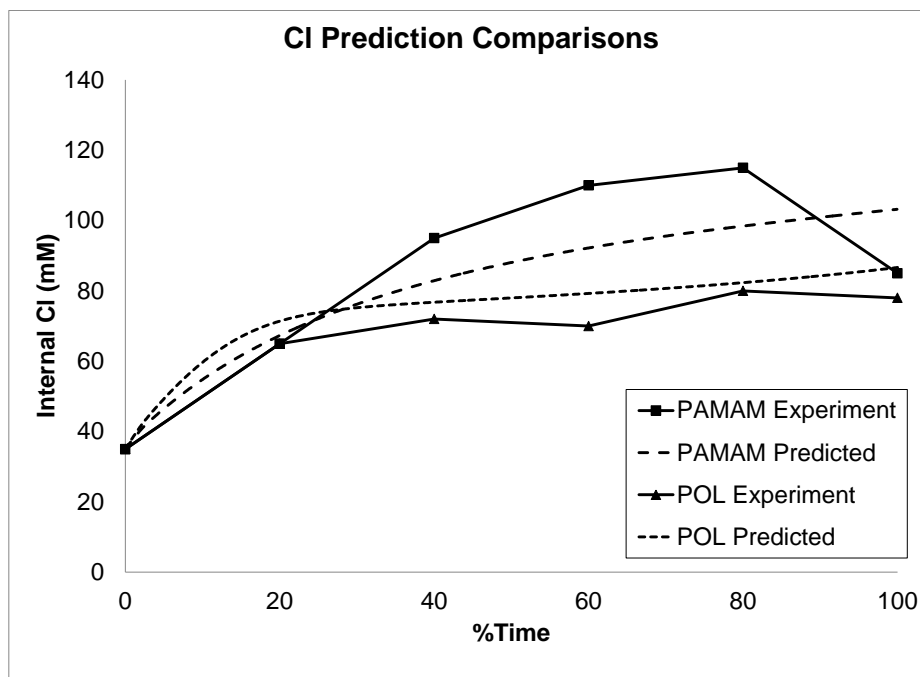


Figure 2.9. Predicted Cl^- accumulation vs. experimental Cl^- accumulation for PAMAM and POL.

This buffering ability leads to an increase in the membrane potential, which in turn causes an inwards diffusion of chloride. The accumulation of trapped protons and chloride then leads to an expansion through osmotic pressure. The increase in internal chloride (figure 2.9) in

both cases is due to the activity of the proton pumps. While the POL case does not include considerable sponge protonation, chloride will continue to diffuse into the endosome as the pumps work to acidify the contents. As mentioned previously, the conditions in this simulation were set to mirror the conditions determined from Sonawane's report[63]. In an actual endosome, the Cl^- accumulation will be much lower as the natural high Cl^- concentration gradient observed in the endosome offsets the membrane potential development due to the proton sponge.

While it appears that the POL case has a faster increase in internal chloride, it must be noted that the measurement is in mM, and is volume dependent. The total number of moles of chloride for the PAMAM case is much higher, but it is also initially offset by the volume expansion. This expansion must also be compared to experiment (equations 2.9-2.11), as seen in figure 2.10.

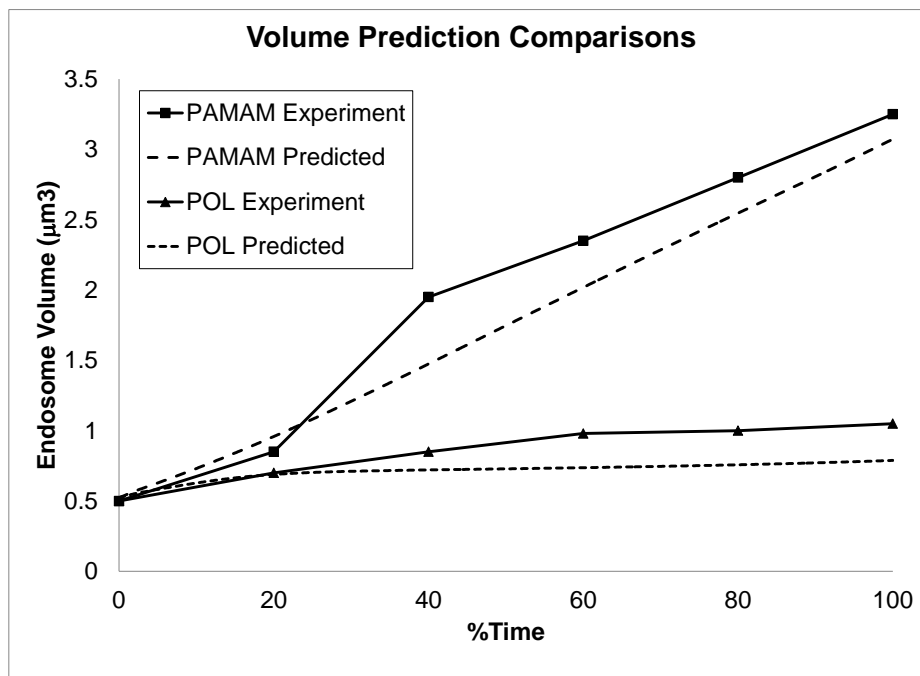


Figure 2.10. Predicted change in volume vs. experimental change in volume for PAMAM and POL.

The total volume change predicted by Sonawane is extraordinarily high, and may be due to the steps required for the isolation of the endosomes themselves. Traditionally a critical area strain of 5% is expected for rupture[76], which will be discussed in the next section. However, the results indicate agreement with the experimental data that the total volume change utilizing the PAMAM sponge is much higher than the volume change expected with POL.

For all three of these plots, the mass of the sponges ($7.85 * 10^{-2}$ pg per endosome) was calibrated from the single PAMAM case for pH change, while the remaining data such as sponge properties was extrapolated from experimental data. The same model conditions were applied for the pH, Cl^- , and volume predictions. This one calibration point then provided validation against both sponge types (PAMAM and POL), predicting the general behavior of steps 1-3 as illustrated in figure 2.4.

2.6.5 Endosome-Sponge Interaction Summarized

The data taken from the previous section may be summarized in table 4, where the information at 50% total time is presented.

Table 4. Sponge-Endosome Comparisons

Values	Experimental		Predicted	
	PAMAM	POL	PAMAM	POL
pH	6.35	5.65	6.63	5.78
Cl (mM)	95	70	88.124	78
Vol (μm^3)	2.1	0.75	1.75	0.729

2.6.6 Endosome Expansion Extension

With these validation steps completed, the model may be used to examine the cases of interest mentioned earlier; specifically Funhoff's sponge and the double protonating PAM-DET from the work of Jin et al. For these studies the values shown in table 2 were employed to closely simulate *in vitro* conditions, and the internal chloride concentration was set to the unmodified value. The goal of these studies was to determine the viability of the selected sponges for ensuring vaccine delivery through endosome burst, and the conditions of the naturally occurring endosome were employed.

For the bursting criteria, standard literature defines the critical area strain for membranes to be 5%[76]. Hopkinson in his study of bilayer membrane pores reported a failure pressure ranging from 66 kPa to 20 kPa, dependent on pore size[11]. If the "hoop stress" is calculated as a function of the internal pressure for the endosome study, it is found that a hoop stress of around 60 kPa occurs at this critical area strain of 5%, which is in the range of Hopkinson's predicted values of failure. Therefore the critical area strain of 5% was used as the threshold for endosome burst. ‘

In this simulation the timescale was shortened to 15 minutes, which is a more realistic time frame in intracellular events compared to the longer period (e.g. 75 minutes) used in the experimental work[63].

Three sponges were selected for the comparisons – PAM-DET, PAMAM, and pDAMA5. PAM-DET was selected as it demonstrated the highest buffering capacity from the sponges selected for the titration validation study between the pH values of endocytosis between 7.4 and 5.5. This sponge was employed as the baseline case, where the total mass selected for each

sponge matched the total mass required for PAM-DET to cross the expected threshold for burst at 5% critical areal strain.

PAMAM was selected for comparison to the PAM-DET case. In Sonawane's experiments, 2nd generation PAMAM demonstrated the best potential for increasing DNA vaccine delivery through endosome burst. Data for the 4th generation from PAMAM was used to simulate this sponge since the information from Jin et al. provides all of the necessary model inputs without any required extrapolation.

Finally, pDAMA5 was selected from the research of Funhoff et al. [71] as a contrarian case. Funhoff et al. reported that a polyamine with pKa values of 9.5 and 5.5 (primary and tertiary amines) did not increase transfection efficiency. Based on this the authors raised questions about the validity of the proton sponge effect [71]. This sponge was recreated in the model, and the volume plots were compared to the other sponges to assess this null result. For the comparison pDAMA5 was selected out of the sponges listed in Funhoff's study, with a particle size of 105 nm and an estimated 59 amines based on the reported MW.

The resulting volume predictions for these three sponges may be seen in figure 2.11. The shaded grey region indicates the expected region of burst, centered on roughly $0.565 \mu\text{m}^3$.

The minimal polyamine concentration required to reach 5% critical area strain within 15 minutes is roughly 1.8 mg/ml for PAM-DET. While this concentration may be initially alarmingly high to the vaccine community, the exposure to the cell is much less, given that the volume of the endosome is much smaller than the volume of the cytoplasm.

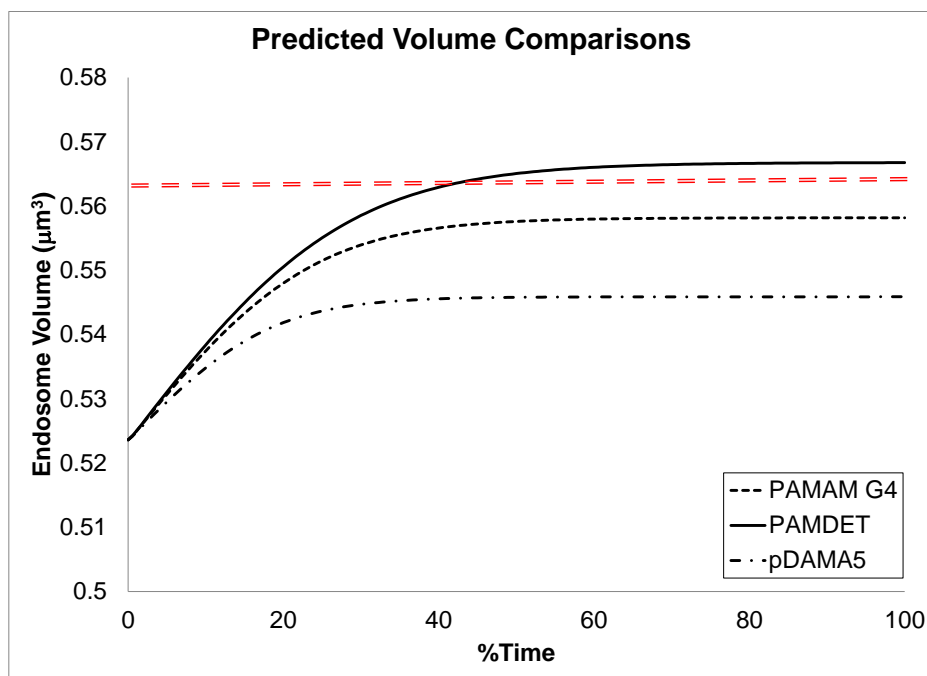


Figure 2.11. Predicted change in volume comparisons for sponges of interest. The dashed red line indicates expected region of burst.

The predicted volume expansions agree with the observations from the literature. pDAMA5 is unable to reach the critical area strain when compared to the other sponges considered, which is in agreement with the observations made by Funhoff. This is due to the reported pDAMA5 pKa values not aligning as well with the naturally occurring pH range expected in the endosome when compared to other sponges such as PAM-DET. Therefore the model accurately captures the seemingly contrarian report, while remaining in agreement with the proton sponge hypothesis[71]. In addition, PAM-DET increases transfection efficiency through a sizeable increase in expansion. The double protonation effect yields an increase in buffering ability at the naturally occurring endosome pH values, and results in a net increase[71, 72].

Another point of interest is the geometry of the sponge itself. The radius of the PAM-DET sponge was increased substantially to imitate a branched system rather than a cluster.

With this modification the model predicts an increase in volume as seen in figure 2.12. However this does not indicate that branched is necessarily better for increasing transfection efficiency. Increasing the radius increases the distance between the protonation sites, which results in lower levels of site interaction. In cases where the initial pKa of the sites are already in the ideal range, site interaction will lower the pKa values and reduce performance. In cases where the initial pKas were above the desired range of 7.0-6.0, site interaction lowers the pKas into the desired range. The internal protonation sites for PAM-DET are already within the desired range with an initial pKa of 6.7, so the increased radius reduces the site interactions and consequently increases the buffering ability. This is in agreement with the observation that the buffering potential of the sponge does not directly correlate with the radius[77].

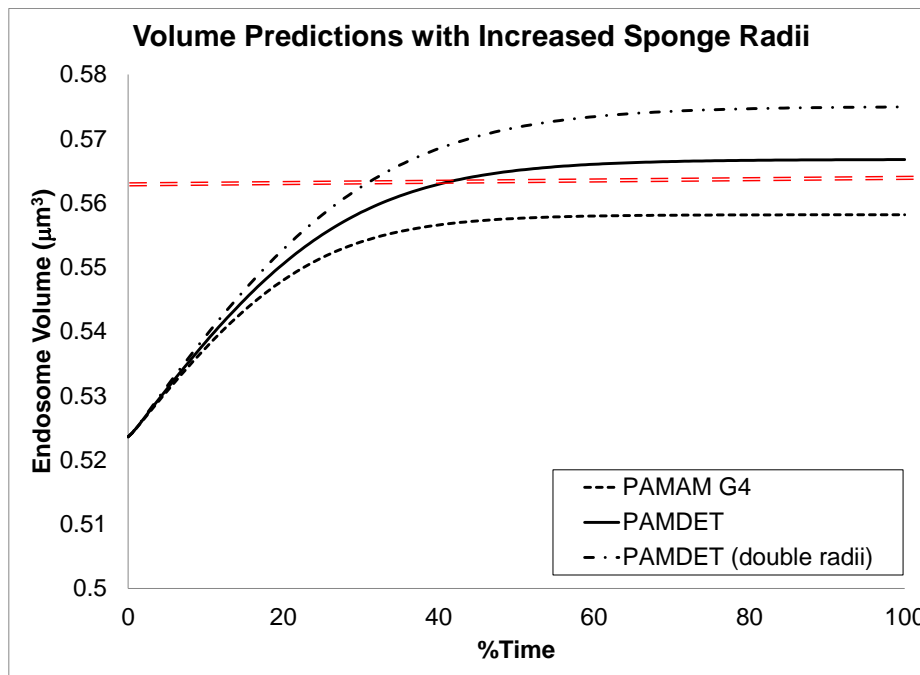


Figure 2.12. Predicted change in volumes for changes in sponge radii.

Finally, a test to ensure vaccine survival was conducted, measuring internal pH as the volume increases (figure 2.13). The regular PAM-DET case was selected for illustration. The

internal pH at the critical volume is reported to be around 6.4. At this point significant degradation will not have occurred, and the released vaccine will remain effective.

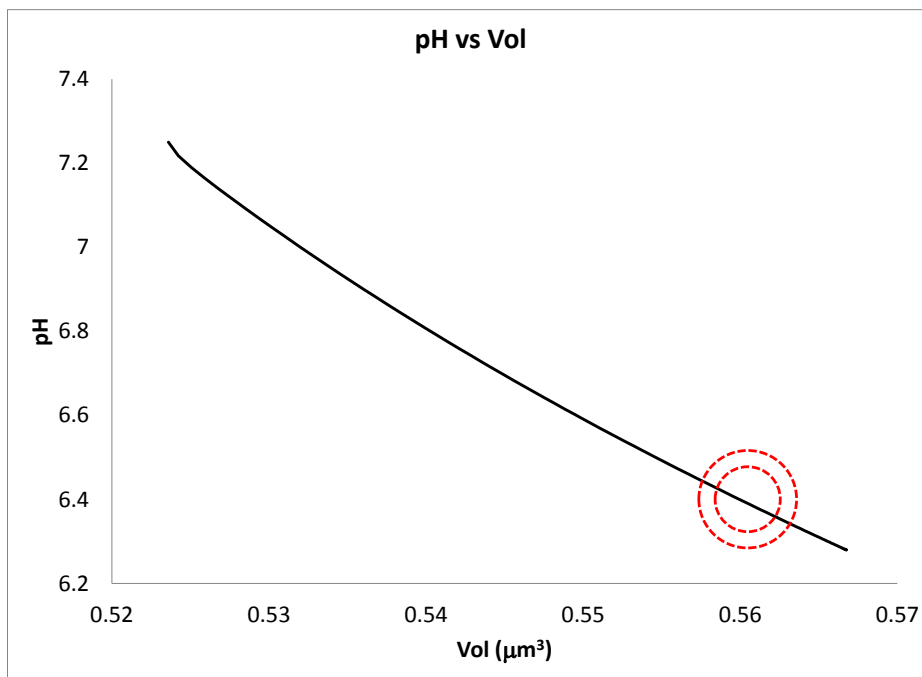


Figure 2.13. Predicted internal pH with respect to change in volume for unmodified PAM-DET.

2.6.7 Dendrimer Study Summary

The proton sponge effect is supported by the predictions of the system of equations selected for this study. The model correctly captured the experimental results of Sonawane [63] through predicting the three steps shown in figure 2.4, and also agreed with the assessments of Jin et al. [72] and the seemingly contrarian results of Funhoff et al [71]. The results show that dendrimers cause the expected expansion of the endosome, resulting in changes in internal ionic concentrations and membrane potential consistent with experimental data. Specifically, the simulation shows that polymer pKa is a critical parameter when attempting to induce endosome burst and therefore illustrate why the Funhoff dendrimers were simply ill-suited for displaying

the desired effect. An amine with a high pKa will be protonated prior to endosome entry and will not have a high change in protonation rate as the endosome acidifies, while a sponge with a somewhat lower pKa will be unable to produce significant expansion before the proton diffusion term is equal to the proton pump flow, causing the pH plateau and limiting further expansion.

The geometry of the polymer itself does not directly correlate with increased performance. While increasing the polymer radius will in certain cases increase the possible volume expansion, there is not a straight forward relationship. The initial polymer pKas play a major role in determining the level of endosome expansion, while the polymer protonation rate k does not play a major role as the lower reaction rates appear sufficient to buffer incoming protons via the ATPase pumps. All of this indicates that a polyamine with pKas within the range of 7.25-6.25 (post site interactions) are favorable for enhancing drug delivery.

This research offers a unique mathematical explanation of the behavior of dendrimers, and offers insights into the boundary conditions in designing polyamines intended for enhancing endosomal drug release.

2.7 ENDOSOME CONCLUSIONS

In this chapter, the core computational model established for analyzing biomimetic membranes was used to study endocytosis. The motivation for this study may be broken in three parts.

- Validate the model for combinations of transport and expansion.
- Determine cause of endosome acidification and the role each transporter plays in the process.
- Explore a viable method for enhancing vaccine delivery through endosome burst.

Each of these goals has been reached. The model has been successfully calibrated and validated for endosome behavior, lending strength to the reliability of the underlying equations. The cause of the endosome acidification was explored and found to be primarily due to the presence of H^+ ATPase, and volume expansion as found to be a function of osmotic pressure. Several methods were explored for enhancing vaccine delivery, and it was determined that the use of proton sponges was the most appropriate method. These sponges were simulated in the model, and ideal sponge qualities were identified for informing future sponge design.

This chapter provides both a general calibration case for predicting the behavior of biomembranes, and illustrates how the selected transporters work in parallel to control acidity, cellular contents, and expansion. The following chapters move towards a more engineering-centric approach, utilizing these biomembranes for applications such as filtration and actuation.

3.0 WATER PURIFICATION STUDIES

Eutrophication due to excess nutrients such as unbound nitrates and phosphates in water is currently contributing to the formation of “dead zones” in regions such as the Gulf of Mexico. These aptly-named aquatic regions are bodies of water that are no longer able to support the natural ecosystem due to a depletion of dissolved oxygen in the water, resulting in a massive loss of life.

Eutrophication occurs when an abundance of nutrients in the water causes explosive growth in the local algae or single-cell organism population. This explosive growth is not sustainable, and results in a subsequent bust phase. During this phase the death of the organisms depletes the surrounding oxygen through cellular respiration, choking out other life forms in the vicinity[78, 79].

The nutrients driving the eutrophication process are present in man-made fertilizing compounds for the promotion of plant growth, and are typically unbound in this form. Because of this they may be routed towards the watershed during rain. This is the catalyst for the explosive growth of algae and other single cell organisms, which lead to the formation of the dead zones. For reference, a dead zone the size of New Jersey has been reported [80] in the Gulf of Mexico, and dead zones are present all along the American coasts.

While these effects are reversible[81], the sources remain unaddressed. Therefore research must be conducted to suggest possible methods for nutrient retrieval before

eutrophication may occur. Currently these nutrients are removed through enhanced biological removal systems[82, 83]. These approaches involve the cultivation of a bacteria or algae to filter out the nutrients before releasing the treated water back into the main flow. While these methods are effective, the cost of upgrading a standard water purification center to additionally remove nitrates and phosphates is prohibitive[84].

Another novel method being explored utilizes a photo bioreactor which employs the excess nutrients to facilitate the growth of algae in a controlled environment, where the algae may be harvested for use in biofuels[85]. This approach, while highly promising for reducing the cost of algae-based biofuels through adding value to the algae cultivation stage through water purification, still requires the presence of a water purification station and is not portable. Algae cultivation in the wild due to high concentrations of nutrients is the driving force behind eutrophication, which this study aims to prevent.

3.1 WATER PURIFICATION CONCEPTS

The research presented here focuses on the proof of concept for the creation of a biomembrane capable of removing both nitrates and phosphates while enabling their retrieval for future, more sustainable, use towards alleviating fertilizer shortage crises[86]. The criteria for the system were specified as follows:

1. Demonstrate high potential for nutrient removal
2. Minimal impact on surrounding region besides nutrient removal
3. Minimal energy required for nutrient removal
4. Provide a mechanism for nutrient retrieval

The inspiration for this research was the ability of plant roots to remove nutrients such as nitrates and phosphates from the surrounding soil against very high concentration gradients[29]. This ability has been attributed to the activity of cellular mechanisms in the roots, mainly through protein-driven selective transport. Thus nature has already created selective transporters appropriate to the target species. The key challenge was identifying an appropriate combination of transporters for addressing this man made (not naturally occurring) transport goal.

The approach was intended to reclaim the nitrates and phosphates as resources rather than as pollutants. This was accomplished through the use of a selective “sponge” that absorbs the incoming nutrients and locks them for retrieval. This not only reclaims nutrients for use, but in a form that will not recreate the deadzone problem. In this study biochar has been considered for use as the nutrient “sponge.”

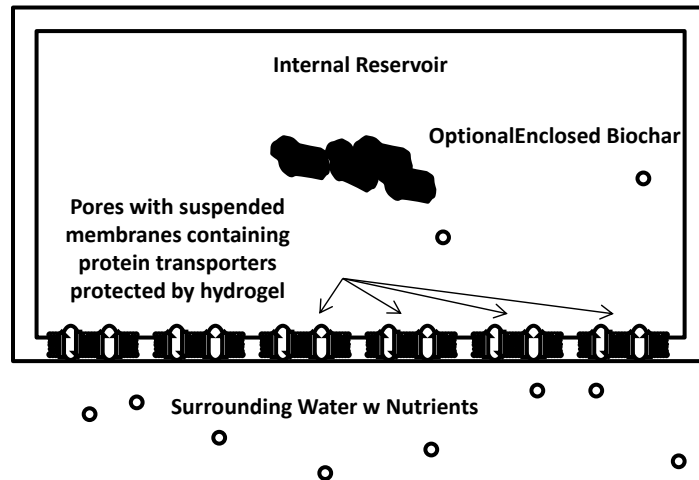


Figure 3.1. Envisioned removal scheme.

An initial sketch for the system may be seen in figure 3.1. In this envisioned configuration tailored biomembranes will be constructed across micro-pores, and protected by a hydrogel scaffold. This pore-based approach to cellular mechanics is similar to the one employed in the early nastic actuation studies[24, 25, 46]. These biomembranes will then

provide the mechanism for removing nutrients from the surrounding water and locking them into the internal reservoir. This internal reservoir may then be combined with the biochar.

3.1.1 Protein Transporter Selection

Several transporter combinations were considered for this study. The earliest incarnations of this study sought applications of transporters that would “self-start” the transport of nitrates and phosphates into a reservoir. The thought process was that the absence of the use of fuel or external power would avert creation of other pollutants. Subsequently, the first inspiration for this work may be seen in figure 3.2. This system combined a phosphate/proton exchanger with a nitrate/proton cotransporter, relying on a linking proton concentration. Since the average Nitrate concentration is typically high compared to phosphate concentration (i.e. 0.16 mM vs. 0.0025 mM in the Mississippi[87]), the goal was to use the higher nitrate concentration gradient to boost the removal of the phosphate gradient. In theory, this system would not require an external power supply, and would use the electrochemical energy present in the water from the nutrient concentration gradient to simultaneously remove both nutrients.

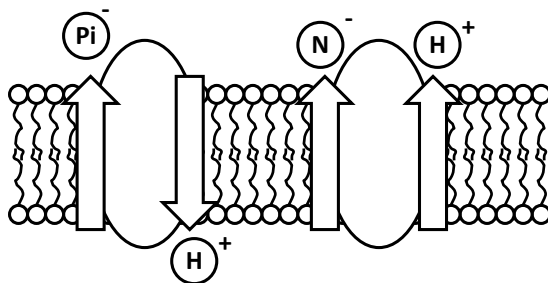


Figure 3.2. Phosphate/proton exchanger coupled with a nitrate/proton cotransporter (system 1).

It was of course anticipated that a self-powered system may be problematic in application, so powered cases were also considered. In addition, the literature suggested that the

proton/phosphate exchanger may not exist due to hyperpolarization effects[88]. Therefore a secondary system was proposed based on the natural configuration seen in figure 3.3. Plants use the hydrolysis of ATP to establish a proton motive force and link this driving potential to dual cotransporters for both nitrates and phosphates as seen in figure 3.3[89]. Because nature has “designed” this system to target the species of interest, the case was of course compelling.

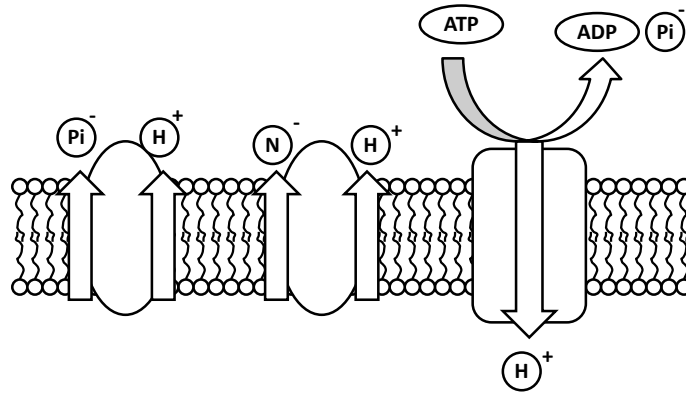


Figure 3.3. Standard nutrient removal protein system seen in plant root cells.

The downside of the system was the requirement of establishing access to ATP for pollutant removal, which would require multiple protein steps, increasing the complexity and the cost of the system. It could however be argued that this system may have access to light, where a photosystem generates the ATP fuel sources directly. Thus a somewhat modified system as illustrated in figure 3.4 was proposed. This was simplified in the system, as the photosystem that generates the ATP fuel sources found in plant cells generates an initial proton motive force for the creation of ATP. For this system the phosphate/proton cotransporter was based on transporters found in algae[83], the nitrate/proton cotransporter was based on transporters located in plant roots[90], and the photosystem was based on photosystem II described by Allen[91]. Since both transporter species are located in plant life, their chance of compatibility is increased.

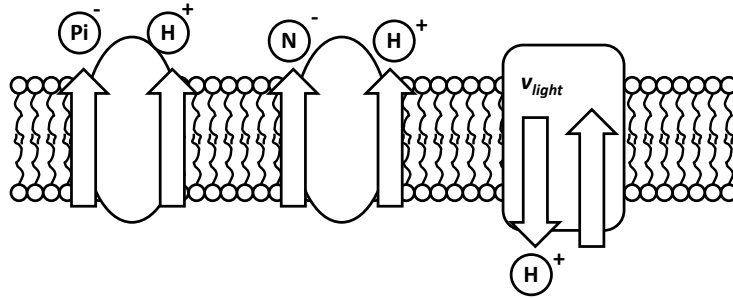


Figure 3.4. Photosystem coupled with phosphate/proton and nitrate/proton cotransporters (system 2).

During the initial assessment, the net hyperpolarization effect of the transporters was found to detrimentally impact the nutrient removal. This will be discussed in detail later in the chapter. To offset the hyperpolarization effect, calcium voltage gated channels were added to the model, as seen in figure 3.5. These were based on calcium voltage gated channels found in rice [92] which should still remain compatible with the previously selected transporters.

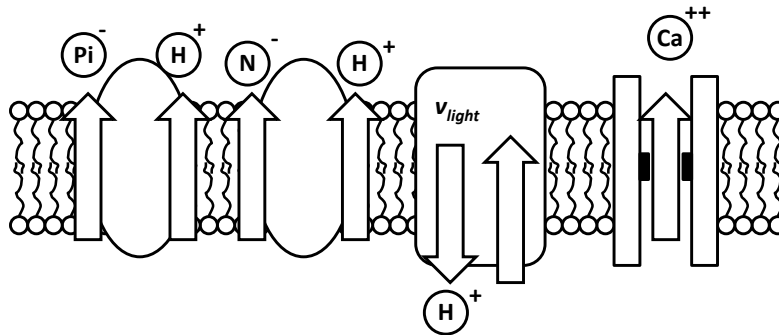


Figure 3.5. System 2 coupled with voltage gated calcium channels (system 3).

With the protein transporter schematic determined, a method for nutrient retrieval was still necessary. The thought-process in seeking a retrieval scheme was two-fold. First, in the absence of a retrieval scheme the membranes will enable collection of the nitrates and phosphates, but in an unbound form they are essentially pollutants. The question of disposal would then need to be addressed. In contrast, natural systems respond to bound nitrates and phosphates as nutrients, when bound they are available when needed, but remain in the bonding system until targeted (i.e., no rain water run off). Creating a retrieval system within the proposed

device will mimic this naturally occurring sake-keeping configuration. Put simply, retrieval will allow for further use of the nutrients, allowing for their recycled use and reducing waste[86]. Second, the addition of a buffering “sponge” for the reclamation of the nutrients may enhance the overall uptake of the system, similar to the observations from the proton sponge studies.

3.2 BIOCHAR INTRODUCTION

With the transporters selected, the next step focused on providing a mechanism for reclaiming and trapping the nutrients for further use. Ideally this method would also allow for increased system effectiveness by removing the nutrients from the transport region, alleviating the concentration gradient and consequently the Nernst equilibrium potentials. The reclaiming process considered here employs biochar. Biochar is a carbonaceous substance resulting from the thermal decomposition of organic matter under restricted ambient oxygen. This organic matter is referred to as biomass. Biochar has a known affinity to organic compounds[93], and has been observed to absorb phosphate groups [94] and particular biochar samples have been demonstrated to reduce nutrient leaking for nitrates[93]. This makes it an appealing candidate for nutrient reclamation. In this study biochar is akin to the proton sponges of the previous chapter, where binding of the charged species to the buffer facilitates further transport through the active biomembrane.

3.2.1 Biochar Creation

Biochar has not been sufficiently studied in relation to nitrate/phosphate uptake to enable a literature review approach to be taken here. Further, biochar is not a readily available off-the-shelf material available for characterization. Therefore it was created and characterized in-house for the purposes of this study. Samples of biochar were created in the laboratory using the apparatus seen in figure 3.6. The method used is Top-Lit Up Draft, or TLUD.

In this process, gasifiers exhibit a thermal decomposition process known as flaming pyrolysis where a pyrolysis front moves downward through the stationary, except for movement due to shrinkage, feedstock which results in the release of volatile gasses from the biomass. This process is depicted in figure 3.7.

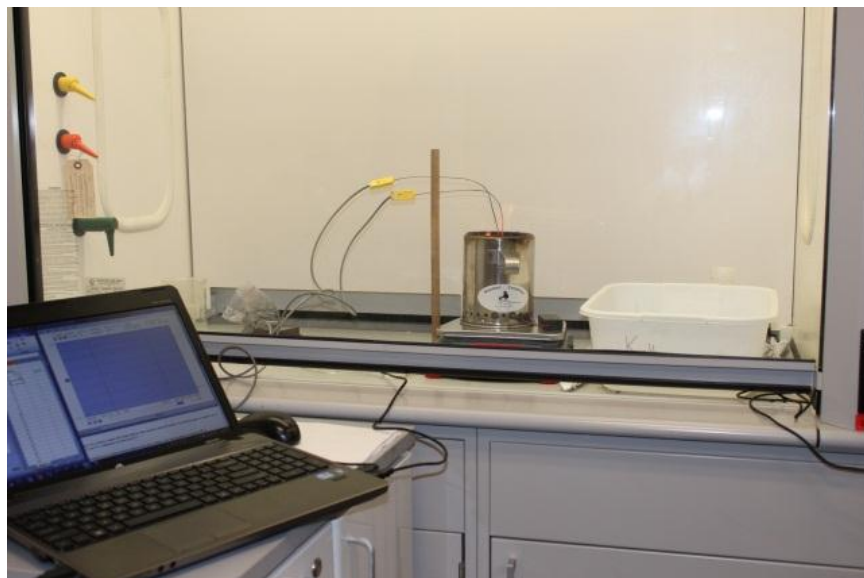


Figure 3.6. System used for creating biochar in the laboratory.

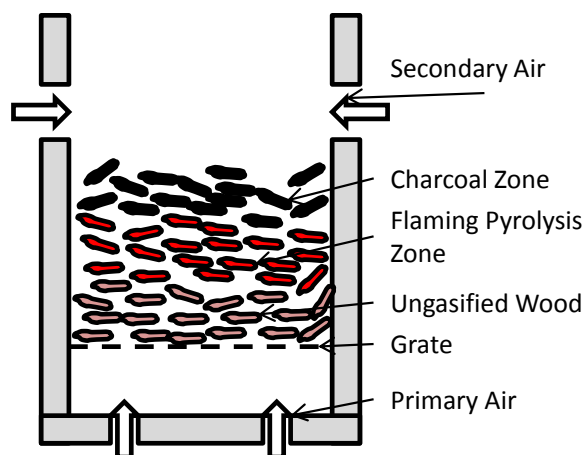


Figure 3.7. Flaming pyrolysis in TLUD sketch [95].

These off-gassed volatiles, consisting of various aliphatic and aromatic hydrocarbons, are then burned at the top of the combustion chamber producing a clean and luminescent flame. Once off-gassing is complete the thermal decomposition reaction changes pathways from pyrolysis to gasification of the produced char resulting in a clean but significantly less luminescent flame than the previous reaction. If the reaction is allowed to proceed by gasification the result would be an ash consisting of various inorganics. The char may be saved by closing all air intakes to shut off the supply of oxygen, or other gasification reactants, or by liquid quenching.

The process for generating the char was performed in several stages which are listed below.

- A camp stove (Woodgas Campstove) was placed on a scale (Ohaus Navigator XT, 0.1 g accuracy), and the weight was recorded and zeroed.
- Hickory chips (Cowboy) were loosely packed in the stove.
- Because it had previously been established that the properties of the resultant char are a strong function of the processing temperature, the internal temperature is a point of interest. Two type K (Omega) thermocouples were placed at different levels in the char as shown in figure 3.6. These thermocouples were hooked to a laptop through a

DAQ (Omega OM-USB-TC-A1), and data was printed to a text file through the software package TracerDAQ. Temperature data recorded from the char itself, and not the flame above. The plot may be seen in figure 3.8.

- The initial weight of the hickory chips was recorded.
- The chips were then ignited, and the stove was turned on to facilitate the flow of air upwards through the chips as illustrated in figure 3.7.
- The weight of the char and chips was recorded every minute as shown in figure 3.9.
- Once the flame changed to a less luminescent flame indicating that the process was completed, the char was quenched in a bath of deionized water and stored for future use.

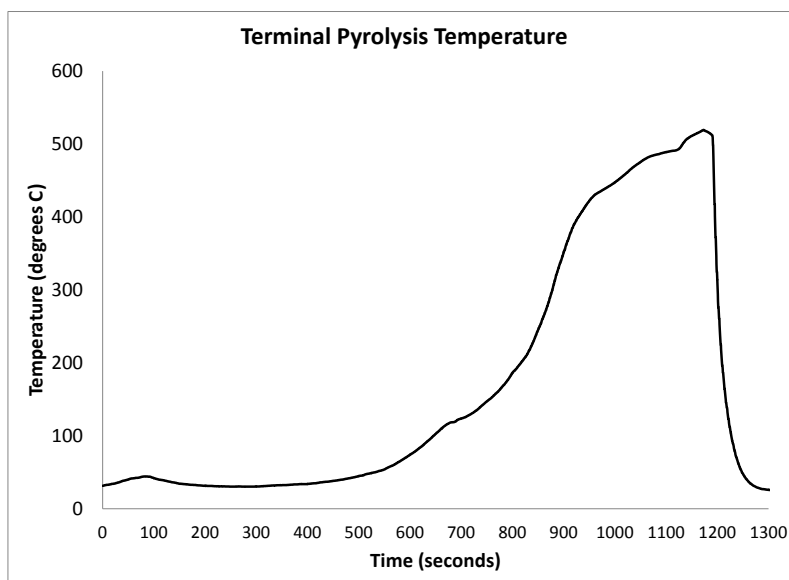


Figure 3.8. Measured terminal temperature of pyrolysis.

If the ultimate uptake of the nitrates by the biochar is primarily a function of adsorption, then the surface area of the char is the determining factor. The terminal pyrolysis temperature observed of 525 °C corresponds to a near-peak surface area when compared to data from McLaughlin et al. as seen in figure 3.10 [95].

It should be noted that research done by Kameyama et al. [96] and Banno et al. [97] indicate that Nitrate uptake of biochar is dependent on the formation of basic functional groups, which continue to increase as temperature increases. The overall uptake reported by Kameyama is negligible until terminal pyrolysis temperatures of 600 °C, and the uptake is reported to continue well past the peak surface area reported by McLaughlin et al.

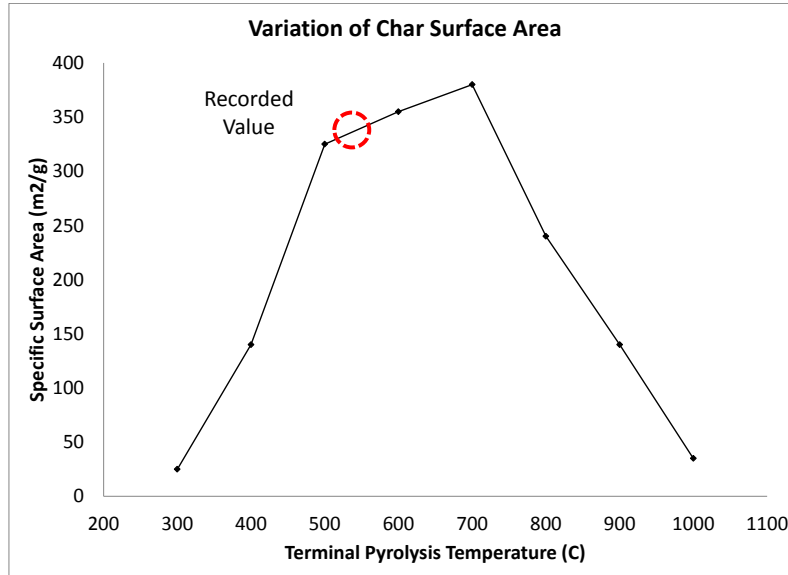


Figure 3.9. Changes in char surface area with respect to the terminal pyrolysis temperature[95].

This illustrates the importance of the char fabrication temperature. While sincere efforts were made to refine the TLUD, future efforts should give sincere consideration to process temperature.

The mass of the char was also measured during this process and may be seen in figure 3.9. During the pyrolysis process, significant mass was lost; approximately 90% of the mass was lost where an ideal process would display considerably less. This process may be refined for future applications to reduce the loss, but it addressed the immediate needs of this proof-of-principle study.

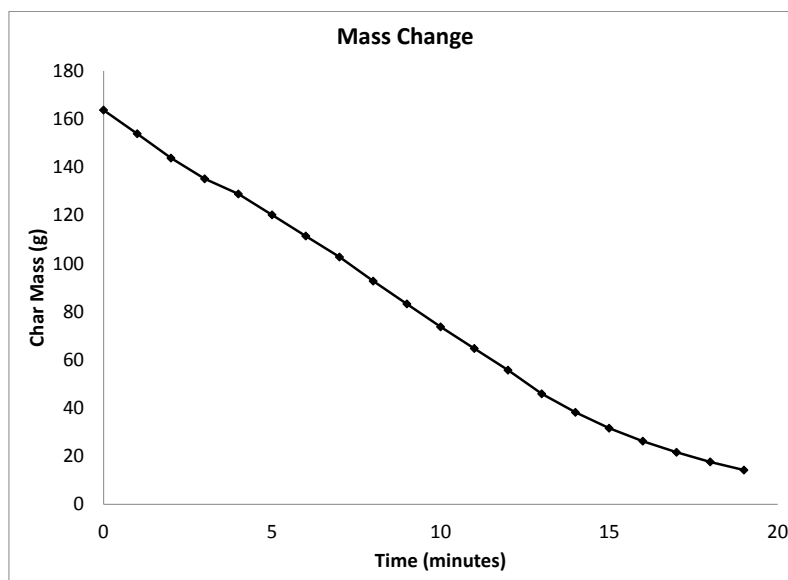


Figure 3.10. Measured change in char mass during pyrolysis.

3.2.2 Biochar Quantification

Once the char was created, it's capability for nitrate uptake and phosphate uptake had to be quantified. These measurements were performed in several stages.

- Generated char was placed in an oven (Carbolite) at 90 °C for 2 hours until char was fully dry. Dry char was then weighed using a scale (Mettler-Toledo AB204-S/FACT, accuracy of 0.01 g), and weights were recorded for future quantification.
- Generated char was placed in deionized water and allowed to soak for over 24 hours until peak water absorption was observed.
- Fixed concentrations of nitrate and deionized water were prepared with a total volume of 50 mL. 1000 ppm Nitrate Standard (Ricca Chemical Company) was pipetted into various mixtures. Samples were stirred at 120 rpm on a magnetic stirring plate

(Corning PC-420D) to ensure thorough mixing. Wet char was added to each sample, and the samples were covered to avoid evaporation

- Char + Nitrate samples were allowed to soak for a 72 hour period to ensure full uptake (literature indicates that 20 hour is time for peak absorption[96]). Samples were then stirred and filter paper (Whatman) was applied to separate fluid from the char.
- 2 mL Liquid Ionic Strength Adjustor (ISA) Buffer (HACH) was added to the samples to eliminate matrix effects from other ions leached from the char during the soaking process. Samples were stirred at 120 rpm for 5 minutes to ensure complete mixing.
- Two known mixtures at the expected upper and lower concentration values were created using the same approach as described earlier for calibration. The samples were stirred at 120 rpm with an insulating sheet of cardboard between the sample and the plate to avoid heat influx during measurements.
- Measurements were taken with a nitrate-sensitive electrode (Mettler Toledo perfection Combination Nitrate Electrode, 7×10^{-6} mM to 1 mM) connected to multimeter (Mettler Toledo Seven-Multi) (figure 3.11). Measurements were recorded, rinsing the electrode and glassware with deionized water and wiping down with KIMwipes between measurements. Records were taken from lowest concentration to highest concentration to avoid electrode drift.
- Nitrate concentrations were obtained using the direct fit method, where the calibration points were plotted on a semi-log plot (mV reading vs. mM concentration). Concentration values for the samples were then extrapolated from fitting the points to the connecting line, and compared to the original concentration values before

exposure to the char. The total mass of absorbed char was then calculated for each sample.

- The levels were then divided by the total mass of dried char added to each sample, and results were plotted comparing the total char uptake to the external nitrate concentration. This may be seen in figure 3.12.



Figure 3.11. System used for measuring nitrate concentrations in the laboratory.

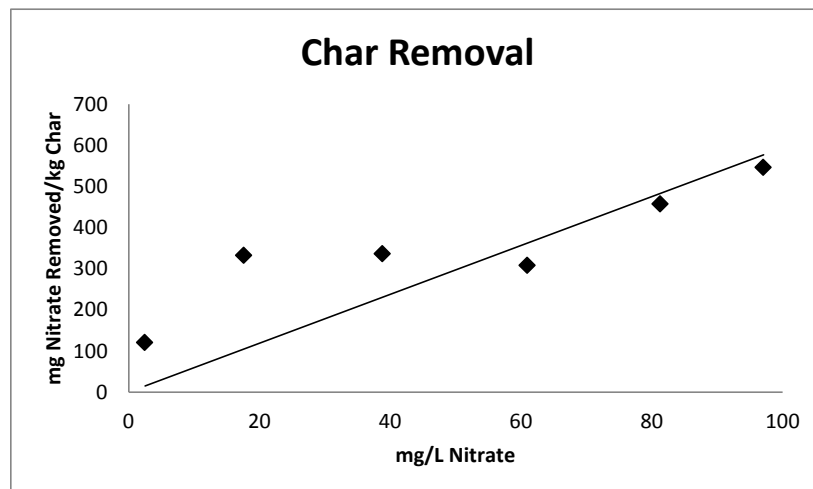


Figure 3.12. Measured nitrate removal by the char with respect to the external concentration of the nitrate.

The slope is comparable to removal capabilities from the literature review [96], with roughly 6 mg of Nitrate removed per kg of biochar present per mg/L of Nitrate in the surrounding area as seen in figure 3.12.

An additional observation on the nature of the uptake was made during the measuring process. When the char was added back to nitrate solutions containing ISA, the formation of a precipitate was observed. This precipitate is thought to be Aluminum Hydroxide, which is a result of the Aluminum Sulfate contained in the ISA. This precipitate is formed in neutral and slightly alkaline solutions, and suggests that the char contains primarily basic functional groups. Since the generated char absorbs surrounding nitrates, this observation is in agreement with those of Banno and Kameyama.

3.3 EQUATIONS FOR WATER PURIFICATION

This section is broken into multiple sections, as several configurations were proposed. Each of the configurations uses a similar core of equations as illustrated in the initial section.

In accordance with the Hodgkin Huxley model, the membrane was treated as a capacitance circuit separating the intracellular and extracellular space, which is consistent with the previously defined core equations. From this the membrane potential may be calculated through the transport $i_{transport}$ across the membrane divided by the membrane capacitance C (based on equation 1.1).

$$\frac{dv}{dt} = -\frac{1}{C} \left(\sum i_{transport} \right) \quad (3.1)$$

The potential was counteracted by the development of Nernst equilibrium potentials for each of the transported species (based on equation 1.2), which were calculated as a function of Boltzmann's constant k_B , the temperature T , the valence z , the basic charge e , and the ratio of the external and internal concentrations $[S]_e$ and $[S]_i$. In this case, the tracked ions are $[H]^+$, $[NO_3]^-$, $[P_{io}]^-$, and $[Ca]^{2+}$.

$$v_s = \frac{k_B T}{e} \ln \left(\frac{[S]_e}{[S]_i} \right) \quad (3.2)$$

The membrane was assumed to be permeable to protons through a standard diffusion equation. This diffusion currents were calculated as a function of the transport surface area A , the permeability P_H , Faraday's constant F , the membrane potential v , the concentrations of $[H]^+$, the Universal Gas Constant R , and the temperature T (based on equation 1.34).

$$i_{Hdiff} = -AP_H F \left(\frac{Fv}{RT} \right) \left[\frac{[H]_i - [H]_e e^{\left(\frac{-Fv}{RT} \right)}}{1 - e^{\left(\frac{-Fv}{RT} \right)}} \right] \quad (3.3)$$

Similar to the previous sections, the change in concentrations was calculated as a function of the transporter flow, repeated for each of the tracked concentrations. The changes in concentrations are universally calculated functions of the currents i_S (which vary dependent on system), the internal volume Vol , and Faraday's constant F . This equation was repeated for each concentration, including $[H]^+$, $[NO_3]^-$, $[P_{io}]^-$, and $[Ca]^{2+}$ (based on equation 1.3).

$$\frac{d[S]}{dt} = \frac{\sum i_S}{Vol * F} \quad (3.4)$$

Since several transporter configurations were proposed as seen in table 5, the equations vary from system to system. These will be discussed in the following sections.

Table 5. Purification Transport Configurations

#	Configuration	Description
1		Nitrate/Proton Cotransporter [90] with Phosphate/Proton Exchanger
2		Phosphate/Proton Cotransporter[83], Nitrate/Proton Cotransporter[90], PMF [91]
3		Phosphate/Proton Cotransporter[83], Nitrate/Proton Cotransporter[90], PMF[91], Calcium Voltage Gated Channels [92]

3.3.1 Transport Equations for System 1

The flow through the cotransporter and exchanger in system 1 were modeled through the following equations. The flow through the Nitrate/Proton Cotransporter was not electrogenic, and was consequently not dependent on a membrane potential term. However, the flow through the Phosphate/Proton Exchanger contributes doubly to the generation of the membrane potential (based on equation 1.16). The flow through these transporters were calculated as functions number of transporters N_{NitH} and N_{PhoH} , the basic charge e , Boltzmann's constant k_B , rate constants λ_{NitH} and λ_{PhoH} , the concentrations $[Nit]^-$, $[H]^+$, and $[Pho]^-$, the membrane potential v , and the Nernst equilibrium potentials $v_{Nitrate}$, $v_{Phosphate}$, and v_H .

$$i_{NitH} = 2N_{NitH}e\lambda_{NitH}\sqrt{[Nit]_e^1[Nit]_i^1[H]_e^1[H]_i^1}\sinh\left(\frac{e(v_{Nitrate} + v_H)}{2k_B T}\right) \quad (3.5)$$

$$i_{PhoH} = 2N_{PhoH}e\lambda_{PhoH}\sqrt{[Pho]_e^1[Pho]_i^1[H]_e^1[H]_i^1}\sinh\left(\frac{e(-2v + v_{Phosphate} - v_H)}{2k_B T}\right) \quad (3.6)$$

The first transporter (Nitrate/Proton) was found in the literature [90]. However, the Phosphate/Proton exchanger was not found in the literature review; in fact its existence was argued against due to its strong hyperpolarization effects [88].

3.3.2 Transport Equations for System 2

The proton motive force generation through the photosystem was modeled as a proton pump, with the current calculated as a function of a driving force v_{pmf} rather than v_{ATP} , the membrane potential v , Boltzmann's constant k_B , temperature T , and an experimental coefficient k_{rate} (based on equation 1.11).

$$i_{H+Influx} = k_{rate}\tanh\left(\frac{e(-v + v_H - v_{pmf})}{2k_B T}\right) \quad (3.7)$$

The transport through the cotransporters was modeled through the following equations. Since the equations are not electrogenic (generating a membrane potential), the membrane potential term was not included in the calculations. The transporters were observed in nature [83, 88, 90], and may be found primarily in plant roots (based on equation 1.16). The flow through these transporters were calculated as functions number of transporters N_{NitH} and N_{PhoH} , the basic charge e , Boltzmann's constant k_B , rate constants λ_{NitH} and λ_{PhoH} , the concentrations $[Nit]^-$, $[H]^+$, and $[Pho]^-$, and the Nernst equilibrium potentials $v_{Nitrate}$, $v_{Phosphate}$, and v_H .

$$i_{NitH} = 2N_{NitH}e\lambda_{NitH}\sqrt{[Nit]_e^1[Nit]_i^1[H]_e^1[H]_i^1}\sinh\left(\frac{e(v_{Nitrate} + v_H)}{2k_B T}\right) \quad (3.5)$$

$$i_{PhoH} = 2N_{PhoH}e\lambda_{PhoH}\sqrt{[Pho]_e^1[Pho]_i^1[H]_e^1[H]_i^1}\sinh\left(\frac{e(v_{Phosphate} - v_H)}{2k_B T}\right) \quad (3.8)$$

3.3.3 Transport Equations for System 3

The final system considered employs similar transporters to the ones found in system 2. The equations for the proton motive force generation and nitrate/phosphate cotransport remained the same (based on equation 1.16).

$$i_{H+Influx} = k_{rate}\tanh\left(\frac{e(-v_{membrane} + v_H - v_{pmf})}{2kT}\right) \quad (3.7)$$

$$i_{NitH} = 2Ne\lambda\sqrt{[Nit]_e^1[Nit]_i^1[H]_e^1[H]_i^1}\sinh\left(\frac{e(v_{Nitrate} + v_H)}{2kT}\right) \quad (3.5)$$

$$i_{PhoH} = 2Ne\lambda\sqrt{[Pho]_e^1[Pho]_i^1[H]_e^1[H]_i^1}\sinh\left(\frac{e(v_{Phosphate} + v_H)}{2kT}\right) \quad (3.8)$$

In this case calcium voltage gated channels were added to the system through equations 3.9 and 3.10. These channels were found in the literature review in plant cells[92, 98]. Because the timescale of the simulation was significantly longer than the gating time, steady state was assumed when calculating the ratio of open channels (based on equations 1.22 and 1.32). The current across the channels was calculated as a function of a transport coefficient k_{Ca} , membrane potential v , Nernst equilibrium potential for calcium v_{Ca} , channel activation voltage v_{Caact} , Boltzmann's constant k_B , and temperature T .

$$i_{Cachannel} = k_{Ca}X_{open}\sinh\left(\frac{e(v - v_{Ca})}{k_B T}\right) \quad (3.9)$$

$$X_{open} = \frac{1}{2}\left[1 + \tanh\left(\frac{2e(v - v_{Caact})}{k_B T}\right)\right] \quad (3.10)$$

Since the timescale for biochar nutrient uptake was expected to be significantly shorter than the timescale for nutrient removal from an open waterway, a steady-state assumption was employed for calculating the amount of nutrient trapped by the char. This was modeled directly as a function of the total nitrate transported:

$$Nitrate_{char} = Nitrate_{total} \left[1 - \frac{1}{(1 + q(mass_{char})/(Vol))} \right] \quad (3.11)$$

where q is the experimentally determined removal potential and $mass_{char}$ is the total mass of the char in the system.

3.4 WATER PURIFICATION CALIBRATION/VALIDATION

Inputs for the water purification study were taken from a combination of literature review and biochar experiments. The total internal volume of the device (figure 3.1) was set at 1 liter for proof-of-concept, assuming a cubical shape with transport membranes embedded on one face with 50% porosity, and folded in a manner to protect the membranes from transverse flows.

Internal concentrations were set to 0.0001 mM. The initial state was assumed to be near-pure water. Concentrations of 0 mM result in a discontinuity in the Nernst equilibrium potential calculation (equation 3.2), so this minimal level was employed.

For nutrient transport coefficients, the peak transporter area (i.e., protein transporters per unit area) was scaled to be similar to values taken from plant vacuoles [99] as well as membrane capacitance (a function of transport surface area). Protein packing was assumed; increasing the

protein density to 80% from a standard 50% value [100]. The photosystem coefficient was taken from total transport observed in Aspen leaves [101].

The literature review indicated that the standard proton motive force generated was found to be 200 mV [62]. This value may vary dependent on system efficiency at converting the incoming light energy into electrochemical energy.

Initially the capacitance was set to 0.4 mF/cm². This value was employed during the initial evaluation stages for quick assessment of system performance. Once the desired system attributes were determined, the capacitance was set to the standard value of 0.6 μF/cm².

Table 6. Water Purification Inputs

Variable	Symbol	Value	Source
Transport Coefficient	$Ne\lambda$	3 pA/pF	[99, 100]
Photo Coefficient	k_{rate}	40 μmol/m ²	[101]
External Nitrate	[Nit] _e	0.16 mM	[87]
External Phosphate	[Pho] _e	0.0025 mM	[87]
External Calcium	[Ca] _e	0.05 mM	[102]
Internal Volume	Vol	1 L	Variable
Transport Area	A	0.1 m ²	Variable
Proton Motive Force	v_{pmf}	200 mV	[29, 103]
Capacitance (system 1 and 2)	C	0.6 mF/cm ²	Variable for initial predictions
Capacitance (system 3)	C	0.6 μF/cm ²	Standard
Internal pH	pH	5.4	Variable
[H ⁺] Permeability	P_H	6.7E-3 cm/sec	[61]
Ca ⁺⁺ Gating Voltage	v_{Caact}	60 mV	Standard
Simulation Time	t_{max}	3 Weeks	[16]
Char Coefficient	q	6*	Experiment
Char Mass		100 g	Variable
Internal Concentrations	$mass_{char}$	0.00001 mM	Pure Water

*Units are (Vol(liters)*mg Trapped Nitrate)/(mg Free Nitrate*kg Char)

The total simulation time was set at 3 weeks, which is taken from a long life membrane system observed by Kaufman et al[16]. Actual membrane lifespan may differ dependent on external conditions.

Currently, no experimental data exists to validate the model predictions. Previous studies (nastic and endosomal) have provided reasonable predictions for cellular systems, and this study utilizes the same core of equations. It is assumed that the predictions presented represent a general proof-of-concept for the water purification system, with reasonable accuracy based on experimentally determined coefficients and a previously-validated approach.

3.5 WATER PURIFICATION RESULTS

As the study evolved, the complexity of the simulation continued to increase and approach natural conditions. The evolution of this study is presented here, presenting data from each of the cases summarized in table 5.

Initial cases focused on the activity of the proteins with the absence of the char material. Once the final transport system is determined, char will be added to the configuration through equation 3.10.

3.5.1 Nutrient Removal for System 1

The first case envisioned utilizes the electrochemical energy of the existing concentration gradients, as seen in row 1 of table 5. The results for uptake may be seen in figure 3.13.

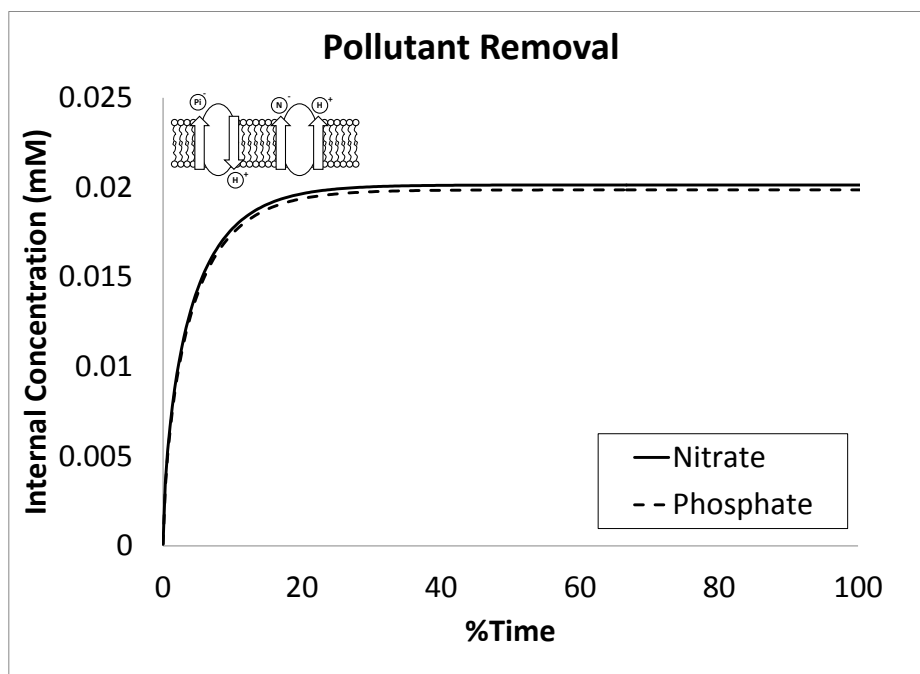


Figure 3.13. Predicted nutrient removal for system 1.

The linking concentration leads to similar removal potential for both nutrients. However, the total amount removed for the Nitrate is considerably lower than the external concentration of 0.16 mM. In addition, no evidence of a phosphate/proton exchanger was found in the literature review, as this transporter would lead to a rapid hyperpolarization of the cellular contents. Thus, while this self-powered configuration was theoretically intriguing, in practice it became clear that even nature invokes power sources.

3.5.2 Nutrient Removal for System 2

This null initial result led to adapting the second system seen in row 2 of table 5, which was based directly on configurations found in nature with the ATP-dependency replaced by a self-sustaining photosystem. This approach decoupled the nitrate and phosphate removal processes, and was dependent on the generation of a proton motive force through a photosystem step (as

modeled in equation 3.7). The initial results for this system may be seen in figures 3.14 and 3.15.

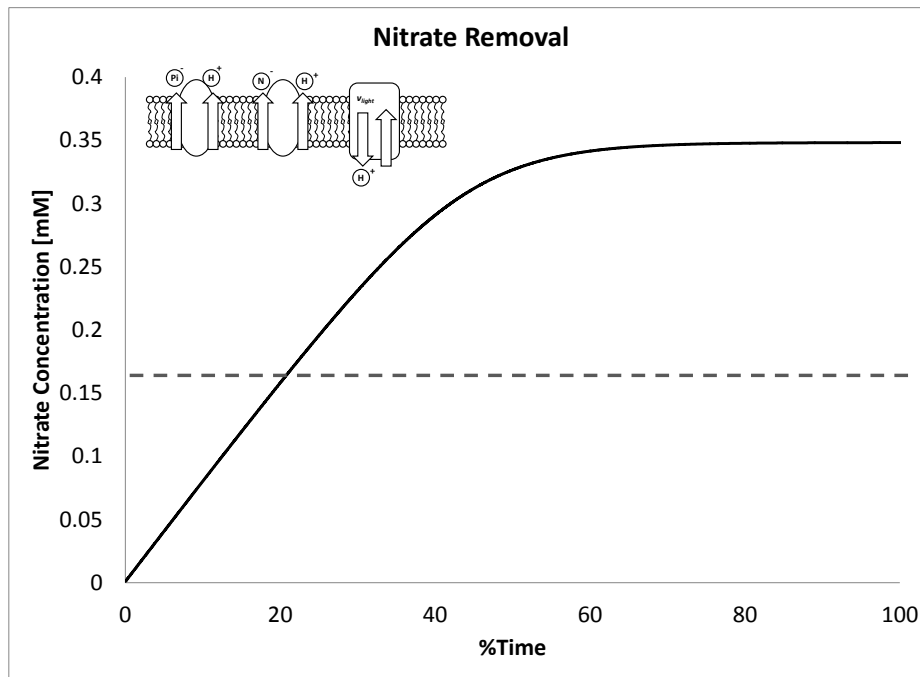


Figure 3.14. Predicted nitrate removal for system 2. The dashed line represents the external concentration.

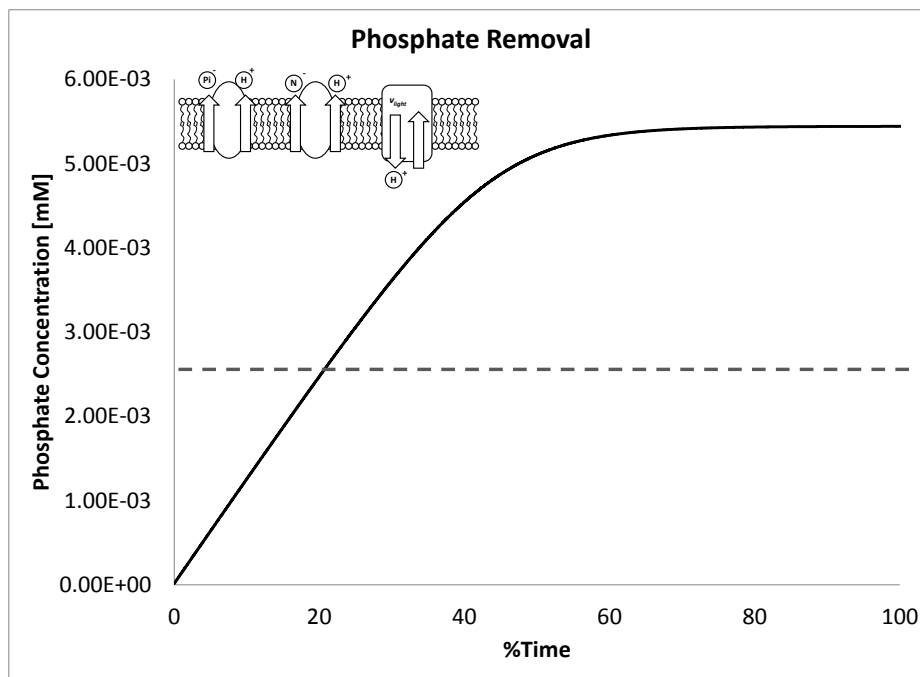


Figure 3.15. Predicted phosphate removal for system 2. The dashed line represents the external concentration.

The uptake for both cases exhibits a similar ratio to the external nutrient concentrations (table 6). The initial success of this system prompted a deeper analysis of the system, where conditions closer to the expected value were applied for further consideration.

One input that had been problematic in initial studies was the capacitance. In this case, with a volume of 1L (table 6), the surface area to internal volume ratio is much lower than cases observed in natural cellular systems. This led to problems with transporter stagnation as a membrane potential rapidly developed due to hyperpolarization effects (equation 3.1), which limited the nutrient uptake of the system which is a function of the volume (equation 3.4). This hyperpolarization step is due to the generation of the proton motive force, which lowers the membrane potential through the removal of protons. Transporter stagnation leads to a breakdown in the Hodgkin-Huxley approximation of the biomembrane as a capacitance circuit, as the approximation assumes ion current is solely responsible for potential behavior. When the transporters stop, the membrane potential will remain constant under this assumption rather than naturally decay. This capacitance-dependent phenomenon may be seen in figure 3.16. The lower line where uptake is negligible employs a capacitance value of $0.4 \mu\text{F}/\text{cm}^2$, which is close to values for bilayer membranes observed in experiment.

From the results it becomes apparent that the development of a hyperpolarization effect is inhibiting the nutrient removal process. The reason for this reduction in capability is due to a combination of factors. First, the Hodgkin Huxley model used in this study assumes constant transporter flow, as the membrane potential will not naturally decay once transport ceases. Because of this a stagnation effect on the transport activity is observed once the generated membrane potential becomes equal to the proton motive force and the Nernst equilibrium potential for the protons. This occurs rapidly, as the volume considered in this study (1 L) is

much larger than standard cellular dimensions (5 μm diameter), and consequently the capacitance to internal volume ratio is much lower than natural cellular systems.

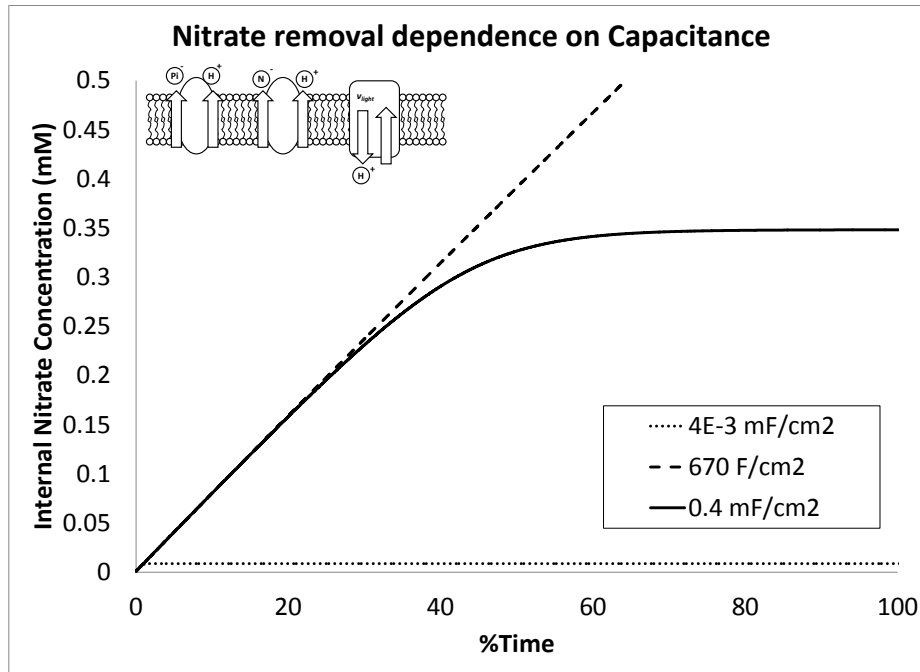


Figure 3.16. Predicted nitrate removal with varying capacitance for system 2.

3.5.3 Nutrient Removal for System 3

The hyperpolarization effect may be alleviated by adding an additional rectifying current to balance the hyperpolarization effect. Here, calcium voltage gated channels are selected, where the external calcium concentration was found to be around 0.05 mM[102]. If calcium voltage gated channels are added to the system (system 3), the overall removal improves dramatically as seen in figures 3.17 and 3.18.

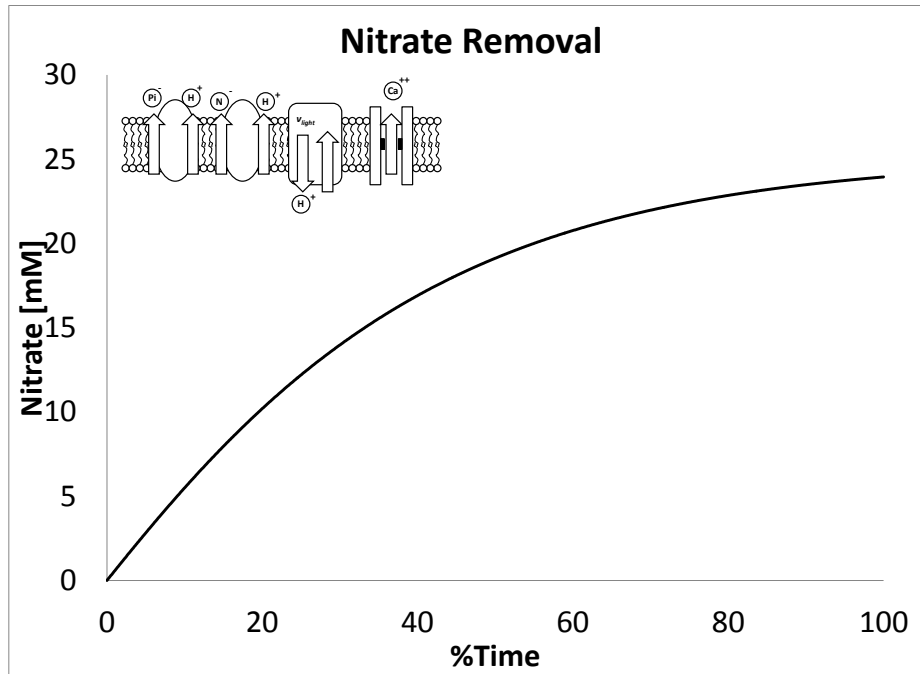


Figure 3.17. Predicted nitrate removal for system 3.

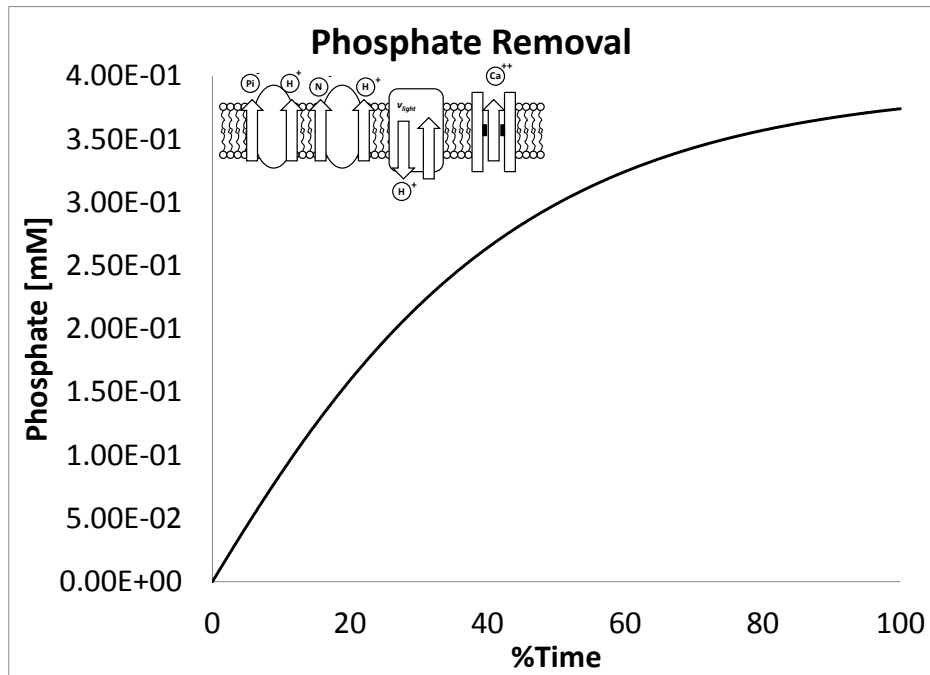


Figure 3.18. Predicted phosphate removal for system 3.

In both cases the total removal is far beyond the external concentration. System 3 offered the highest uptake with all inputs taken directly from experiment, moving the proof-of-concept study closer to reality.

The uptake by the system continues until the generated proton motive force v_{pmf} is equivalent to the Nernst equilibrium potential combined with the generated membrane potential. If the reaction is not balanced as seen in system 2, the membrane potential will increase linearly with the incoming concentrations (equation 2.1). This leads to a rapid development of the membrane potential, and the Nernst equilibrium concentrations are not allowed to increase substantially. If the membrane potential is balanced, then the Nernst equilibrium potentials are the limiting factor, which increase logarithmically (equation 2.2). Because of this, the balanced system (system 3) offers significantly more uptake than the unbalanced system (system 2). This may be summarized in figure 3.19.

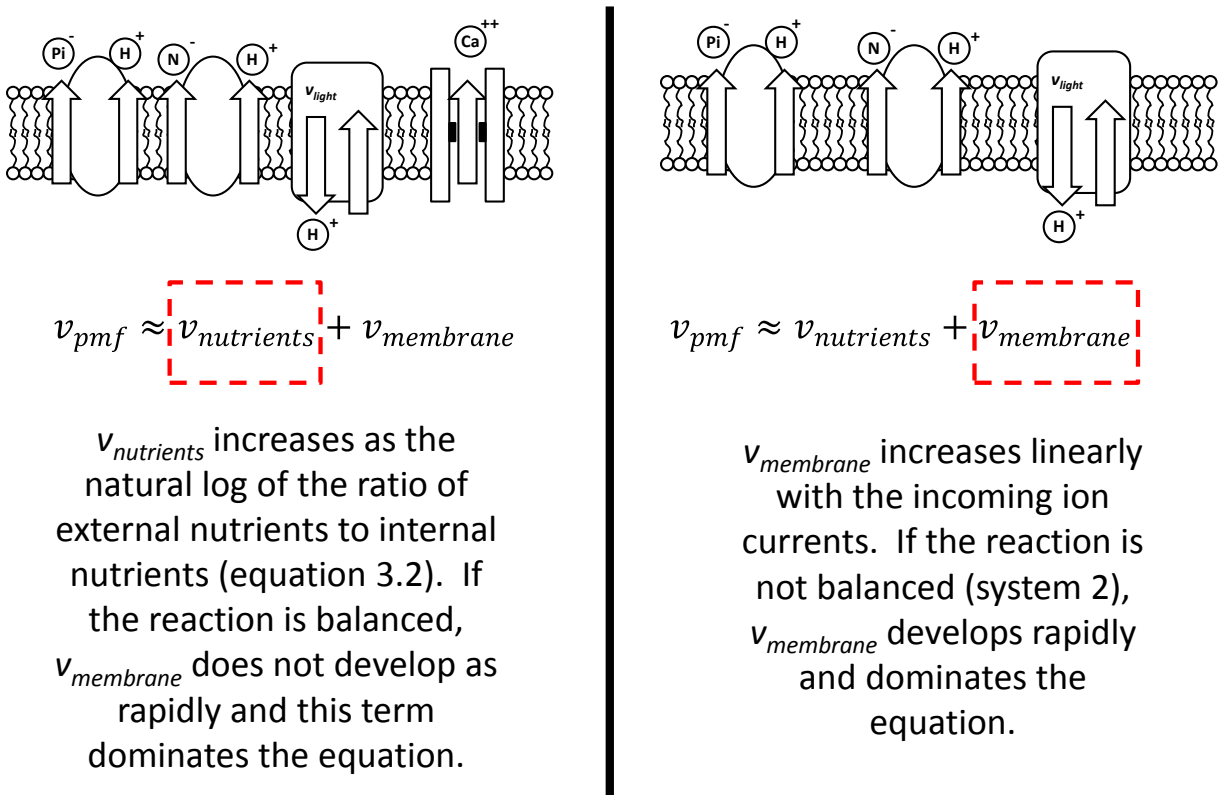


Figure 3.19. Illustration of nutrient vs. membrane potential development with and without calcium voltage gated channels.

Biochar was introduced to the system interior through equation 3.11. It was assumed that trapped nitrates and phosphates are absorbed in a similar fashion, and it was assumed that trapped nutrients no longer contribute to their respective Nernst equilibrium potentials (equation 3.2). 100 g of biochar was added to the systems and plotted for comparison in figures 3.20 and 3.21.

For the inclusion of the char, the total amount removed from the system by the char is roughly 1/3 of the total amount. This alleviates the Nernst equilibrium potentials, and allows for further removal while simultaneously allowing for nutrient retrieval. It was assumed that the char is held in place by a hydrogel, and is not allowed to interact with the transport membranes themselves.

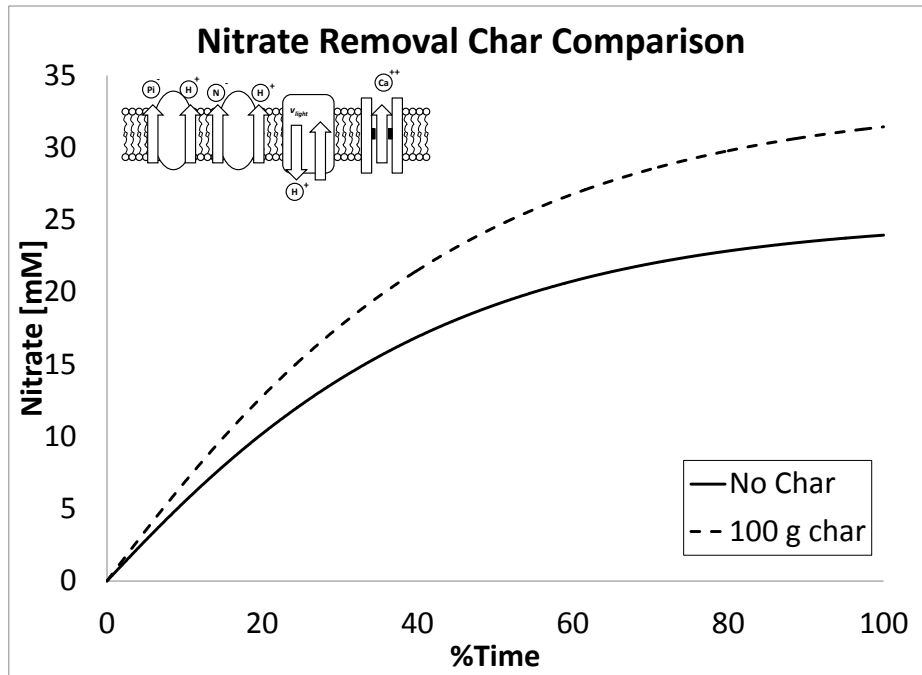


Figure 3.20. Predicted nitrate removal for system 3 with and without 100g of biochar.

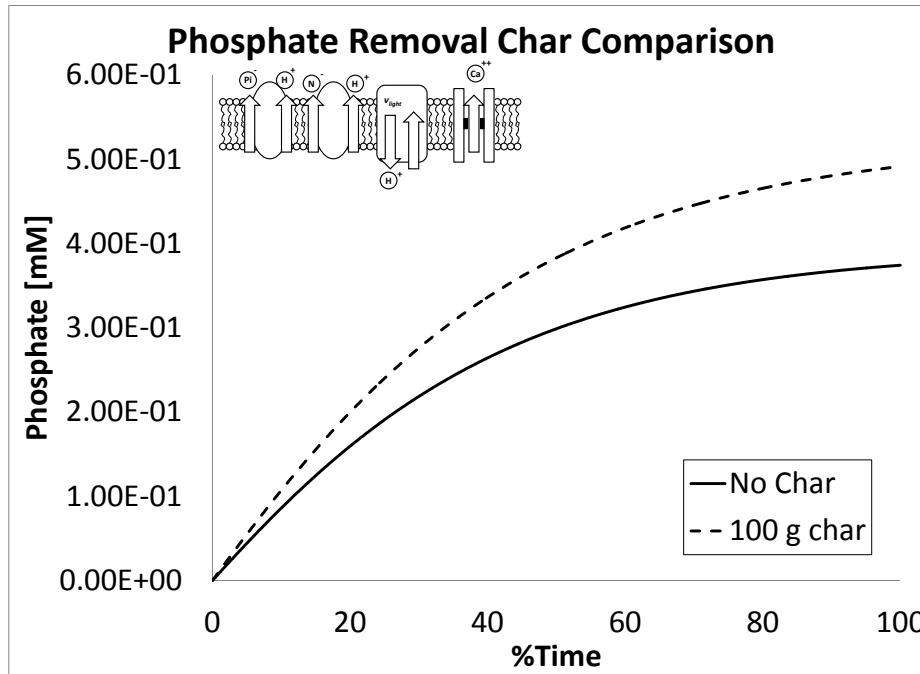


Figure 3.21. Predicted phosphate removal for system 3 with and without 100g of biochar.

A final series of simulations were performed where the proton motive force was varied between 150 mV to 250 mV. The results for this study may be seen in figure 3.22. From the results it becomes clear that variations in the applied proton motive force lead to substantially altered nutrient uptake characteristics.

As the proton motive force increases, the total amount of nutrients removed from the exterior increases exponentially, which may be inferred from equation 3.2. For the 250 mV case, it may be observed that the total amount of nutrient removed is still not at the equilibrium value. If the membrane stability is increased to last beyond three weeks, then the potential for removal will also increase with increasing photosystem efficiency.

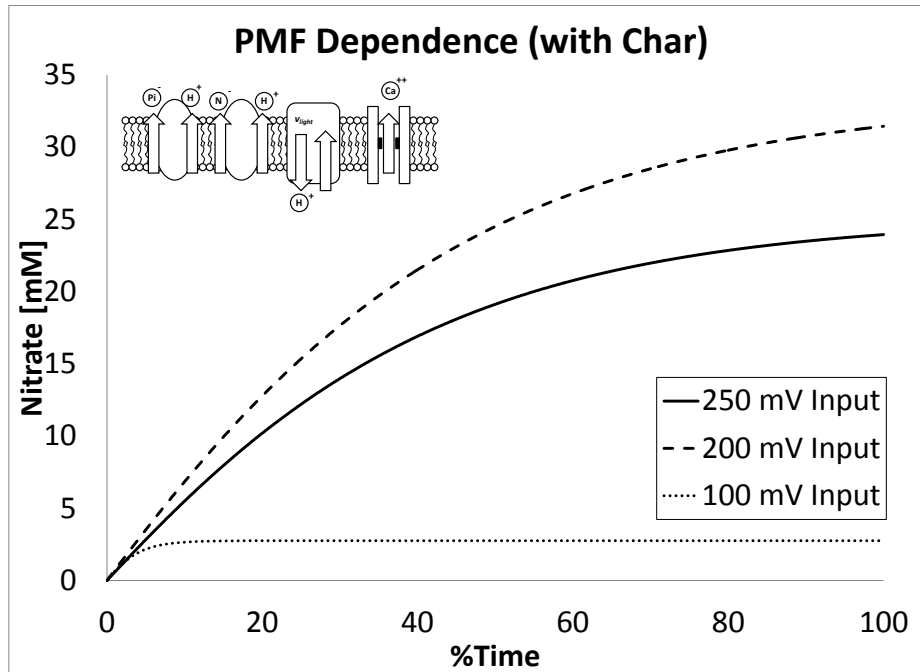


Figure 3.22. Predicted nitrate removal for system 3 with 100g of biochar and varied v_{pmf} .

3.6 WATER PURIFICATION CONCLUSIONS

The foregoing case study offers a preliminary proof-of principle for applying biological transport proteins in the development of a nitrate-phosphate removal system including the identification of several key design challenges. The first point of interest was the reduction in transport effectiveness when applying the biomembrane system to large-scale geometries (significantly larger than a standard cellular system). The increase in volume when compared to the system capacitance due to the reduction of the surface area to volume ratio had a detrimental impact on the system effectiveness. Use of the biomembrane model suggests that the inclusion of voltage gated calcium channels for balancing the hyperpolarization effect may be an effective strategy to mitigating this scaling effect.

Secondly, membrane durability and compatibility must be enhanced. The surrounding currents may result in membrane rupture (device failure). Work is being performed to increase membrane durability through altered membrane composition or the introduction of a scaffold material[7]. In the interim it may be appropriate to consider development of a device maintenance plan.

Finally, the surrounding ion concentrations are not controllable, and blocking ion currents may result in reduction of transporter effectiveness. Certain protein transporters are sensitive to external concentrations beyond the scope of their own transported species, and in some cases a “blocking” ion may be present which inhibits the flow across the transporter. In this preliminary proof-of-principle study, these are beyond the scope of the effort. However, it is appropriate to be aware of the future design challenge.

Overall however, this research has illustrated the preliminary efforts in determining a feasible combination of transporters for a unique dual-pollutant removal system. These studies establish that purely passive approaches without an external impetus are unlikely to be effective. However introduction of a photosynthetic power source coupled with a buffer-like ion sponge in the form of biochar is predicted to yield high pollutant removal rates. The peak uptake indicates a total removal potential of roughly 150 (volume of purified water to system volume). This effort establishes sufficient theoretical proof-of-principle to begin meaningful consideration of experiment and design constraints.

4.0 REVERSIBLE OSMOTIC ACTUATION STUDIES

The final section considered in the dissertation focuses on employing the biomembrane model toward developing an osmotic actuator that demonstrates reversible deformation with minimal driving input. The envisioned actuation system utilizes principles of osmotic transport from the plant kingdom. The system proposed here has some basis in the early nastic model discussed in the Master's thesis [27] but with focus on osmotic transport instead of cotransport of water and sucrose to aid in actuation. The initial nastic actuator utilized the cotransport of sucrose and water to drive the actuation of a flexible diaphragm, and was demonstrated experimentally[24]. This actuation system showed potential for cellularly-driven actuation systems, however several changes may be implemented to improve performance.

The main concern is reversibility. The nastic configuration relies on the development of a proton concentration gradient to enable cotransport of sucrose and protons. Once the concentration gradient is established, no mechanism is in place to alleviating the gradient so that the motion may be reset. This osmotic design aims to produce an actuation method that is fully reversible.

The second concern is controllability. When the nastic process was modeled, emphasis was placed on the active transport portion of the volume change, and was mainly driven by the cotransport rather than osmotic pressure. This results in an initial spike followed by a gradual decay as the resisting pressure gradually forces water back out of the interior. This design aims

to utilize osmotic pressure for actuation rather than cotransport, which reconsiders the modeling elements employed.

4.1 INSPIRATION

The inspiration for the osmotic actuator was taken from the plant kingdom, where the majority of cellular energy transfer and communication is handled through the motion of potassium ions[104]. As a specific example, consider that K^+ accumulation is the main osmotic agent in the expansion of guard cells, which are responsible for the opening and closing of pores that allow for the exchange of gases in leaves. The closing is triggered by the introduction of Ca^{++} to the system, where the calcium inhibits further K^+ accumulation and due to its strong charge allows for the loss of 2 K^+ ions for each Ca^{++} ion introduced to the cytosol. In this fashion the osmotic pressure is reduced and reversed, and the pore is closed[28]. This displacement behavior was mimicked for the controlled deformation of the osmotic actuator.

The transport itself was handled by two currents. There are two modes of diffusion observed in cellular transport – the first is the natural slow decay of concentration gradients or membrane potentials due to bilayer permeability, and the second is rapid ion current due to the opening of the voltage gated channels. It is this second mode of transport that allows for rapid changes in the system state, and this was the main force for the osmotic actuation. These voltage gated channels require a signal to open, (action potential), which is generated by the cell. Once the action potential threshold is achieved in the cell, the voltage gated channels become fully open and allow for movement of the selected ions until equilibrium is restored[18, 105].

The proposed actuator employs voltage gated calcium and potassium channels obtainable from plants [92, 98, 106, 107] combined with generated action potentials for the rapid generation of osmotic pressure. In nature action potentials must occur very rapidly to overcome pump and exchanger activity; here the applied action potential will be sustained until the ion current returns the sum membrane potential to equilibrium values.

4.2 PROPOSED SYSTEM

The proposed system for osmotic actuation combined these two aspects of cellular activity, and may be seen in figure 4.1. Two chambers will be connected through a system of pores with bilayer membranes and voltage activated calcium channels. Voltage gated calcium channels exist in a variety of forms, and may be obtained from many plant cells [92, 98]. A theoretical driving potential was applied to this interior membrane (membrane 2), which activated the calcium channels and created a concentration gradient of Ca^{++} between the two chambers (chambers I and II). This generated another potential at membranes 1 and 3, which in turn activated the K^+ voltage gated channels, driving K^+ into and out of the inclusion to balance the flow of calcium. Through this the transport was sustained and deformation through osmotic pressure between the chambers and the surrounding reservoirs was accomplished.

This osmotic pressure drove an influx of water into the central chambers (I and II). Aquaporins, which contribute to the higher water permeability of plant cells[108], were present in the two potassium membranes (1 and 3) which ensured that the water transport is primarily between the external reservoirs and chambers, and not between the chambers themselves.

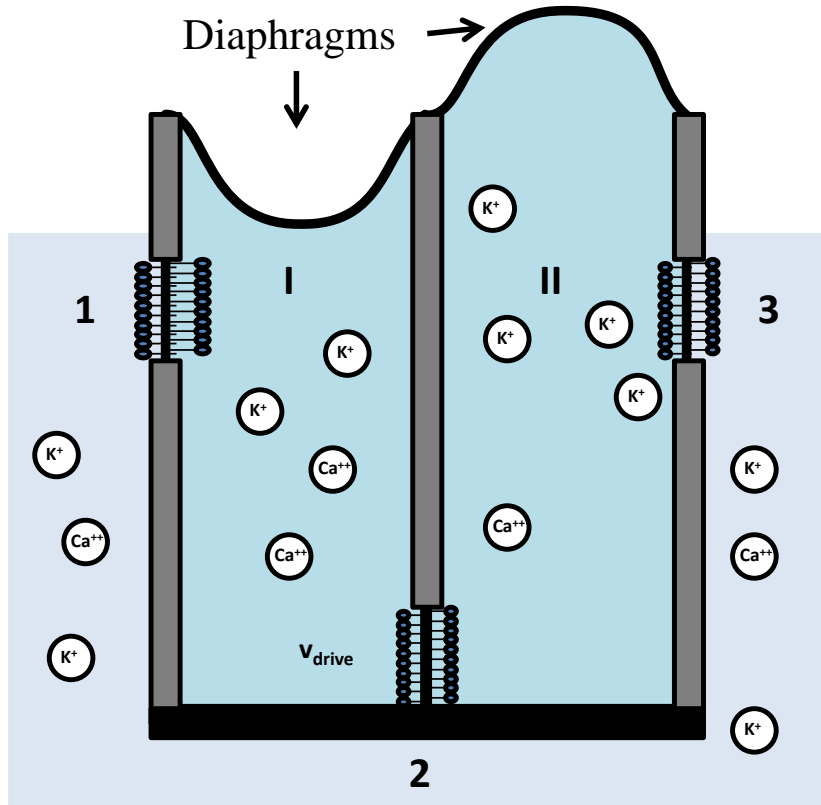


Figure 4.1. The proposed osmotic actuation system. Driving membranes are labeled 1, 2, and 3, while chambers are labeled I and II.

The generation of the membrane potential at membranes 1 and 3 is a point of contention, and requires experimental observation. Traditionally the membrane potential is calculated as a function of the currents across the membrane, but most literature is not concerned with pore structures. Fournier [18] discusses that impermeant negatively charged proteins impact the development of membrane potentials in living cells, and Skotheim [109] observed the elimination of inward K^+ currents when introducing Ca^{++} to the system. Based on these observations it may be inferred that the accumulation or reduction of Ca^{++} on either side of the central divider will result in the expulsion or accumulation of K^+ . For the purpose of this study,

the ion transport across membrane 2 will be applied directly to membranes 1 and 3, treating the two chambers as individual cells with a connecting interface.

For ease of visualization, the system may also be represented in an encapsulated form as illustrated in figure 42; this configuration has previously been experimentally demonstrated for alternate cellularly inspired system[5].

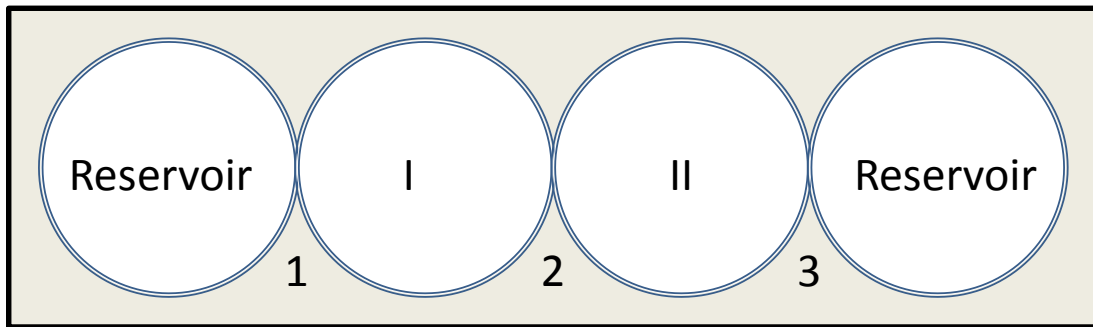


Figure 4.2. Encapsulated cells with connecting transport membranes. Membranes 1 and 3 allow for potassium transport to the reservoirs, membrane 2 contains the driving input and allows for calcium transport between the two motor cells I and II

There are a variety of options for generating the energy required for the action potential, ranging from external application of an electrical stimulus to introducing ATP to simulate the ATPase. Identification of the proper method of generating the potential while ensuring maximum efficiency will be necessary for attaining peak actuation performance. In this study an externally applied potential was imposed on membrane 2 to stimulate activity.

4.3 EQUATIONS FOR OSMOTIC ACTUATION

In accordance with the Hodgkin-Huxley model[21], the membrane was treated as a capacitance circuit separating the intracellular and extracellular space. The membrane potential v was determined by summing the currents across each transporter $i_{transport}$ divided by the membrane capacitance C . This equation was repeated for primary transport of both chambers I and II (based on equation 1.1).

$$\frac{dv}{dt} = -\frac{1}{C} \left(\sum i_{transport} \right) \quad (4.1)$$

The Nernst equilibrium potentials were calculated based on the transport as a function of Boltzmann's constant k_B , the temperature T , the valence z , the basic charge e , and the ratio of the external and internal concentrations $[S]_e$ and $[S]_i$. In this case, the tracked ions are $[K]^+$ and $[Ca]^{2+}$. This equation was repeated for each transport membrane (1, 2, and 3) (based on equation 1.3).

$$v_s = \frac{k_B T}{e} \ln \left(\frac{[S]_e}{[S]_i} \right) \quad (4.2)$$

The transporters considered in this case are voltage gated channels. A variable driving potential function $v_{drive}(t)$ was applied to these channels, and the current was calculated as a function of a transport coefficient $k_{channel}$, membrane potential v , Nernst equilibrium potential for calcium v_{Ca} , channel activation voltage v_{Caact} , Boltzmann's constant k_B , and temperature (based on equation 1.22 and 1.32).

$$i_{Cachannel} = k_{channel} X_{open} \sinh \left(\frac{e(v - v_{Ca} + v_{drive}(t))}{k_B T} \right) \quad (4.3)$$

$$X_{open} = \frac{1}{2} \left[1 + \tanh \left(\frac{2e(v - v_{Caact})}{k_B T} \right) \right] \quad (4.4)$$

The potassium channel current was calculated in a similar fashion without the addition of the driving potential, and the use of the Nernst equilibrium potential for potassium v_K (based on equations 1.22 and 1.32).

$$i_{Kchannel} = k_{channel} X_{open} \sinh\left(\frac{e(v - v_K)}{2k_B T}\right) \quad (4.5)$$

$$X_{open} = \frac{1}{2} \left[1 + \tanh\left(\frac{2e(v - v_{Kact})}{k_B T}\right) \right] \quad (4.6)$$

In each case, the channel gating equation used the steady-state form. Initial calculations implemented the differential form, but the differences between the two predictions were found to be negligible, while the steady state assumption reduced the computational time significantly.

The membranes were assumed to be permeable to potassium through a standard diffusion equation, since plant cells are highly permeable to potassium. This diffusion currents were calculated as a function of the transport surface area A , the permeability P_K , Faraday's constant F , the membrane potential v , the concentrations of $[K]^+$, the Universal Gas Constant R , and the temperature T (based on equation 1.34).

$$i_{Kdiff} = -AP_K F \left(\frac{Fv}{RT}\right) \left[\frac{[K]_i - [K]_e e^{\left(\frac{-Fv}{RT}\right)}}{1 - e^{\left(\frac{-Fv}{RT}\right)}} \right] \quad (4.7)$$

Similar to the previous sections, the change in concentrations was calculated as a function of the transporter flow, repeated for each of the tracked concentrations. This was repeated for all 4 regions; the two driving chambers (I and II), and the external reservoirs (based on equation 1.2).

$$\frac{d[S]}{dt} = \frac{\sum i_S}{Vol * F} \quad (4.8)$$

Changes in concentrations generated osmotic pressure, which was determined from the van't Hoff equation. This osmotic pressure is dependent on the difference between the external ($[S]_e$) and internal ($[S]_i$) concentrations, multiplied by the gas constant R , the temperature T , and the osmotic coefficient of the membrane θ . A constant C is enforced to ensure that the initial osmotic pressure is set to zero. This equation was repeated for both potassium transport membranes (based on equation 1.35).

$$\pi = RT\theta \sum ([S]_i - [S]_e) - C \quad (4.9)$$

This osmotic pressure generation resulted in osmotic transport across the membrane, which increased or decreased the volume of the chamber through diaphragm displacement. The volume change was dependent on the generation of osmotic pressure rather than the active transport across the channels. This was linked to the presence of aquaporins (water channels) [108] in the potassium transport membranes. However, the water permeability of the calcium membrane was assumed to be negligible due to lack of aquaporins. The total change in chamber volume was calculated as a function of the hydraulic conductivity K , the difference between the osmotic pressure π and the generated resistance pressure p_r , and the summation of the volumes V_s of the transported species (based on equation 1.36):

$$\frac{dV}{dt} = KA \left(\sum_s \pi_s - p_r \right) + \sum_s \bar{V}_s \frac{d}{dt} (n_s)_i \quad (4.10)$$

This equation was repeated for both chambers. The resistance to deformation calculation assumes linear hyperelastic expansion of a circular rubber diaphragm, and the resulting pressure from the deformation was calculated through [42] (based on equation 1.48):

$$p_r = \frac{16Et^3\Delta V}{\pi r^6(1 - \nu^2)} \quad (4.11)$$

where E is young's modulus for the diaphragm material, t is the diaphragm thickness, ν is Poisson's ratio for the diaphragm material, and r is the radius of the diaphragm.

The displacement at the center W was calculated through[42]:

$$W = \frac{P_r r^4}{64 \left(\frac{Et^3}{12(1 - \nu^2)} \right)} \quad (4.12)$$

For strain calculations, the shape of the diaphragm during chamber expansion was assumed to be a dome. The total surface area A was calculated through:

$$A = 2\pi \left(\frac{W^2 + (d/2)^2}{2h} \right) W \quad (4.13)$$

where d is the diameter of the diaphragm and W is the central displacement calculated through equation 4.12. The strain was calculated by comparing the deformed surface area to the initial flat diaphragm area (πr^2).

4.4 MODEL CALIBRATION/VALIDATION

The baseline inputs from the study were taken from both the previous nastic studies and values found in the literature for plant cells, and may be seen in table 7. A range of activation potentials for both calcium channels and potassium channels were noted in the literature review, with a high degree of tailorability. Therefore, values of +/-45 mV for the calcium channels and +/-60

mV for the potassium channels were selected from the expected ranges of channel activation values. The central membrane was assumed to be relatively impermeable to water while the outer membranes were assumed to be highly permeable. This was achieved through assuming the presence of aquaporins in the outer membranes[108]. These are pressure-activated water channels found in plant cells, and their presence is the reason that plant cell membranes are generally more permeable to water diffusion than animal cell membranes. This variation in aquaporin presence ensures that the water flow occurs mainly between the chambers and the external reservoirs, and not between the two central chambers.

The voltage gated channels were based on transporters located in plant cells. The potassium channels were modeled after the KAT1 family[110-112]. Protein packing was assumed, increasing the total transport coefficient by 1.5[100]. The calcium voltage gated channels were similarly located in plant cells to increase compatibility and were modeled after the OsTPC1 family[92]. I-V plots were not readily available for this transporter so it was assumed that the calcium channel density was sufficient to match the coefficient determined for the potassium transporters. This approach resulted in a value of 12 nA for the channel flow coefficient. The value assumed does not risk over-estimating the channel density, as it is still lower than the value employed by Endresen [49] which was validated against experimental data.

Additionally cell membranes are highly permeable to potassium. This diffusion flow was accounted for across all membranes with a standard plant cell potassium permeability value of $1.6E-7$ cm/sec[113].

The dimensions of the chambers and diaphragms themselves were taken directly from the values from the nastic actuation computational study for direct comparison purposes.

Table 7. Osmotic Actuator Baseline Inputs

Variable	Symbol	Value	Source
Diaphragm Radius	R	250 μm	[46]
Diaphragm Thickness	T	2.5 μm	[46]
Diaphragm Elastic Modulus	E	0.1 GPa	Rubber
Diaphragm Poisson's Ratio	V	0.5	Rubber
Chamber Height	H	1000 μm	[46]
Transport Surface Area	A	98174 μm^2	Variable
Channel Coefficient	$k_{channel}$	12 nA	[100, 110-112]
K+ Activation Voltage	v_{actK+}	50 mV	Variable
Ca++ Activation Voltage	$v_{actCa++}$	40 mV	Variable
Initial K+ Concentrations	$[\text{K}]_{ie0}^+$	100 mM	Variable
Initial Ca++ Concentrations	$[\text{Ca}]_{ie0}^{++}$	50 mM	Variable
Membrane Capacitance	C	1 $\mu\text{F}/\text{cm}^2$	Standard
Potential Input	v_{drive}	500 mV	Variable
Potassium Permeability	P_k	1.6E-7 cm/sec	[113]
Water Permeability	P_{OS}	300E-4 cm/sec	[108]

Similarly to the previous section, direct validation may not be achieved for this study. Chamber dimensions were taken directly from data for previous nastic actuation simulations, and the study employed the same approach as the previously validated cases for endocytosis and nastic actuation. Several observations from the results do lend credence to the results.

First, the overall length of time for full actuation is in line with the expected timescale for observed swelling/shrinking motions in the plant kingdom[109]. The expected timescale for the motion only exceeds this value when v_{drive} exceeds values of the membrane tolerance (1 V).

Secondly, the transporter current ratio for comparing the ion diffusion currents to channel currents demonstrated that the channel currents, while higher than the diffusion currents, do not

overwhelm them. The overall flow is still comparable. This was in line with expected transporter behavior[18].

4.5 OSMOTIC ACTUATION RESULTS

Several indicators of performance must be examined. Free displacement, blocked force, and rate of response are all of importance. The inputs from table 7 were used as a baseline, with modifications as noted for individual cases. For each case the predicted results may be compared to the results from the nastic actuation case[46].

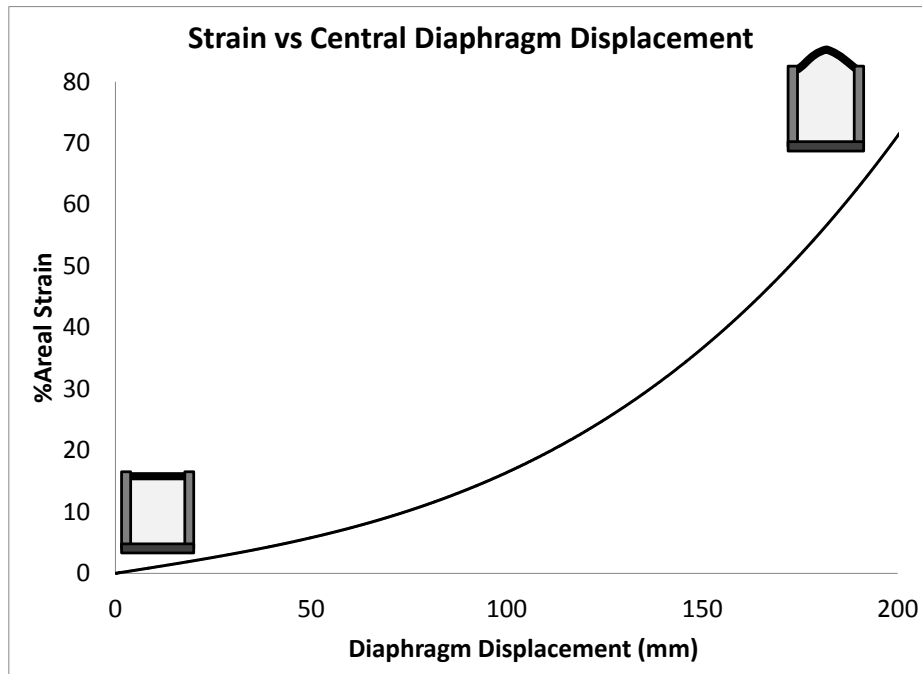


Figure 4.3. Converting Central Displacement to %Areal Free Strain

For displacements, the results will be presented as the central displacement of the diaphragm, calculated through equation 4.12. This may be converted into a %Areal Strain as seen in figure 4.3, calculated through equation 4.13. The original nastic simulation reported

deformations in central displacement values, so the results for the revised osmotic actuator will also be reported in central displacements for comparison.

4.5.1 Relating v_{drive} to generated membrane potentials

For the majority of these plots, the baseline voltage v_{drive} of 500 mV will be applied. The maximum sustainable potential across these membranes was found to be 200 mV[110]. Therefore the driving potential must be applied gradually in practice. As v_{drive} is applied across the calcium transport membrane (membrane 2), the voltage gated calcium channels open to provide a rectifying flux, reducing the membrane potential across the membrane. The motion of the calcium ions then generates additional membrane potentials across the two potassium transport membranes (membranes 1 and 3) and in doing so splits v_{drive} across the three membranes as illustrated in figure 4.4.

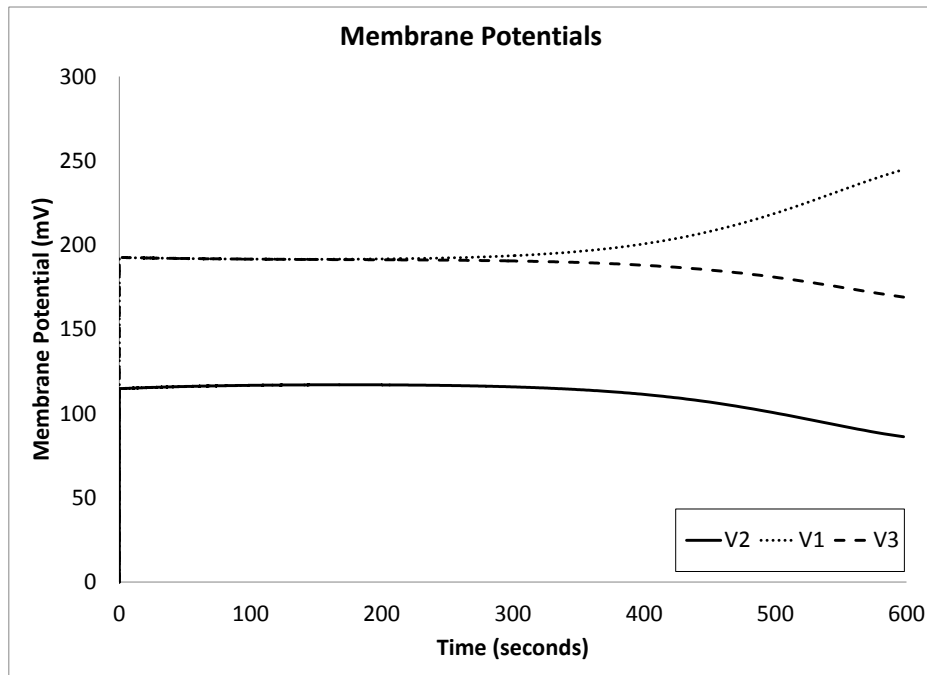


Figure 4.4. The input potential is distributed across the three transport membranes.

As noted, during the expansion the maximum potential is located across the potassium transport membranes at just under 200 mV. The drift once displacement has halted is due to the difference in the gating behavior, which may be adjusted to avoid surpassing the maximum voltage. Therefore this 500 mV driving potential still generally yields developed membrane potentials below the maximum observed threshold of 200 mV.

4.5.2 Baseline Actuation Performance

The first point of interest is the maximum displacement achievable. This was achieved by allowing the diaphragm to expand without the application of any external loads.

As illustrated in figure 4.5, the overall displacement compares favorably to results predicted by the optimized nastic actuation study[46], with a peak displacement of 208 μm (compared to 250 μm). It should be noted that the maximum stroke is equivalent to double this value, as the actuator is able to fully reverse in the opposing direction as well, for a total stroke of 416 μm . As shown in figure 4.3, this is equivalent to roughly 75% areal strain.

Next, the blocked force was predicted. This was accomplished by holding the diaphragm rigidly in place, setting the total displacement to zero for the duration of the simulation. From the balance of forces, the pressure required to hold the diaphragm rigidly in place (blocked force) will be equivalent to the maximum osmotic pressure developed.

As illustrated in figure 4.6, peak hydrostatic pressure is given as 0.28 MPa. This value is smaller than the initial spike seen in the nastic computational studies with a peak of 1.0 MPa, but the pressure is sustained rather than transient.

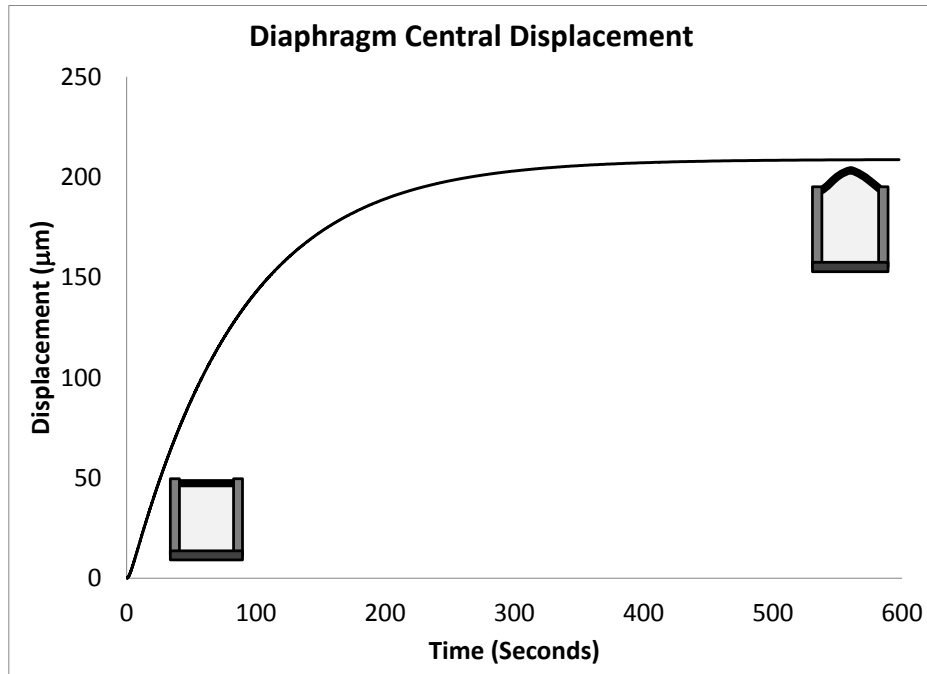


Figure 4.5. Predicted free central diaphragm displacement for osmotic actuation.

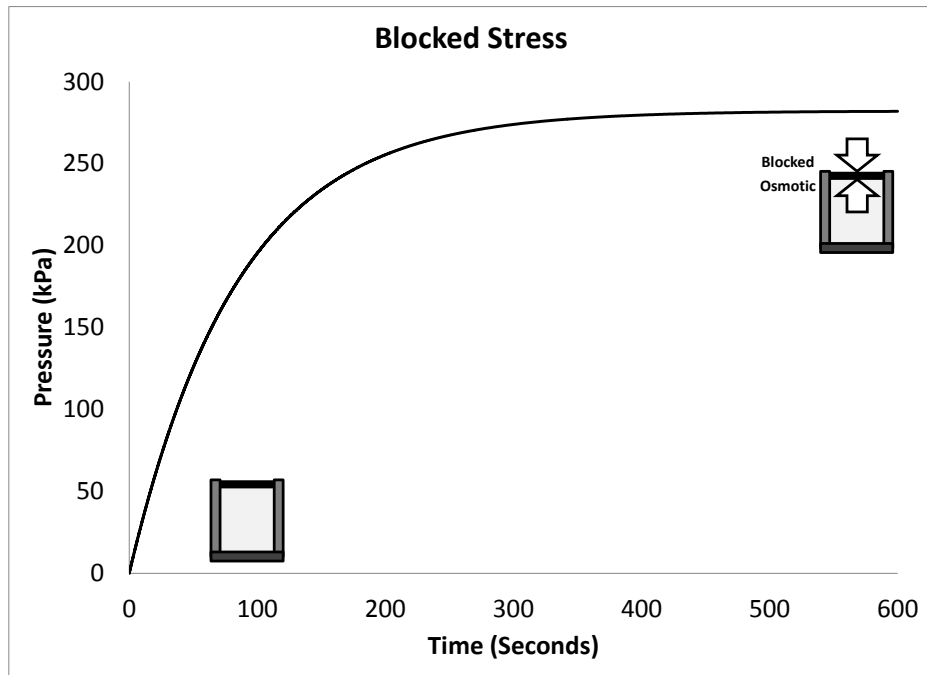


Figure 4.6. Predicted blocked stress for osmotic actuation.

Finally changing the internal concentration will be examined. It should be noted that the value of Ca^{++} concentration originally selected for the baseline case was found to be much higher than regular cytosol concentrations. The impact of reducing the concentration to 5 mM

was plotted and may be seen in figure 4.7. The potassium values are left as is as they fall within the accepted range of cytosol concentrations[114].

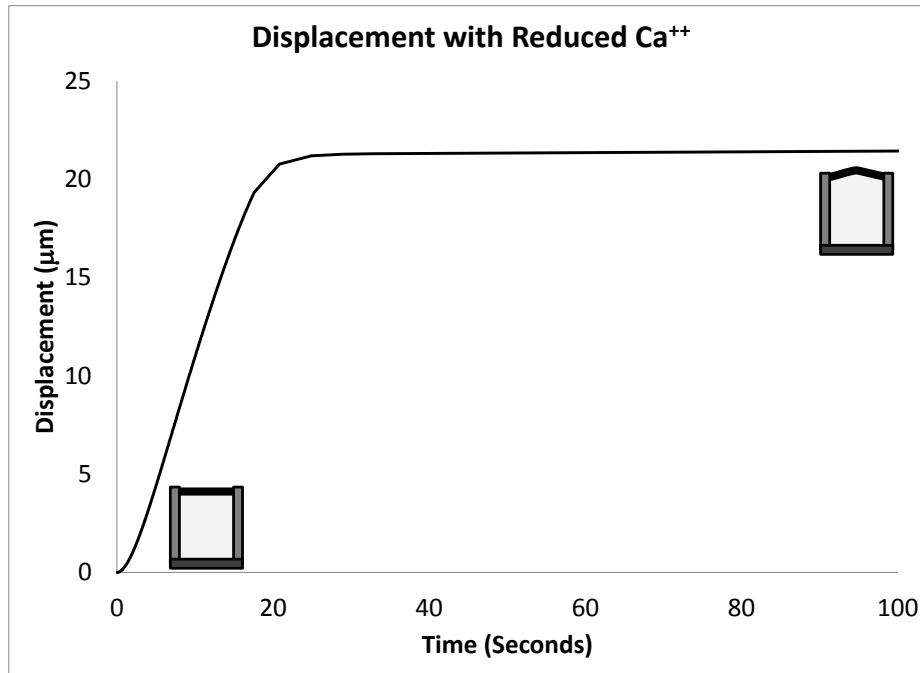


Figure 4.7. Predicted central diaphragm displacement with reduced calcium (5 mM).

The reduction of the calcium concentration results in a much lower overall displacement, and much lower time to the peak displacement. The total displacement for this case is around 20 μm. Based on the earlier nastic study where naturally occurring systems of transporters were employed, the magnitude of this prediction is consistent with expectations for natural systems (but is too small for engineered systems).

4.5.3 Input Potential Dependence

Control over the actuator is exerted by manipulating the potential $v_{drive}(t)$ on membrane 2. It is therefore appropriate to explore the implications of varying this input parameter.

4.5.3.1 Varied Input Magnitude Impact

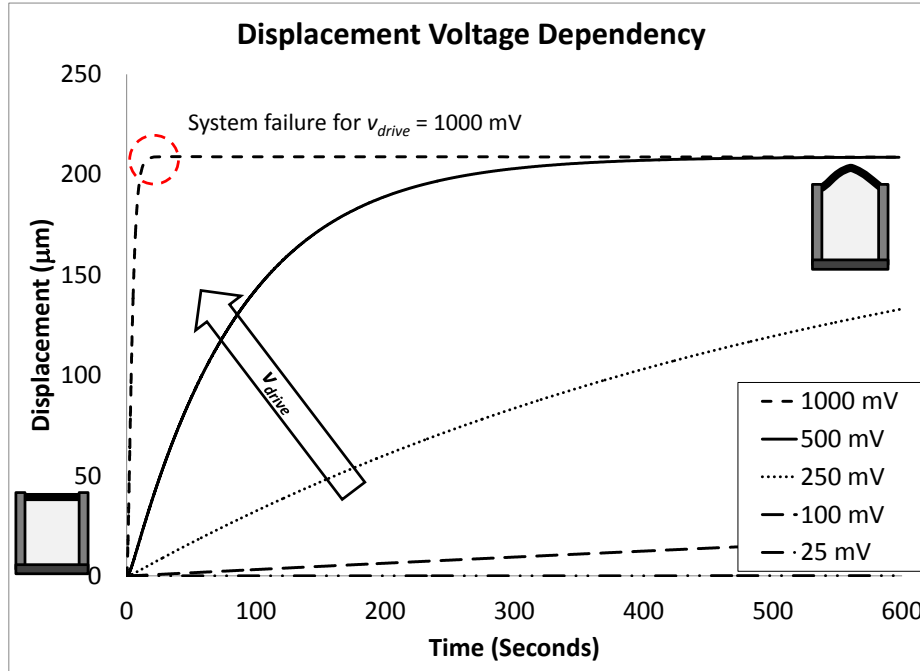


Figure 4.8. Predicted central diaphragm displacement with varied v_{drive} . With v_{drive} set to 1000 mV, the generated membrane potentials surpass the individual membrane threshold of 200 mV which will result in system failure. The first test examines the impact of varying the level of the input potential. The v_{drive} input was held constant at several values, ranging from 25 mV to 1000 mV, and the resulting displacements may be seen in figure 4.8.

From the results it appears that the overall displacement is not directly dependent on the driving potential, but the rate of expansion is highly dependent on the potential. The 25 mV case falls below the required channel activation potentials, and consequently no displacement occurs. All other cases exhibited actuation.

The driving potential relates directly to the Nernst equilibrium potentials. As the Nernst potentials (equation 4.2) are directly linked to the concentration gradient, consequently the driving potential is directly linked to the osmotic pressure and the displacement of the diaphragm. However, since the osmotic pressure increases linearly with concentration gradient

and the Nernst potentials increase as the natural log of the concentration ratio, the gain from the input potential will decrease with each additional volt. This is why the model predicts that doubling the driving potential from 500 mV to 1000 mV (see figure 4.8) will only result in an increased displacement of 0.1 μm at equilibrium. While the 1000 mV simulation predicted much faster increases, the overall work done by the actuator remains at a similar level. Because of this relationship, the most effective way to alter the free displacement and blocked force of the actuator is through varying the concentrations, as seen in figure 4.7.

The rate of response appears to be linked to the driving potential. For the case with a 1000 mV potential, the total response time for peak displacement is roughly 30 seconds. This is not in accordance with the predicted rate of response for swelling/shrinking movements observed in the plant kingdom[109]. The membrane potentials developed in this case are well beyond the previously defined threshold of 200 mV, and membrane failure is expected to occur. In general, higher membrane potentials have an inverse effect on the average lifespan of the membrane, and early experimental studies noted that higher values the membrane became increasingly unstable[115].

4.5.3.2 Input Removal Impact

Prompted by the behavior from the previous study, the impact of removing the input potential was studied. The input was held initially at 500 mV, and then was reduced to zero at a predefined point in the simulation.

Figure 4.9 indicates that the removal of the voltage causes a cessation in motion of the actuation diaphragm. The concentrations remain constant, and the osmotic pressure is maintained. Two cases were plotted. The first case removed the driving potential halfway through, and the second case removed the driving potential one quarter through the simulation.

In both cases, the displacement stopped and held at a near-constant value once the driving potential was removed.

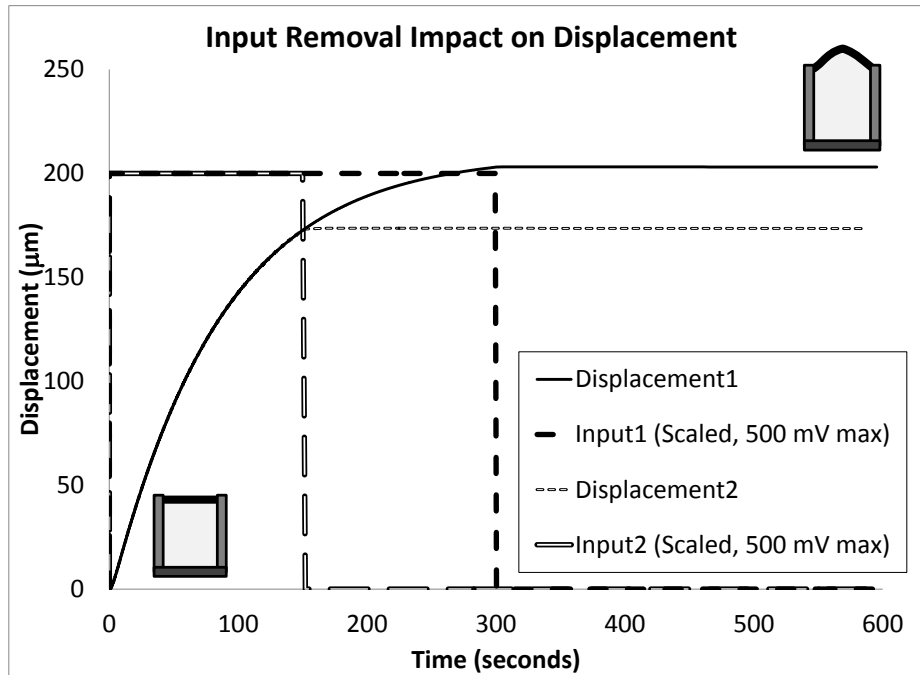


Figure 4.9. Predicted central diaphragm displacement with removed input v_{drive} at $\frac{1}{2}$ time and $\frac{1}{4}$ time.

These phenomena may be explained through the relation between the driving potential and the voltage gated channels. As the displacement occurs, the overall membrane potentials between the chambers are kept low as the overall transport has a neutral impact on the charge (2 K^+ out for every Ca^{++} in). Once the potential is relieved, the existing membrane potentials quickly move back towards equilibrium by shifting the concentrations back minutely, and the voltage activated channels close. The displacement does gradually begin to dissipate due to K^+ diffusion currents, but it is held relatively constant as the balancing Ca^{++} transport is solely a function of the channel activity, and the membrane potential does not approach the required values for channel activation.

4.5.3.3 Varied Input Direction Impact

The next step involves determining the reversibility of the displacement. The input potential is varied to provide an initial negative potential, followed by an increase back to the baseline value of 500 mV. Displacements for both chambers are presented to demonstrate reversibility.

This figure is of particular interest. The two displacements are calculated separately, but the total displacements have opposite directions with similar magnitudes. In addition, the displacement does not appear to change until the input potential reverses direction, in agreement with the previous section. The peak displacements are the same as the ones observed with the constant input (figure 4.5). The process is reversible.

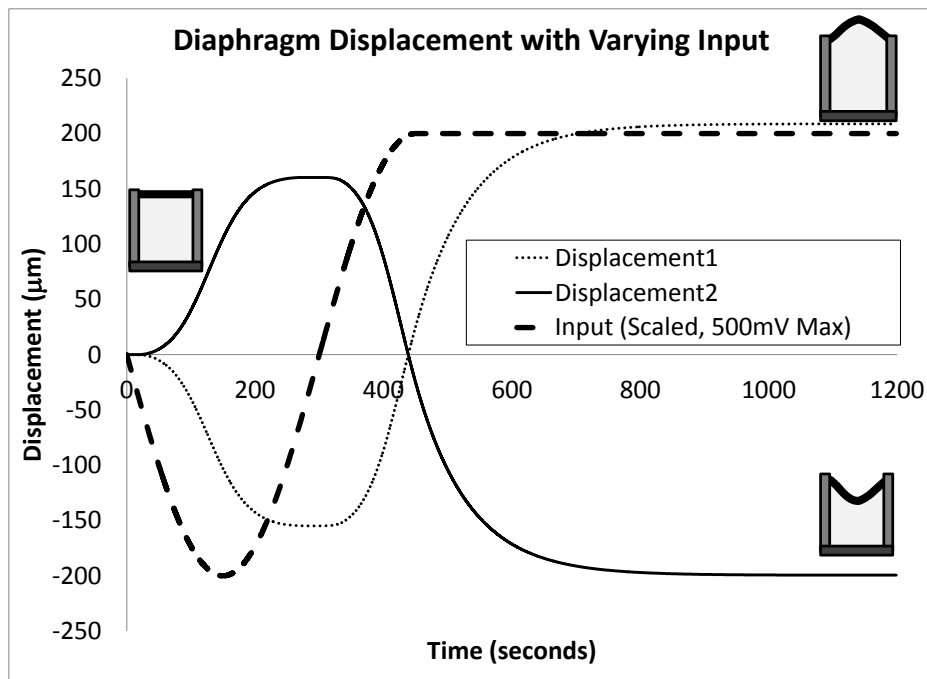


Figure 4.10. Predicted central diaphragm displacement with varied input $v_{drive}(t)$.

Upon further examination of the results seen in figures 4.8-4.10, it was observed that the following relationship exists between the input potential and the Nernst equilibrium potentials across the membranes once the system reaches equilibrium.

$$v_{drive} \approx v_{1K} + v_{3K} + v_{2Ca} \quad (84)$$

This assumes that the transport across the lower Ca^{++} driving membrane directly impacts the secondary K^+ transport membrane with minimal loss in signaling, and no interference from the applied potential at the secondary transport membranes. This relation explains several of the results of the plots.

4.5.4 Role of Membrane Capacitance.

In the previous chapter on Water Purification, the membrane capacitance input played a large role in selecting protein transporters. In addition, for the original Nastic Actuation case study, the capacitance value was set to be 670 F/cm^2 to ensure that the data fit the general curve, essentially increasing the capacitance value to the point that the hyperpolarization effect no longer played a role in limiting the actuation motion.

Consequently varying the capacitance is examined here in detail. The baseline value was derived directly from the standard value for a bilayer membrane at $1 \mu\text{F/cm}^2$. The results for this capacitance value were compared directly to the value previously employed for nastic actuation (670 F/cm^2)

It is observed that increased capacitance of the cell membrane results in a negative displacement. This is because the membrane potential created by the transported Ca^{++} is diminished to the point that the membrane potentials remain far below the activation threshold of $\pm 60 \text{ mV}$ for the voltage activated K^+ channels. This loss of signal conductance is also observed in nature when cell capacitance is increased through high cholesterol content[116].

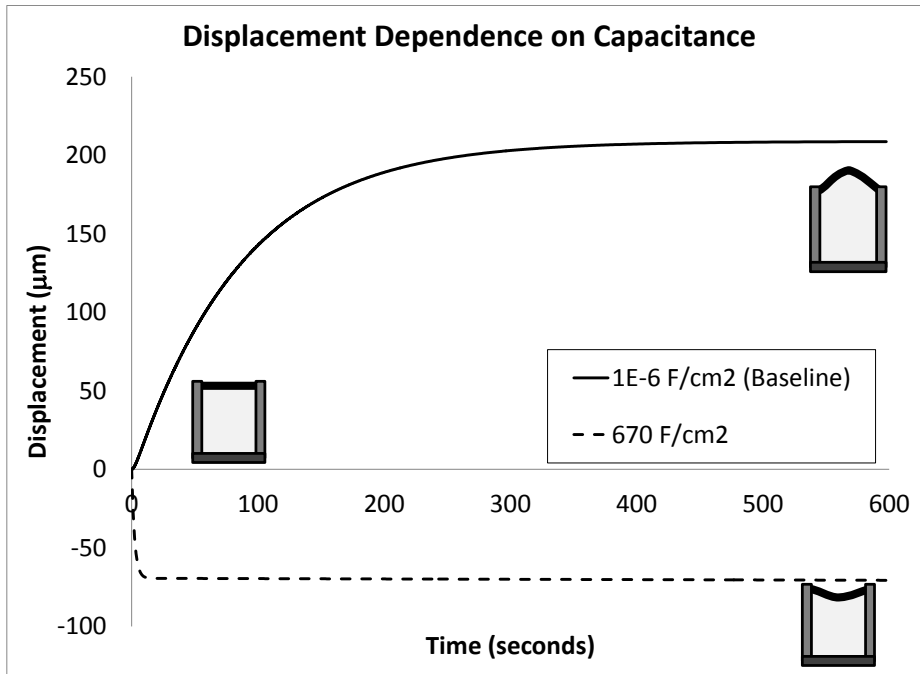


Figure 4.11. Predicted central diaphragm displacement with varied membrane capacitance C .

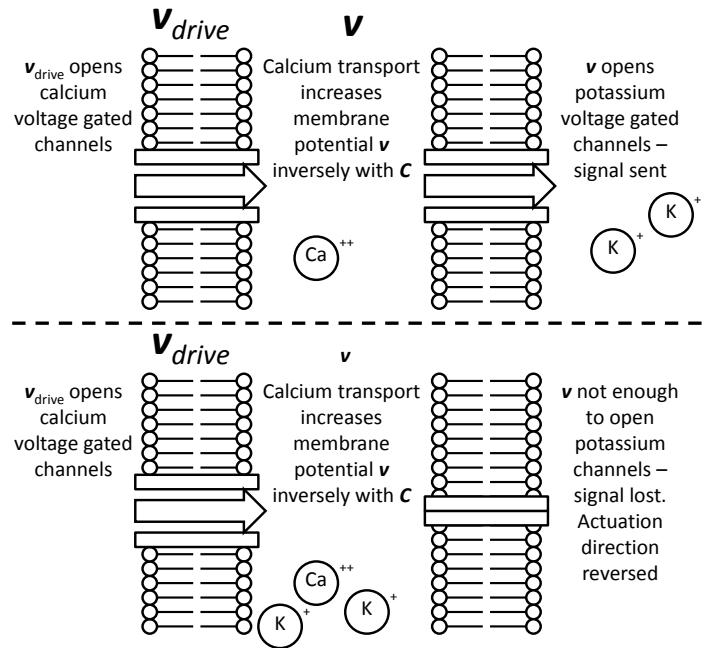


Figure 4.12. Illustration of capacitance's relation to signaling – membrane potential development inversely related to membrane capacitance, increasing the membrane capacitance reduces signal development, reducing action potential generation. The upper image corresponds to baseline capacitance case in figure 4.10, and the lower image corresponds to increased capacitance case.

4.6 DISCUSSION

The predicted results for this system compare favorably with the previous nastic actuation system, with the addition of reversibility and a higher level of control over the deformation behavior. The osmotic system proposed is wholly original, and the predicted performance for the considered baseline system compares favorably with similar smart materials. The highest reported deflection with no external loading was 208 μm (416 μm total stroke), with an internal pressure of 0.228 MPa, both of which are sustainable with no further input. Assuming a dome shaped diaphragm, the total strain in the diaphragm material may be approximated as roughly 80%.

The presented actuation system is highly tailorable. Through altering the diaphragm material, biomembrane surface area, driving potential, and ion concentrations, the user may create a diverse range of actuation systems for a variety of tasks. An expected universal behavior is high levels of deformation with a slower rate of response.

The rate of response was found to be on the order of 10 minutes for full scale deformation for an input of 250 – 500 mV, which is in alignment with other swelling/shrinking movements[109]. The rate of response may be increased by an increased input potential, but this increased potential may rupture the membranes.

The internal pressure (which matches the osmotic flow when volume is at equilibrium) is above the recommended limit of 66 kPa for pore membrane rupture[11]. It is suggested that the diaphragm material and dimensions be varied to yield larger deformations – in this way the osmotic pressure will be relieved and failure pressures will not be reached. In addition, high levels of hydrostatic pressure may interfere with the performance of the voltage gated channels[117]. If pressures still remain above desired values, then the membrane may be

supported with a hydrogel scaffold. Cholesterol has been used to increase membrane strength[12], but high levels of cholesterol may increase capacitance, causing loss of actuation as seen in figure 4.11.

Overall the input required for motion is equivalent to the channel activation voltages, and increasing the input beyond the channel activation threshold only impacts the rate and has minimal impact on total displacement. The displacement may be maintained for long period of time without sustained input, as seen in figure 4.9. The osmotic actuation system therefore is ideal for large deformation actuation requirements that are not dependent on rapid rate of response.

One benefit of the proposed system is the simultaneous swelling/expansion that occurs across the central membrane. This behavior lends itself well to bimorph applications, as seen in figure 4.13. This is similar to the original vision for the nastic actuation program[118], and would allow for high deflection values. But in addition, the system is now capable of fully controllable and reversible deformation through the use of action potential generation and voltage gated channels, moving the biomembrane facilitated actuation concept closer to the desired goals.

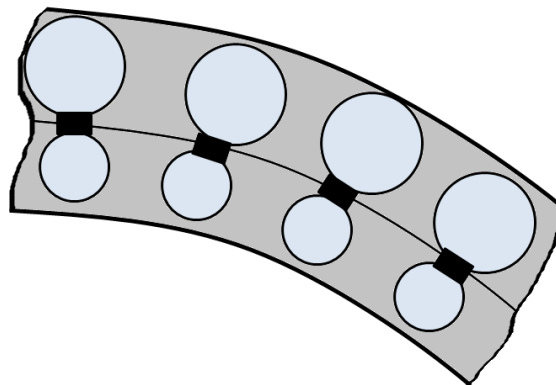


Figure 4.13. Illustration of a possible bimorph application of the dual chamber apparatus for large scale deflections.

4.7 OSMOTIC ACTUATION CONCLUSIONS

This chapter details proof of principle for the creation of a novel osmotic actuation system based on transport systems found in plant guard cells. The system was built using a computational approach similar to the one employed in previous chapters, with the intent of demonstrating potential actuation applications for these novel biomembranes. Inputs were taken from the literature or assumed to follow predefined ranges of values found in nature. All of the selected variables fall within experimentally obtainable values. Initial results show that the actuator is fully reversible and controllable, and that the peak displacement and pressure may be controlled by varying the applied voltage or ion concentrations.

The strengths of this approach to actuator design is the creation of a highly-tailorable actuation system built on biomimetic principles allowing for reversible and controllable deformation through osmotic pressure and ion channel activity. While companion experimental studies are required as future work, the preliminary results are promising. The work presented here supports the viability of the concept, and provides guidelines for osmotic actuation design.

5.0 CONCLUSIONS

The primary goal of this dissertation has been to define (a) the core governing equations to a new class of active materials, and (b) the generalized approach toward their application. To enable illustration of the approach as well as the extraordinarily broad range of potential applications three distinctly different demonstration cases have been offered. In each demonstration case the core equations first required calibration. They were then coupled to additional case-specific equations, akin to defining boundary conditions. Moreover, each case has been motivated as compelling in their own right.

While the concepts are still in early stages of development, the presented results provide motivation for further explorations of these cellular mechanics for engineering applications. Further refinements improving the membrane stability and compatibility will allow for the widespread use of these cellular systems, opening up new avenues in micro sensing and micro actuation studies.

The following sections focus on the conclusions from each of the respective case studies. The final contributions may be seen in the following chapter.

5.1 ENDOSOME SUMMARY

- The endosome study demonstrated the utility of the active membrane modeling methodology through using engineering principles to advance biological research goals.
- DNA vaccine delivery is crucial for successful gene therapy, and endocytosis is a primary barrier to successful vaccine delivery.
- The endosome study focused on applying the computational model towards understanding and subsequently manipulating endosomes.
- Endosome behavior was successfully calibrated from experimental data and validated against common characteristics observed in endocytosis
 - pH plateau of roughly 6.5 due to combination of pump and diffusion effects
 - Reduction in acidification through Na^+K^+ pump activity
 - Resting membrane potential of roughly 90 mV due to external concentrations, diffusion, and transporter activity
- Once the naturally occurring endosome model was successfully modeled, an approach for inducing burst-release of DNA vaccine was studied. The proton Sponge effects were deemed the most promising, and it was determined that tertiary pKa values of roughly 6.5 were ideal for inducing burst, with primary pKa values of 10 for binding to the vaccine.

5.2 WATER PURIFICATION SUMMARY

- The water purification study sought to demonstrate how a naturally occurring process could be amplified via adoption of the active membrane modeling approach.

- The motivation for the research was addressing the formation of “dead zones”, or aquatic regions no longer capable of sustaining life. These zones are formed through a boom-bust eutrophication cycle in which dissolved oxygen is reduced through cellular respiration.
- Plant roots were used as inspiration for the selection of transporters. A photosynthetic device was suggested for the creation of a proton motive force, allowing for the continued removal of negatively charged nitrates and phosphates from surrounding regions of water
- An internal locking mechanism analogous to buffering was proposed. Biochar was selected because of observations of reduced nutrient leeching in fertilization applications. Biochar was created in the lab, and its ability to reduce nitrate concentrations was studied.
- Inclusion of the biochar was found to offer a compelling pathway for enabling effective uptake as well as a subsequent re-use of the nitrates and phosphates.
- The peak uptake indicates a total removal potential of roughly 150 (volume of purified water to system volume).

5.3 OSMOTIC ACTUATION SUMMARY

- The osmotic actuator study demonstrated a classic engineering approach toward application of a novel active material.
- The motivation was revisiting the original nastic actuation system and enhancing controllability and reversibility.
- The concept of an osmotic actuator drew specific inspiration from behavior seen in plant guard cells.
- The resulting actuator was capable of high deformations with moderate blocked force.

- The input potential had a high impact on rate of deformation but the relation between the total deformation and input demonstrated diminishing returns for the input potential in relation to the peak.
- Predicted results must be tempered with experimental observations.

6.0 CONTRIBUTIONS

The contributions of the research are measured here.

- The dissertation presents a novel class of active materials; biologically inspired active membranes, or biomembranes. These tailored membranes similar to ones found in nature allow for cellularly inspired devices for purification, actuation, sensing, etc.
- Numerical methods were employed to simulate the behavior of these biomembranes. The simulation results were validated against experimental observations, and offered insight into the nature of the results through varying inputs and transport configurations.
- The model was successfully applied towards simulating the endocytosis process. A computational model for the protonation of a dendrimer was constructed and included with the transport model. This allowed for the study of the effectiveness of the proton sponge with varying dimensions, pKa values, and densities for vaccine delivery applications. It was found that the geometry of the sponge did not directly link to the sponge's effectiveness; instead the sponge pKa values should remain close to the internal pH for effective burst.
- A water purification case was constructed. It was found that an imbalance in incoming vs. outgoing charges resulted in reduced transport effectiveness, particularly when dealing with system volumes greater than that of a regular cell due to the dominance of

volume effects (concentration change) in relation to surface effects (membrane capacitance).

- Biochar was created and tested for nitrate uptake capabilities. It was found that the char does have a natural affinity for absorbing nutrients such as nitrates and phosphates, and that the uptake ability is dependent on both surface area and temperature of pyrolysis.
- A novel actuation design was proposed. From this study it was demonstrated that osmotic actuation may be enhanced through using two separate species with varying charges, and that osmotic actuation demonstrates high ranges of deformation with minimal driving input.
- Overall the dissertation demonstrates the varying range of abilities involving the use of biomembranes, and provides impetus for their future studies.

7.0 PUBLICATIONS

The following lists are publications from the research discussed in this dissertation.

7.1 REFERRED JOURNAL PAPERS

Freeman, Eric, Weiland, Lisa, and Meng, Wilson, 2010 “Application of Proteins in Burst Delivery Systems”, *Smart Mater Struct*, 19 09401

Freeman, Eric and Weiland, Lisa, 2009, “High Energy Density Nastic Materials: Parameters for Tailoring Active Response”, *Journal of Intelligent Material Systems and Structures*, *Jan 2009*.

Freeman, Eric, Weiland, Lisa, submitted 8/30/2011, “Biologically Inspired Reversible Osmotic Actuation through Voltage-Gated Ion Channels”, *Journal of Intelligent Material Systems and Structures*

Freeman, Eric, Weiland, Lisa, and Soncini, Ryan, 2012, “Biologically Inspired Water Purification through Active Transport”, *TBD*

Freeman, Eric, Weiland, Lisa, and Meng, Wilson, 2012, “Towards a Predictive Modeling of Intracellular Gene Delivery through a Computational Study of Endosome Buffering”, *TBD*

7.2 NON-REFEREED CONFERENCE PAPERS WITH PRESENTATION

Freeman, Eric, Weiland, Lisa, Soncini, Ryan, 2011, “Water Purification through Selective Transport”, Proc of ASME-SMASIS 2011, Sept 18th – Sept 21st, Scottsdale, AZ.

Freeman, Eric, Weiland, Lisa, and Meng, Wilson, 2010, “Computational Study of Inclusion Burst Via the Proton Sponge Hypothesis”, Proc of ASME-SMASIS 2010, Sept 28th - Oct 1st, Philadelphia, PA.

Freeman, Eric, Weiland, Lisa, and Meng, Wilson, 2009 “Endosomal Vaccine Delivery through the Nastic Model”, Proc of ASME SMASIS 2009, Sept 20th -24th, Oxnard, CA.

Freeman, Eric, Weiland, Lisa, 2008, “Applications of Biologically Inspired Materials”, Proc of ASME-SMASIS 2008, Oct 28th-30th, Ellicott City, MD.

Freeman, Eric, Weiland, Lisa, 2007, “Parametric Studies of a Coupled Transport/Hyperelastic Model for High Energy Density Nastic Materials”, Proc of ASME-IMECE 2007, Nov 11th-15th, Seattle, WA.

7.3 NON-REFEREED CONFERENCE PAPERS WITH POSTER

Freeman, Eric, Weiland, Lisa; 2011, “Development of Protein-Based Water Purification Systems”, Proc of CMMI 2011, Jan 4th – Jan 7th, Atlanta, GA.

APPENDIX A

SUMMARY OF EQUATIONS USED IN THE INDIVIDUAL CASES

ENDOSOME EQUATIONS

$$\frac{dv}{dt} = -\frac{1}{C} \left(\sum i_{transport} \right) \quad (2.1)$$

$$v_s = \frac{k_B T}{ze} \ln \left(\frac{[S]_e}{[S]_i} \right) \quad (2.2)$$

$$i_{Hrpump} = M_H e \lambda_H * \tanh \left(\frac{e(-v - v_{ATP} + v_H)}{2k_B T} \right) \quad (2.3)$$

$$i_{NaKpump} = M_{NaK} e \lambda_{NaK} * \tanh \left(\frac{e(-v - v_{ATP} + 3v_{Na} - 2v_K)}{2k_B T} \right) \quad (2.4)$$

$$i_{HDiff} = -AP_{H^+} F \left(\frac{Fv}{RT} \right) \left[\frac{[H]_i - [H]_e e^{\left(\frac{-Fv}{RT}\right)}}{1 - e^{\left(\frac{-Fv}{RT}\right)}} \right] \quad (2.5)$$

$$i_{ClDiff} = -AP_{Cl^-} F \left(\frac{-Fv}{RT} \right) \left[\frac{[Cl]_i - [Cl]_e e^{\left(\frac{Fv}{RT}\right)}}{1 - e^{\left(\frac{Fv}{RT}\right)}} \right] \quad (2.6)$$

$$\frac{d[S]}{dt} = \frac{\sum i_s}{Vol * F} \quad (2.7)$$

$$\frac{dpH}{dt} = \frac{\sum i_{H^+}}{Vol * F * C_{buff}} \quad (2.8)$$

$$\pi = RT\theta \sum ([S]_i - [S]_e) - C \quad (2.9)$$

$$\frac{dV}{dt} = KA \left(\sum_s \pi_s - p_r \right) + \sum_s \bar{V}_s \frac{d}{dt} (n_s)_i \quad (2.10)$$

$$p_r(\lambda) = \frac{2\mu_0 t_0}{r_0 \lambda} \left[1 - \frac{1}{\lambda^6} \right] e^{\gamma(2\lambda^2 - \lambda^{-4} - 3)} \quad \lambda = \frac{r}{r_0} \quad (2.11)$$

PROTON SPONGE EQUATIONS

$$\frac{d[H^+]_{sponge}}{dt} = k_{prot}[X]_{free} - k_{loss}[X]_{prot} \quad (2.12)$$

$$k_{prot} = k * \frac{10^{pKa-pH}}{1 + 10^{pKa-pH}} \quad (2.13a)$$

$$k_{loss} = k * \frac{10^{pH-pKa}}{1 + 10^{pH-pKa}} \quad (2.13b)$$

$$pK_i = pK_{i0} - \sum_{i \neq j} \epsilon_{ij} \langle x \rangle_j \quad (2.14)$$

$$\epsilon_{ij} = \frac{W(r_{ij})}{k_B T \ln 10} \quad (2.15)$$

$$W(r) = \frac{e^2}{4\pi\epsilon_0 D_w} \cdot \frac{e^{-\kappa r}}{r} \quad (2.16)$$

$$\kappa^{-1} = \sqrt{\frac{D_w \epsilon_0 k_B T}{2N_A e^2 I}} \quad (2.17)$$

$$I = \frac{1}{2} \sum [X]_i z_i^2 \quad (2.18)$$

WATER PURIFICATION

$$\frac{dv}{dt} = -\frac{1}{C} \left(\sum i_{transport} \right) \quad (3.1)$$

$$v_s = \frac{k_B T}{e} \ln \left(\frac{[S]_e}{[S]_i} \right) \quad (3.2)$$

$$i_{Hdiff} = -APF \left(\frac{Fv}{RT} \right) \left[\frac{[H]_i - [H]_e e^{\left(\frac{-Fv}{RT} \right)}}{1 - e^{\left(\frac{-Fv}{RT} \right)}} \right] \quad (3.3)$$

$$\frac{d[S]}{dt} = \frac{\sum i_s}{Vol * F} \quad (3.4)$$

$$i_{NitH} = 2N_{NitH} e \lambda_{NitH} \sqrt{[Nit]_e^1 [Nit]_i^1 [H]_e^1 [H]_i^1} \sinh \left(\frac{e(v_{Nitrate} + v_H)}{2k_B T} \right) \quad (3.5)$$

$$i_{PhoH} = 2N_{PhoH} e \lambda_{PhoH} \sqrt{[Pho]_e^1 [Pho]_i^1 [H]_e^1 [H]_i^1} \sinh \left(\frac{e(-2v + v_{Phosphate} - v_H)}{2k_B T} \right) \quad (3.6)$$

$$i_{H+Influx} = k_{rate} \tanh \left(\frac{e(-v + v_H - v_{pmf})}{2k_B T} \right) \quad (3.7)$$

$$i_{PhoH} = 2N_{PhoH} e \lambda_{PhoH} \sqrt{[Pho]_e^1 [Pho]_i^1 [H]_e^1 [H]_i^1} \sinh \left(\frac{e(v_{Phosphate} + v_H)}{2k_B T} \right) \quad (3.8)$$

$$i_{Cachannel} = k_{Ca} X_{open} \sinh \left(\frac{e(v - v_{Ca})}{k_B T} \right) \quad (3.9)$$

$$X_{open} = \frac{1}{2} \left[1 + \tanh \left(\frac{2e(v - v_{caact})}{k_B T} \right) \right] \quad (3.10)$$

$$Nitrate_{char} = Nitrate_{total} \left[1 - \frac{1}{(1 + q(mass_{char})/(Vol))} \right] \quad (3.11)$$

OSMOTIC ACTUATION EQUATIONS

$$\frac{dv}{dt} = -\frac{1}{C} \left(\sum i_{transport} \right) \quad (4.1)$$

$$v_s = \frac{k_B T}{e} \ln \left(\frac{[S]_e}{[S]_i} \right) \quad (4.2)$$

$$i_{cchannel} = k_{channel} X_{open} \sinh \left(\frac{e(v - v_{ca} + v_{drive}(t))}{k_B T} \right) \quad (4.3)$$

$$X_{open} = \frac{1}{2} \left[1 + \tanh \left(\frac{2e(v - v_{caact})}{k_B T} \right) \right] \quad (4.4)$$

$$i_{Kchannel} = k_{channel} X_{open} \sinh \left(\frac{e(v - v_K)}{2kT} \right) \quad (4.5)$$

$$X_{open} = \frac{1}{2} \left[1 + \tanh \left(\frac{2e(v - v_{Kact})}{k_B T} \right) \right] \quad (4.6)$$

$$i_{Kdiff} = -AP_K F \left(\frac{Fv}{RT} \right) \left[\frac{[K]_i - [K]_e e^{\left(-\frac{Fv}{RT}\right)}}{1 - e^{\left(-\frac{Fv}{RT}\right)}} \right] \quad (4.7)$$

$$\frac{d[S]}{dt} = \frac{\sum i_s}{Vol * F} \quad (4.8)$$

$$\pi = RT\theta \sum ([S]_i - [S]_e) - C \quad (4.9)$$

$$\frac{dV}{dt} = KA \left(\sum_s \pi_s - p_r \right) + \sum_s \bar{V}_s \frac{d}{dt} (n_s)_i \quad (4.10)$$

$$p_r = \frac{16Et^3 \Delta V}{\pi r^6 (1 - v^2)} \quad (4.11)$$

$$W = \frac{P_r r^4}{64 \left(\frac{Et^3}{12(1 - v^2)} \right)} \quad (4.12)$$

$$A = 2\pi \left(\frac{W^2 + (d/2)^2}{2h} \right) W \quad (4.13)$$

APPENDIX B

VACCINE DELIVERY CODE

Module Solvers

```
Public Sub Simulation(ByRef strMessage As String, ByVal locSim As String, ByVal locTime As String,
ByVal locOut As String, ByVal bATP As Boolean, ByVal bBuffer As Boolean, ByVal bP As Boolean, ByVal bDamp
As Boolean, ByVal bHydro As Boolean, ByVal bPump As Boolean, ByVal bCT As Boolean, ByVal bDiff As Boolean,
ByVal bChann As Boolean, ByVal bIon As Boolean, ByVal bSuc As Boolean, ByVal bCl As Boolean, ByVal bCa As
Boolean, ByVal bK As Boolean, ByVal bNa As Boolean, ByVal bEx As Boolean, ByVal bNaK As Boolean, ByVal
bSponge As Boolean, ByVal bSpongeVar As Boolean)
```

NOTE: REMOVED MAJORITY OF DIMENSION LINES FOR BREVITY

```
If IO.File.Exists(locSim) = True Then
'Read File
oRead = IO.File.OpenText(locSim)
'Sim Variables
pH_e = oRead.ReadLine      'External pH
Suc_ef = oRead.ReadLine    'External Suc
Cl_ef = oRead.ReadLine     'External Chloride
Na_ef = oRead.ReadLine     'External Sodium
K_ef = oRead.ReadLine      'External Potassium
Ca_ef = oRead.ReadLine     'External Calcium
Protein_ef = oRead.ReadLine 'External final protein
N_SUT4 = oRead.ReadLine    'Number of Cotransporters
l_SUT4 = oRead.ReadLine    'Rate constant for Cotransporters
N_EX = oRead.ReadLine      'Number of Exchangers
l_EX = oRead.ReadLine     'Rate constant for exchangers
N_NaK = oRead.ReadLine     'Number of NaK ATPase
l_NaK = oRead.ReadLine    'Rate constant for NaK ATPase
n_W = oRead.ReadLine       'Water Stoichiometry for SUT4
CapS = oRead.ReadLine     'Water Capacitance (F/m2)
alpha = oRead.ReadLine    'Membrane Hydraulic Conductivity
ARadius = oRead.ReadLine  'Larger Radius
BRadius = oRead.ReadLine  'Smaller Radius
sigma = oRead.ReadLine    'Osmotic Reflection Coefficient
M_HPump = oRead.ReadLine  'Number of proton pumps in the membrane
l_HPump = oRead.ReadLine  'Rate Constant for pumps
n_H = oRead.ReadLine      'Number of protons transported per pump cycle
DATP0 = oRead.ReadLine    'Free energy release from ATP
Beta_H = oRead.ReadLine
D_H = oRead.ReadLine
HDiff = oRead.ReadLine    'Diff Constant
ClDiff = oRead.ReadLine
KDiff = oRead.ReadLine
delta = oRead.ReadLine    'Membrane Thickness
```

```

damp = oRead.ReadLine      'Expansion Damping
tau = oRead.ReadLine

'mobilities
u_H = oRead.ReadLine      'mobility of ions
u_S = oRead.ReadLine      'mobility of sucrose
u_W = oRead.ReadLine      'mobility of water
u_Cl = oRead.ReadLine     'mobility of Cl
u_K = oRead.ReadLine      'mobility of K
u_Na = oRead.ReadLine     'mobility of Na
u_Ca = oRead.ReadLine     'mobility of Ca

'Initial Conditions
pH_i0 = oRead.ReadLine    'Initial internal pH
Suc_i0 = oRead.ReadLine   'Initial internal Suc
Cl_i0 = oRead.ReadLine    'Initial internal Cl
Na_i0 = oRead.ReadLine    'Initial internal Na
K_i0 = oRead.ReadLine     'Initial internal K
Ca_i0 = oRead.ReadLine    'Initial internal Ca
Protein_i0 = oRead.ReadLine 'Initial internal Protein
Rho_0 = oRead.ReadLine    'Initial density of internal fluid
n0_ATP = oRead.ReadLine   'Initial scale of ATP (21 kb T default)
n0_P = oRead.ReadLine     'Initial amount of P_io available
n0_ADP = oRead.ReadLine   'Initial amount of ADP available
Mass_0 = oRead.ReadLine   'Initial mass of internal fluid
Temp_0 = oRead.ReadLine   'Initial internal temperature
bufferval = oRead.ReadLine 'Bufferval
spongeval = oRead.ReadLine 'ratio of H+ not absorbed by the sponge
Poissons = oRead.ReadLine 'Poisson's Ratio
YMod = oRead.ReadLine     'youngs modulus
RoC = oRead.ReadLine      'Rate of Change
'DATP0 = oRead.ReadLine * -k * Temp_0 / e
DATP0 = oRead.ReadLine * -(1 / (6.022 * 10 ^ 23)) * 10 ^ 6 * 1 / e
pKa1 = oRead.ReadLine
pKa2 = oRead.ReadLine
pKa3 = oRead.ReadLine
pKa4 = oRead.ReadLine
capmm = oRead.ReadLine
MW = oRead.ReadLine
ProtAm1 = oRead.ReadLine
ProtAm2 = oRead.ReadLine
ProtAm3 = oRead.ReadLine
ProtAm4 = oRead.ReadLine
d12 = oRead.ReadLine      'primary interaction
d23 = oRead.ReadLine      'secondary interaction
d13 = oRead.ReadLine      'tertiary interaction
kr1 = oRead.ReadLine
kr2 = oRead.ReadLine
kr3 = oRead.ReadLine
kdiss = oRead.ReadLine    'disassociation constant (rate)
sponger = oRead.ReadLine  'sponge radius
v_0 = oRead.ReadLine      'initial membrane potential
'num sponge = oRead.ReadLine
oRead.Close()
Else
iCase = 1
bRun = False
Call ErrorHandler(iCase, strMessage)
End If

If IO.File.Exists(locTime) = True Then
'Read File
oRead = IO.File.OpenText(locTime)
DT0 = oRead.ReadLine     'Initial timestep
DTMax = oRead.ReadLine   'Max Timestep
DTMin = oRead.ReadLine   'Min Timestep
TMax = oRead.ReadLine    'Maximum sim time
KMax = oRead.ReadLine    'Maximum number of steps

```

```

    RMax = oRead.ReadLine 'Maximum number of reiterated steps
    Nwrite = oRead.ReadLine 'Write to output every N steps
    oRead.Close()
Else
    iCase = 1
    bRun = False
    Call ErrorHandler(iCase, strMessage)
End If

If IO.File.Exists(locOut) = True Then
    IO.File.Delete(locOut)
End If
oWrite = IO.File.CreateText(locOut)

'Set variables
pH_i = pH_i0
Suc_i = Suc_i0
K_i = K_i0
Na_i = Na_i0
Cl_i = Cl_i0
Ca_i = Ca_i0
Protein_i = Protein_i0

Suc_e = Suc_ef
K_e = K_ef
Na_e = Na_ef
Cl_e = Cl_ef
Ca_e = Ca_ef
Protein_e = Protein_ef

Suc_eOld = Suc_e
K_eOld = K_e
Na_eOld = Na_e
Cl_eOld = Cl_e
Ca_eOld = Ca_e
Protein_eOld = Protein_e

Vol_0 = 4 / 3 * System.Math.PI * ARadius ^ 3 * 10 ^ -18 'keep in m3
If ARadius = BRadius Then
    A0 = 4 * System.Math.PI * ARadius ^ 2 * 10 ^ -12 'keep in m2
Else
    A0 = 4 * System.Math.PI * (ARadius ^ 2 + BRadius ^ 2 /
(System.Math.Sin(System.Math.Acos(BRadius / ARadius))) * System.Math.Log((1 +
System.Math.Sin(System.Math.Acos(BRadius / ARadius))) / (System.Math.Cos(System.Math.Acos(BRadius /
ARadius))))) * 10 ^ -12
End If

Vol = Vol_0
A = A0
AOld = A
Cap = A * CapS * 10 ^ -2 'Convert to F/m2 from uF/cm2 (10^-2)

ARadiusOld = ARadius
BRadiusOld = BRadius
ARadius0 = ARadius
BRadius0 = BRadius
Dim Radius As Double
Dim Radius0 As Double
Dim RadiusOld As Double

Radius = ARadius * 10 ^ -6
RadiusOld = Radius
Radius0 = Radius

n_ATP = n0_ATP
n_ADP = n0_ADP
DATP = DATP0

```

```

n_P = n0_P
VM = 0
HoopStress = 0
'convert to mV
v_K = (k * Temp) / (e) * System.Math.Log(K_e / K_i)
v_Na = (k * Temp) / (e) * System.Math.Log(Na_e / Na_i)
v_Cl = (k * Temp) / (-e) * System.Math.Log(Cl_e / Cl_i)
v_Ca = (k * Temp) / (2 * e) * System.Math.Log(Ca_e / Ca_i)

v = v_0
Rho = Rho_0      'This is currently constant
DT = DT0

Temp = Temp_0

ProtAm = ProtAm1 + ProtAm2 + ProtAm3 + ProtAm4      'sum up the protonation sites

capconv = capmm / MW * ProtAm      'convert from grams/m3 of sponge to moles * protonation
site

capacity = capconv * Vol      'converts to moles of protonable H+ (low val)

totstruct = capacity * avnum / ProtAm

rk1 = sponger      'outer - Y(16)
rk2 = 7 / 10 * sponger      'middle - Y(17)
rk3 = 4 / 10 * sponger      'inner - Y(18)
mfp = (ProtAm / (rk1 ^ 3 * 4 / 3 * System.Math.PI) * siter ^ 2 * System.Math.PI) ^ (-1)
mod1 = 1
mod2 = System.Math.Exp(-0.5 * (rk1 - rk2) ^ 2 / (mfp ^ 2))
mod3 = System.Math.Exp(-0.5 * (rk1 - rk3) ^ 2 / (mfp ^ 2))

'Divide among 3 sites according to protonation sites
capacity1 = capacity * ProtAm1 / (ProtAm)
capacity2 = capacity * ProtAm2 / (ProtAm)
capacity3 = capacity * ProtAm3 / (ProtAm)
capacity4 = capacity * ProtAm4 / (ProtAm)
H_e = 10 ^ -(pH_i) * 10 ^ 3
H_eOld = H_e
H_ef = 10 ^ -(pH_e) * 10 ^ 3
H_i0 = 10 ^ -(pH_i) * 10 ^ 3
H_si = 0
Y(1) = H_i0 * Vol      'convert pH to ion concentration (mM)
Y(2) = Suc_i * Vol      '* 10 ^ -6
Y(3) = v
Y(4) = Vol
Y(5) = n_ATP
Y(6) = 0      'Pressure Generated
Y(7) = 0.55      'Probability of Activation
Y(8) = K_i * Vol '* 10 ^ -6      'Concentrations are in mM or mol/m3
Y(9) = Na_i * Vol '* 10 ^ -6
Y(10) = Cl_i * Vol '* 10 ^ -6
Y(11) = Ca_i * Vol '* 10 ^ -6
Y(12) = 0.0      'Ca channels - all channels assumed to be shut at sim start
Y(13) = 0.0      'Na channels
Y(14) = 0.0      'Cl channels
Y(15) = 0.0      'K channels
'Introduce iteration loop here to obtain actual values
If bSpongeVar = False Then
    mod1 = 1
    mod2 = 1
    mod3 = 1
End If
'Iteration step - have to determine equilibrium value for each sponge. Begin at pH = 100
(ridiculously high)
'and iterate downwards, modifying pKa as it moves

```

```

'Dim F1, F2, F3 As Double
Y0(16) = 10 ^ (pKa1 - pH_i) / (1 + 10 ^ (pKa1 - pH_i)) * capacity1
Y0(17) = 10 ^ (pKa2 - pH_i) / (1 + 10 ^ (pKa2 - pH_i)) * capacity2
Y0(18) = 10 ^ (pKa3 - pH_i) / (1 + 10 ^ (pKa3 - pH_i)) * capacity3
Y0(19) = 10 ^ (pKa4 - pH_i) / (1 + 10 ^ (pKa4 - pH_i)) * capacity4
bRun = True

While (bRun) = True

    e0 = 8.85 * 10 ^ -12      'in F/m
    Dw = 75                  'consider constant as temperature is constant
    'calculate the ionic strength of the mixture - should be around 0.2 M
    IonS = 0.5 * (Na_i * 1 + Ca_i * 2 ^ 2 + K_i * 1 + Cl_i * 1 + H_i * 1) * 10 ^ -3

    n = (Y(16) + Y(17) + Y(18) + Y(19)) / capacity * 0.75 + 1
    Debl = ((Dw * e0 * k * 10 ^ -3 * Temp) / (2 * avnum * e ^ 2 * IonS)) ^ (1 / 2)
    rtest = (((sponger * n) ^ 3 * 4 / 3 * System.Math.PI) / (ProtAm - ProtAm4)) ^ 3 / (4 *
System.Math.PI) ^ (1 / 3) * 2
    rtest = sponger * n / 2
    r12 = (sponger * n - rtest) * 1 / 4 + rtest
    r23 = (n * sponger - rtest) * 1 / 2
    r13 = (n * sponger - rtest) * 3 / 4 + rtest
    V3 = ((sponger * n - rtest) * 1 / 2) ^ 3 * 4 / 3 * System.Math.PI
    V2 = ((sponger * n - rtest) * 1) ^ 3 * 4 / 3 * System.Math.PI - V3
    V1 = (sponger * n) ^ 3 * 4 / 3 * System.Math.PI - V3 - V2
    r33 = (((V3) / (ProtAm3)) ^ 3 / (4 * System.Math.PI)) ^ (1 / 3) * 2
    r22 = (((V2) / (ProtAm2)) ^ 3 / (4 * System.Math.PI)) ^ (1 / 3) * 2
    r11 = (((V1) / (ProtAm1)) ^ 3 / (4 * System.Math.PI)) ^ (1 / 3) * 2

    W12 = e ^ (2) * System.Math.Exp(-1 / Debl * r12) / (4 * System.Math.PI * e0 * Dw * r12)
    W13 = e ^ (2) * System.Math.Exp(-1 / Debl * r13) / (4 * System.Math.PI * e0 * Dw * r13)
    W23 = e ^ (2) * System.Math.Exp(-1 / Debl * r23) / (4 * System.Math.PI * e0 * Dw * r23)
    W11 = e ^ (2) * System.Math.Exp(-1 / Debl * r11) / (4 * System.Math.PI * e0 * Dw * r11)
    W22 = e ^ (2) * System.Math.Exp(-1 / Debl * r22) / (4 * System.Math.PI * e0 * Dw * r22)
    W33 = e ^ (2) * System.Math.Exp(-1 / Debl * r33) / (4 * System.Math.PI * e0 * Dw * r33)

    e12 = W12 / (k * 10 ^ -3 * Temp * System.Math.Log(10))
    e13 = W13 / (k * 10 ^ -3 * Temp * System.Math.Log(10))
    e23 = W23 / (k * 10 ^ -3 * Temp * System.Math.Log(10))
    e11 = W11 / (k * 10 ^ -3 * Temp * System.Math.Log(10))
    e22 = W22 / (k * 10 ^ -3 * Temp * System.Math.Log(10))
    e33 = W33 / (k * 10 ^ -3 * Temp * System.Math.Log(10))

    pK1 = pKa1 - e12 * Y0(17) / capacity2 - e13 * Y0(18) / capacity3 - 2 * e11 * Y0(16) /
capacity1
    pK2 = pKa2 - e12 * (Y0(16) + Y0(19)) / (capacity1) - e23 * Y0(18) / capacity3 - 2 * e22 *
Y0(17) / capacity2
    pK3 = pKa3 - e23 * Y0(17) / capacity2 - 2 * e33 * Y0(18) / capacity3 - e13 * (Y0(19) + Y0(16))
/ capacity1

    c1 = 10 ^ (-pH_i + pK1) / (1 + 10 ^ (-pH_i + pK1))
    c2 = 10 ^ (-pH_i + pK2) / (1 + 10 ^ (-pH_i + pK2))
    c3 = 10 ^ (-pH_i + pK3) / (1 + 10 ^ (-pH_i + pK3))
    c4 = 10 ^ (-pH_i + pKa4) / (1 + 10 ^ (-pH_i + pKa4))
    c11 = 10 ^ (pH_i - pK1) / (1 + 10 ^ (pH_i - pK1))
    c12 = 10 ^ (pH_i - pK2) / (1 + 10 ^ (pH_i - pK2))
    c13 = 10 ^ (pH_i - pK3) / (1 + 10 ^ (pH_i - pK3))
    c14 = 10 ^ (pH_i - pKa4) / (1 + 10 ^ (pH_i - pKa4))
    Y(16) = (10 ^ (pK1 - pH_i) / (1 + 10 ^ (pK1 - pH_i)) * capacity1 - Y0(16)) * 1 / 2 + Y0(16)
    Y(17) = (10 ^ (pK2 - pH_i) / (1 + 10 ^ (pK2 - pH_i)) * capacity2 - Y0(17)) * 1 / 2 + Y0(17)
    Y(18) = (10 ^ (pK3 - pH_i) / (1 + 10 ^ (pK3 - pH_i)) * capacity3 - Y0(18)) * 1 / 2 + Y0(18)
    Y(19) = (10 ^ (pKa4 - pH_i) / (1 + 10 ^ (pKa4 - pH_i)) * capacity4 - Y0(19)) * 1 / 2 + Y0(19)

    Dim errsum As Double
    errsum = System.Math.Abs(Y(16) - Y0(16)) + System.Math.Abs(Y(17) - Y0(17)) +
System.Math.Abs(Y(18) - Y0(18)) + System.Math.Abs(Y(19) - Y0(19))
    errsum = errsum / capacity

```

```

If (errsum < 0.000000000001) Then
    bRun = False
End If
Y0(16) = Y(16)
Y0(17) = Y(17)
Y0(18) = Y(18)
Y0(19) = Y(19)

End While
'values calculated in titration studies - similar protonation levels at all sponge at onset

sponge0 = (Y(16) + Y(17) + Y(18) + Y(19)) / Y(4)

'Write Initial Data
TIME = 0
TIME0 = TIME
iChannelH = 0
iCT = 0
iHDiff = 0
iClDiff = 0
iPump = 0
iChannelH = 0
dPi0 = R * (10 ^ -3) * Temp * 0.73 * ((H_i - H_e) + (Na_i - Na_e) + (Cl_i - Cl_e) + (K_i - K_e) +
(Ca_i - Ca_e) + (Protein_i - Protein_e))
dPi0 = R * (10 ^ -3) * Temp * 0.73 * ((Na_i - Na_e) + (Cl_i - Cl_e) + (K_i - K_e) + (Ca_i - Ca_e)
+ (Protein_i - Protein_e))
'Determine initial radius
'Radius0 = (Vol * (3 / 4) * (1 / System.Math.PI)) ^ (1 / 3)

oWrite.WriteLine("INC TIME(s) pH_i H_i H_si iDetach DATP Suc_i(mM) Suc_e K_i K_e Na_i Na_e Ca_i
Ca_e Cl_i Cl_e v(mV) VOL(um3) Area(um2) nATP P pHoop VM dPi iCT(pA) iNaCa iNaK iPump iHDiff iClDiff
iChannH iChannS iChannCl iChannK iChannNa iChannCa f DV S1 S2 S3 STot Astrain sumH pH_i pKa1 pKa2 pKa3")
'Header Information
oWrite.WriteLine(KINC & " " & TIME / TMax * 100 & " " & pH_i & " " & " " & H_i & " " & H_si & " "
& iDetach & " " & DATP & " " & Suc_i & " " & Suc_e & " " & K_i & " " & K_e & " " & Na_i & " " & Na_e & " "
& Ca_i & " " & Ca_e & " " & Cl_i & " " & Cl_e & " " & v & " " & Vol * 10 ^ 18 & " " & A & " " & n_ATP & " "
& Pressure & " " & HoopStress & " " & VM & " " & dPi & " " & iCT & " " & " " & iEX & " " & iNaK & " " &
iPump & " " & iHDiff & " " & iClDiff & " " & iChannelH & " " & iChannelS & " " & iChannelCL & " " &
iChannelK & " " & iChannelNa & " " & iChannelCa & " " & Y(7) & " " & DV & " " & Y(16) + Y(19) & " " &
Y(17) & " " & Y(18) & " " & ispongetot & " " & (A - A0) / A0 & " " & (H_i + sponge0sm) * Vol * 10 ^ 18 & " "
& pH_i & " " & pK1 & " " & pK2 & " " & pK3)
oWrite.Close()
'Start Loop
KINC = 1
For i = 1 To Nvar 'Store initial values in case run needs to be restarted.
    Y0(i) = Y(i)
Next
bRun = True
While bRun = True
    'Store old time
    TIME0 = TIME
    For i = 1 To 7

        H_i = Y(1) / Y(4) '* 10 ^ 6
        H_si = (Y(17) + Y(16) + Y(18) + Y(19)) / Y(4) '* 10 ^ 6
        Suc_i = Y(2) / Y(4) '* 10 ^ 6
        K_i = Y(8) / Y(4) '* 10 ^ 6
        Na_i = Y(9) / Y(4) '* 10 ^ 6
        Cl_i = Y(10) / Y(4) '* 10 ^ 6
        Ca_i = Y(11) / Y(4) '* 10 ^ 6
        If pH_i0 < pH_i Then
            pH_i = -System.Math.Log10((10 ^ -(pH_i0)) + ((Y(1) * 10 ^ -3) - (10 ^ -(pH_i0))))
        End If

        'Osmotic Pressure Generated - Pa
        sponge0sm = (H_si * Y(4) - sponge0 * Vol_0) / Y(4)
    
```

```

dPi = R * (10 ^ -3) * Temp * 0.73 * ((spongeOsm) + (Na_i - Na_e) + (Cl_i - Cl_e) + (K_i -
K_e) + (Ca_i - Ca_e) + (Protein_i - Protein_e))
dPi = dPi - dPi0

'Nernst Equilibrium
'Units are in mV - CHECKED
v_H = (k * Temp) / (e) * System.Math.Log(H_e / H_i) * SCALE
v_Suc = (k * Temp) / (e) * System.Math.Log((Suc_e) / (Suc_i)) * SCALE
v_W = (k * Temp) / (e) * V_bar_H2O / F * dPi * SCALE
v_K = (k * Temp) / (e) * System.Math.Log(K_e / K_i) * SCALE
v_Na = (k * Temp) / (e) * System.Math.Log(Na_e / Na_i) * SCALE
v_Cl = (k * Temp) / (-e) * System.Math.Log(Cl_e / Cl_i) * SCALE
v_Ca = (k * Temp) / (2 * e) * System.Math.Log(Ca_e / Ca_i) * SCALE

If n_H > 0 Then
  If bCT = True Then
    'CONVERT TO pA (10^12)
    kCT = 2 * N_SUT4 * e * l_SUT4 * Rho * System.Math.Sqrt(H_e * H_i * Suc_e / Rho *
Suc_i / Rho) * 10 ^ 12
    'Moves ions into the inclusion
    iCT = kCT * System.Math.Sinh(0.5 * (e * (Y(3) - n_W * v_W - v_H - v_Suc) / (k *
Temp)))
  Else
    iCT = 0
  End If
Else
  If bCT = True Then
    'CONVERT TO pA (10^12)
    kCT = 2 * N_SUT4 * e * l_SUT4 * Rho * System.Math.Sqrt(H_e * H_i * Suc_e / Rho *
slue * Suc_i / Rho * slui * (slve * slvi) ^ n_W) * 10 ^ 12
    'Moves ions out of the inclusion
    iCT = kCT * System.Math.Sinh(0.5 * (e * (Y(3) - n_W * v_W + v_H - v_Suc) / (k *
Temp)))
  Else
    iCT = 0
  End If
End If
'Exchanger Calculations
If bEx = True Then
  'CONVERT TO pA (10^12)
  kEX = 2 * N_EX * e * l_EX * Rho * System.Math.Sqrt((Na_e / Rho) ^ 3 * (Na_i / Rho) ^ 3
* (Ca_i / Rho) ^ 2 * (Ca_e / Rho) ^ 2) * 10 ^ 12
  'kEX = 1400
  iEX = kEX * System.Math.Sinh(0.5 * (e * (Y(3) - 3 * v_Na + 2 * v_Ca) / (k * Temp)))
Else
  iEX = 0
End If
'Determine energy release from ATP Hydrolysis
If bATP = True Then
  V_ATP = Vol_0
  V_ADP = Vol_0
  V_P = Vol_0
  n_ADP = n0_ADP
  n_P = n0_P
  n_ADP = n0_ADP
Else
  n_ADP = n0_ADP + n0_ATP - Y(5)
  n_P = n0_P + n0_ATP - Y(5)
  V_ATP = Y(4)
  V_ADP = Y(4)
  V_P = Y(4)
End If
'NaKATPase
If bNaK = True Then
  kNaK = 2 * N_NaK * e * l_NaK * 10 ^ 12
  iNaK = kNaK * System.Math.Tanh((e * (Y(3) - DATP + 3 * v_Na - 2 * v_K) / (2 * k *
Temp)))

```

```

Else
    iNaK = 0
End If
'Pump current
If bPump = True Then
    Dim checkval3 As Double
    checkval3 = e * (n_H * Y(3) - DATP - n_H * v_H) / (2 * k * Temp)
    kPump = M_HPump * e * l_HPump * 10 ^ 12 * A / A0
    iPump = kPump * System.Math.Tanh((e * (n_H * Y(3) - DATP - n_H * v_H) / (2 * k *
Temp)))

Else
    iPump = 0
End If

'Diffusion
If bDiff = True Then
    If (1 - System.Math.Exp((-F * Y(3)) / (R * Temp))) <> 0 Then
        iHDiff = -HDiff * A * A / A0 * F * (F * Y(3) + 0) / (R * Temp) * ((10 ^ -(pH_i) *
10 ^ 3) - H_ef * System.Math.Exp(-1 * F * Y(3) / (R * Temp))) / (1 - System.Math.Exp(-1 * F * Y(3) / (R *
Temp))) * 10 ^ 12
        iKDiff = -KDiff * A * F * (F * Y(3) + 0) / (R * Temp) * (K_i - K_ef *
System.Math.Exp(-1 * F * Y(3) / (R * Temp))) / (1 - System.Math.Exp(-1 * F * Y(3) / (R * Temp))) * 10 ^ 12
        If iKDiff > 0 Then
            iKDiff = 0 'No diffusion inwards from exterior
        End If
    Else
        iHDiff = HDiff * A * A / A0 * (H_e - (10 ^ -(pH_i) * 10 ^ 3)) * 10 ^ 12
        iKDiff = KDiff * A * F * (K_e - K_i) * 10 ^ 12
    End If
    If (1 - System.Math.Exp((F * Y(3)) / (R * Temp))) <> 0 Then
        iClDiff = -ClDiff * A * A / A0 * F * -(F * Y(3) + 0) / (R * Temp) * (Cl_i - Cl_ef
* System.Math.Exp(1 * F * Y(3) / (R * Temp))) / (1 - System.Math.Exp(1 * F * Y(3) / (R * Temp))) * 10 ^ 12
    Else
        iClDiff = ClDiff * A * A / A0 * F * (Cl_e - Cl_i) * 10 ^ 12
    End If
End If
Else
    iHDiff = 0
    iClDiff = 0
    iKDiff = 0
End If

'Channels
If bChann = True Then

    If bIon = True Then
        kCH = 2 * k * u_H * Y(7) * System.Math.Sqrt(H_e * H_i) * 10 ^ 12
        iChannelH = kCH * System.Math.Sinh(e * (Y(3) - v_H) / (2 * k * Temp))
    Else
        iChannelH = 0
    End If

    If bSuc = True Then
        kCSuc = 2 * k * u_S * Y(7) * System.Math.Sqrt(mSuce * slue * mSuci * slui) * 10 ^
12
        iChannelS = kCSuc * System.Math.Sinh(e * (Y(3) - v_Suc) / (2 * k * Temp))
    Else
        iChannelS = 0
    End If

'Declare activation potential = -5
If bCl = True Then
    dinf = 0.5 * (1 + System.Math.Tanh(-2 * e * (Y(3) - 6.6) / (k * Temp)))
    kCCl = 2 * k * u_Cl * Y(14) * dinf

```

```

        iChannelCL = kCCl * System.Math.Sinh(-1 * e * (Y(3) + v_C1) / (2 * k * Temp))

Else
    iChannelCL = 0
End If

If bK = True Then
    kCK = u_K * Y(15) '* dinf
    iChannelK = kCK * System.Math.Sinh(e * (Y(3) - v_K) / (2 * k * Temp))
Else
    iChannelK = 0
End If

If bCa = True Then

    dinf = 0.5 * (1 + System.Math.Tanh(2 * e * (Y(3) + 6.6) / (k * Temp)))
    kCCa = (u_Ca * (1 - Y(12)) * dinf + 0.01645) * 10 ^ -9 'Endresen
    iChannelCa = kCCa * System.Math.Sinh(e * (Y(3) - v_Ca) / (k * Temp))
Else
    iChannelCa = 0
End If

If bNa = True Then
    kCNa = u_Na * Y(13) '* minf 'Endresen
    iChannelNa = kCNa * System.Math.Sinh(e * (Y(3) - v_Na) / (2 * k * Temp))
Else
    iChannelNa = 0
End If
Else 'All channels are disabled. Set flows to zero.
    iChannelS = 0
    iChannelH = 0
    iChannelW = 0
    iChannelCL = 0
    iChannelCa = 0
    iChannelNa = 0
    iChannelK = 0
End If

Radius = (Y(4) / (4 / 3 * System.Math.PI)) ^ (1 / 3)

A = 4 * System.Math.PI * Radius ^ 2

Cap = CapS * A * 10 ^ -2 'CapS is in uF/cm2, convert to F/m2
Radius = (Y(4) * (3 / 4) * (1 / System.Math.PI)) ^ (1 / 3)

'Determine internal pressure from the change in radius
Dim lambda As Double = Radius / Radius0
If bP = False Then
    pStat = 2 * (YMod) / (Radius0 * lambda) * (10 ^ 3) * (1 - 1 / (lambda ^ 6)) *
System.Math.Exp(0.067 * (2 * lambda ^ 2 - lambda ^ -4 - 3))
Else
    pStat = 0
End If

HoopStress = pStat * Radius / (2 * delta * 10 ^ -6)
'If pStat > 10 Then
'pStat = pStat
'End If

'alpha should be 0.052E-2 m/sec
DV = (alpha * V_bar_H20) / (R * 10 ^ -3 * Temp) * A * (sigma * dPi - (pStat)) + (iClDiff *
10 ^ -12) / F * V_bar_C1

'Increase the total number of protons
'convert from pA to A, then divide by Faraday's Constant - results in change in moles

```

```

D(1) = ((-iCT - n_H * iPump - iChannelH + iHDiff) / (F)) * 10 ^ -12

D(16) = 0
D(17) = 0
D(18) = 0
D(19) = 0

'Dim F1, F2, F3 As Double
e0 = 8.85 * 10 ^ -12 'in F/m
Dw = 75 'consider constant as temperature is constant
'calculate the ionic strength of the mixture - should be around 0.2 M
IonS = 0.5 * (Na_i * 1 + Ca_i * 2 ^ 2 + K_i * 1 + Cl_i * 1 + H_i * 1) * 10 ^ -3

n = (Y(16) + Y(17) + Y(18) + Y(19)) / capacity * 0.75 + 1

Debl = ((Dw * e0 * k * 10 ^ -3 * Temp) / (2 * avnum * e ^ 2 * IonS)) ^ (1 / 2)

rtest = (((sponger * n) ^ 3 * 4 / 3 * System.Math.PI) / (ProtAm - ProtAm4)) * 3 / (4
* System.Math.PI) ^ (1 / 3) * 2
rtest = sponger * n / 2
r12 = (sponger * n - rtest) * 1 / 4 + rtest
r23 = (n * sponger - rtest) * 1 / 2
r13 = (n * sponger - rtest) * 3 / 4 + rtest
V3 = ((sponger * n - rtest) * 1 / 2) ^ 3 * 4 / 3 * System.Math.PI
V2 = ((sponger * n - rtest) * 1) ^ 3 * 4 / 3 * System.Math.PI - V3
V1 = (sponger * n) ^ 3 * 4 / 3 * System.Math.PI - V3 - V2
r33 = (((V3) / (ProtAm3)) * 3 / (4 * System.Math.PI)) ^ (1 / 3) * 2
r22 = (((V2) / (ProtAm2)) * 3 / (4 * System.Math.PI)) ^ (1 / 3) * 2
r11 = (((V1) / (ProtAm1)) * 3 / (4 * System.Math.PI)) ^ (1 / 3) * 2

W12 = e ^ (2) * System.Math.Exp(-1 / Debl * r12) / (4 * System.Math.PI * e0 * Dw *
r12)
W13 = e ^ (2) * System.Math.Exp(-1 / Debl * r13) / (4 * System.Math.PI * e0 * Dw *
r13)
W23 = e ^ (2) * System.Math.Exp(-1 / Debl * r23) / (4 * System.Math.PI * e0 * Dw *
r23)
W11 = e ^ (2) * System.Math.Exp(-1 / Debl * r11) / (4 * System.Math.PI * e0 * Dw *
r11)
W22 = e ^ (2) * System.Math.Exp(-1 / Debl * r22) / (4 * System.Math.PI * e0 * Dw *
r22)
W33 = e ^ (2) * System.Math.Exp(-1 / Debl * r33) / (4 * System.Math.PI * e0 * Dw *
r33)

e12 = W12 / (k * 10 ^ -3 * Temp * System.Math.Log(10))
e13 = W13 / (k * 10 ^ -3 * Temp * System.Math.Log(10))
e23 = W23 / (k * 10 ^ -3 * Temp * System.Math.Log(10))
e11 = W11 / (k * 10 ^ -3 * Temp * System.Math.Log(10))
e22 = W22 / (k * 10 ^ -3 * Temp * System.Math.Log(10))
e33 = W33 / (k * 10 ^ -3 * Temp * System.Math.Log(10))

pK1 = pKa1 - e12 * Y(17) / capacity2 - e13 * Y(18) / capacity3 - 2 * e11 * (Y(16) +
Y(19)) / capacity1
pK2 = pKa2 - e12 * (Y(16) + Y(19)) / (capacity1) - e23 * Y(18) / capacity3 - 2 * e22 *
Y(17) / capacity2
pK3 = pKa3 - e23 * Y(17) / capacity2 - 2 * e33 * Y(18) / capacity3 - e13 * (Y(19) +
Y(16)) / capacity1

c1 = 10 ^ (-pH_i + pK1) / (1 + 10 ^ (-pH_i + pK1))
c2 = 10 ^ (-pH_i + pK2) / (1 + 10 ^ (-pH_i + pK2))
c3 = 10 ^ (-pH_i + pK3) / (1 + 10 ^ (-pH_i + pK3))
c4 = 10 ^ (-pH_i + pKa4) / (1 + 10 ^ (-pH_i + pKa4))
c11 = 10 ^ (pH_i - pK1) / (1 + 10 ^ (pH_i - pK1))

```

```

c12 = 10 ^ (pH_i - pK2) / (1 + 10 ^ (pH_i - pK2))
c13 = 10 ^ (pH_i - pK3) / (1 + 10 ^ (pH_i - pK3))
c14 = 10 ^ (pH_i - pKa4) / (1 + 10 ^ (pH_i - pKa4))

D(16) += kr1 * (capacity1 - Y(16)) * c1
D(17) += kr2 * (capacity2 - Y(17)) * c2
D(18) += kr3 * (capacity3 - Y(18)) * c3
D(19) += kr1 * (capacity4 - Y(19)) * c4

D(16) = D(16) - kr1 * Y(16) * c11
D(17) = D(17) - kr1 * Y(17) * c12
D(18) = D(18) - kr2 * Y(18) * c13
D(19) = D(19) - kr1 * Y(19) * c14

acidification 'Currently the sponges are releasing into the surroundings - must avoid initial
'if the total is less than the initial concentration, nullify diss
'spongeOsm = (H_si * Y(4) - sponge0 * Vol_0) / Y(4)
If bSponge = False Then
    D(16) = 0
    D(17) = 0
    D(18) = 0
    D(19) = 0
End If

ispongetot = D(16) + D(17) + D(18) + D(19)
D(1) = D(1) - ispongetot

Else
    D(1) = 0
End If

'Sucrose Concentration
If bCT = True Or bSuc = True Then
    D(2) = (-iChannelS - iCT) / (F * Y(4)) * 10 ^ 3 'convert from pA
Else
    D(2) = 0
End If

D(3) = (-1 / Cap) * (iCT - (1) * (iPump + iHDiff) + iChannelH - iKDiff - iChannelCL +
iClDiff + iChannelCa + iChannelK + iChannelNa + iEX - iNaK) * 10 ^ -9 'mV

'Volume Change
D(4) = DV

'New coefficients
'CHANGES SHOULD BE IN moles / sec

D(8) = (-2 * iNaK - iChannelK + iKDiff) / (F) * 10 ^ -12 'Internal K
D(9) = (+3 * iNaK - iChannelNa - 3 * iEX) / (F) * 10 ^ -12 'Internal Na
D(10) = (-iChannelCL + iClDiff) / (F) * 10 ^ -12 'Internal Cl - Cl charge is negative
D(11) = (2 * iEX - iChannelCa) / (2 * F) * 10 ^ -12 'Internal Ca

'ATP used in the ATPases
If bATP = False Then 'Not constant ATP
    D(5) = (-System.Math.Abs(iPump + iEX)) / (F * Y(4)) ' * 10 ^ 3
Else
    D(5) = 0
End If

'Pressure Calculations
If bP = False Then 'Calc Pressure

```

```

'pStat = 0
If bDamp = True Then 'No Damping
    D(6) = 0
Else
    D(6) = (DV * damp) / DT
    D(6) = 0 'temp disabled
    pDyn = ((3 / 4 * 1 / System.Math.PI * (DV + Vo1)) ^ (1 / 3) - (3 / 4 * 1 /
System.Math.PI * (Vo1)) ^ (1 / 3)) * damp / DT
    pDyn = 0
End If
Else
    pStat = 0
    D(6) = 0
End If

'Channel Activation
If bIon = True And bChann = True Then
    D(7) = 1 / tau * System.Math.Cosh(2 * e * (Y(3) + 10) / (k * Temp)) * (0.5 * (1 +
System.Math.Tanh(2 * e * (Y(3) + 10) / (k * Temp))) - Y(7))
    D(7) = 0
Else
    D(7) = 0
End If

If bCa = True And bChann = True Then
    'vx = -25.1 - Endresen
    D(12) = 1 / tau * System.Math.Cosh(2 * e * (Y(3) - 85) / (k * Temp)) * (0.5 * (1 +
System.Math.Tanh(2 * e * (Y(3) - 85) / (k * Temp))) - Y(12))
    Else
    D(12) = 0
End If

If bNa = True And bChann = True Then
    'vh = -91.0 - Endresen
    'was 40
    If bflag = False Then
        D(13) = 1 / (5 * tau) * System.Math.Cosh(2 * e * (Y(3) - 45) / (k * Temp)) * (0.5
* (1 - System.Math.Tanh(2 * e * (Y(3) - 45) / (k * Temp))) - Y(13))
    Else
        D(13) = 1 / (5 * tau) * System.Math.Cosh(2 * e * (Y(3) + 5) / (k * Temp)) * (0.5 *
(1 - System.Math.Tanh(2 * e * (Y(3) + 5) / (k * Temp))) - Y(13))
    End If
Else
    D(13) = 0
End If
'Check calcs
If bCl = True And bChann = True Then
    'activation potential = 100
    D(14) = 1 / tau * System.Math.Cosh(2 * e * (Y(3) - 65) / (k * Temp)) * (0.5 * (1 +
System.Math.Tanh(2 * e * (Y(3) - 65) / (k * Temp))) - Y(14))
    'D(14) = 0
Else
    D(14) = 0
End If
'Select appropriate matrix to copy to (D -> K)
If bK = True And bChann = True Then
    'vx = -25.1 - Endresen - CHECK THIS
    If bflag = False Then
        D(15) = 1 / (15 * tau) * System.Math.Cosh(2 * e * (Y(3) - 40) / (k * Temp)) * (0.5
* (1 - System.Math.Tanh(2 * e * (Y(3) - 40) / (k * Temp))) - Y(15))
    Else
        D(15) = 1 / (15 * tau) * System.Math.Cosh(2 * e * (Y(3) - 75) / (k * Temp)) * (0.5
* (1 - System.Math.Tanh(2 * e * (Y(3) - 75) / (k * Temp))) - Y(15))
    End If
Else
    D(15) = 0
End If
Select Case i

```

```

Case 1
  For j = 1 To Nvar
    K1(j) = D(j)
  Next
Case 2
  For j = 1 To Nvar
    K2(j) = D(j)
  Next
Case 3
  For j = 1 To Nvar
    K3(j) = D(j)
  Next
Case 4
  For j = 1 To Nvar
    K4(j) = D(j)
  Next
Case 5
  For j = 1 To Nvar
    K5(j) = D(j)
  Next
Case 6
  For j = 1 To Nvar
    K2(j) = D(j)
  Next
Case 7
  For j = 1 To Nvar
    K3(j) = D(j)
  Next
End Select

'Every step innocent until proven guilty
bAccept = True

'Calculate next step dependent on current step - integration.
Select Case i
Case 1
  For j = 1 To Nvar
    Y1(j) = Y0(j) + DT * 0.2 * K1(j)
  Next
  If Y1(2) < 0 Or Y1(4) < 0 Or Y1(5) < 0 Then
    bAccept = False
    i = 8
  End If
  TIME = TIME0 + 0.2 * DT
Case 2
  For j = 1 To Nvar
    Y1(j) = Y0(j) + DT * (CDec(3 / 40) * K1(j) + CDec(9 / 40) * K1(j))
  Next
  If Y1(2) < 0 Or Y1(4) < 0 Or Y1(5) < 0 Then
    bAccept = False
    i = 8
  End If
  TIME = TIME0 + 0.3 * DT
Case 3
  For j = 1 To Nvar
    Y1(j) = Y0(j) + DT * (CDec(44 / 45) * K1(j) - CDec(56 / 15) * K2(j) + CDec(32
/ 9) * K3(j))
  Next
  If Y1(2) < 0 Or Y1(4) < 0 Or Y1(5) < 0 Then
    bAccept = False
    i = 8
  End If
  TIME = TIME0 + 0.8 * DT
Case 4
  For j = 1 To Nvar
    Y1(j) = Y0(j) + DT * (CDec(19372 / 6561) * K1(j) - CDec(25360 / 2187) * K2(j)
+ CDec(64448 / 6561) * K3(j) - (212 / 729) * K4(j))
  Next
  If Y1(2) < 0 Or Y1(4) < 0 Or Y1(5) < 0 Then

```

```

        bAccept = False
        i = 8
    End If
    TIME = TIME0 + 0.8 / 0.9 * DT
    Case 5
        For j = 1 To Nvar
            Y1(j) = Y0(j) + DT * (CDec(9017 / 3168) * K1(j) - CDec(355 / 33) * K2(j) +
CDec(46732 / 5247) * K3(j) + CDec(49 / 176) * K4(j) - CDec(5103 / 18656) * K5(j))
        Next
        If Y1(2) < 0 Or Y1(4) < 0 Or Y1(5) < 0 Then
            bAccept = False
            i = 8
        End If
        TIME = TIME0 + DT
    Case 6
        For j = 1 To Nvar
            Y1(j) = Y0(j) + DT * (CDec(35 / 384) * K1(j) + CDec(500 / 1113) * K3(j) +
CDec(125 / 192) * K4(j) - CDec(2187 / 6784) * K5(j) + CDec(11 / 84) * K2(j))
        Next
        For j = 1 To Nvar
            K2(j) = CDec(71 / 57600) * K1(j) - CDec(71 / 16695) * K3(j) + CDec(71 / 1920)
* K4(j) - CDec(17253 / 339200) * K5(j) + CDec(22 / 525) * K2(j)
        Next
    Case 7
        For j = 1 To Nvar
            'K4(j) = (K2(j) - (1 / 40) * K3(j)) * DT
            K4(j) = DT * K2(j) - CDec(1 / 40) * K3(j) * DT
        Next
    End Select
ERR:
    If bAccept = True Then
        'Shift forwards
        For j = 1 To Nvar
            Y(j) = Y1(j)
        Next
    End If
Next
CheckErr:
    'Check error
    Dim Err As Double
    Dim Denom As Double
    Dim storeval As Double
    Dim EPS As Double = 0.000005
    Dim DTNew As Double
    If bAccept = True Then 'If the step hasn't been rejected yet, check for errors
        Err = 0
        For i = 1 To Nvar
            storeval = System.Math.Max(System.Math.Abs(Y1(i)), System.Math.Abs(Y0(i)))
            Denom = System.Math.Max(EPS, storeval)
            Err = Err + (K4(i) / Denom) ^ 2
        Next
        Err = System.Math.Sqrt(Err / Nvar)
        DTNew = DT * System.Math.Min(5, System.Math.Max(0.1, (EPS / Err) ^ (1 / 5) * 0.85))
        If Double.IsNaN(DTNew) = True Then
            DTNew = DT * 0.5
        End If

        'Check for negative concentrations
        If Y1(8) < 0 Or Y1(9) < 0 Or Y1(10) < 0 Or Y1(11) < 0 Or Y1(1) < 0 Or Y1(16) < 0 Or Y1(17)
< 0 Or Y1(18) < 0 Then
            bAccept = False
        End If

        If System.Math.Abs(Err) > EPS Or Double.IsNaN(Err) = True Or Double.IsInfinity(Err) = True
Then
            bAccept = False
        End If
    End If
End If

```

```

'Check for criteria for each step
If bAccept = True Then
    KREJ = 0
    For i = 0 To (Nvar - 1)
        Y(i) = Y1(i)
        K1(i) = K3(i)
    Next
    Vol = Y(4)

    If Y(13) > 0.9 And Y(3) < 5 And TIME > 17 Then
        bflag = True
    End If

    Pressure = Y(6) + pStat
    Pressure = pStat '+ pDyn

    v = Y(3)

    pH_i = (pH_i0 - (Y(1) - H_i0 * Vol_0) / Y(4) * 1 / (bufferval))

    H_i = Y(1) / Y(4)
    H_si = (Y(18) + Y(17) + Y(16) + Y(19)) / Y(4)
    Suc_i = Y(2) / Y(4) '* 10 ^ 6
    K_i = Y(8) / Y(4) '* 10 ^ 6
    Na_i = Y(9) / Y(4) '* 10 ^ 6
    Cl_i = Y(10) / Y(4) '* 10 ^ 6
    Ca_i = Y(11) / Y(4) '* 10 ^ 6

    spongeOsm = (H_si * Y(4) - sponge0 * Vol_0) / Y(4)
    Radius = (Vol * (3 / 4) * (1 / System.Math.PI)) ^ (1 / 3)
    A = 4 * System.Math.PI * Radius ^ 2
    pStatOld = pStat
    pDynOld = pDyn
    'Determine internal pressure from the change in radius
    Dim lambda As Double = Radius / Radius0
    If bP = False Then
        'Units are in N/m2 (0.006 is in dyne/cm,
        'Shear Modulus is only listed as "VERY LOW" - modify by 10^-10
        pStat = 2 * (0.006) / (Radius0 * lambda) * (10 ^ -10) * (1 - 1 / (lambda ^ 6)) *
System.Math.Exp(0.067 * (2 * lambda ^ 2 - lambda ^ -4 - 3))
        pStat = 0
    Else
        pStat = 0
    End If
    If pStat > 10 Then
        pStat = pStat
    End If

    'Write information to the output file
    If Nwritecount >= Nwrite Then
        owrite = IO.File.AppendText(locOut)
        owrite.WriteLine(KINC & " " & TIME / TMax * 100 & " " & pH_i & " " & " " & H_i & " " &
H_si & " " & iDetach & " " & DATP & " " & Suc_i & " " & Suc_e & " " & K_i & " " & K_e & " " & Na_i & " " &
Na_e & " " & Ca_i & " " & Ca_e & " " & Cl_i & " " & Cl_e & " " & v & " " & Vol * 10 ^ 18 & " " & A & " " &
n_ATP & " " & Pressure & " " & HoopStress & " " & VM & " " & dPi & " " & iCT & " " & " " & iEX & " " &
iNaK & " " & iPump & " " & iHDiff & " " & iClDiff & " " & iChannelH & " " & iChannelS & " " & iChannelCL &
" " & iChannelK & " " & iChannelNa & " " & iChannelCa & " " & Y(7) & " " & DV & " " & Y(16) + Y(19) & " "
& Y(17) & " " & Y(18) & " " & ispongetot & " " & (A - A0) / A0 & " " & (H_i + spongeOsm) * Vol * 10 ^ 18 &
" " & pH_i & " " & pK1 & " " & pK2 & " " & pK3)
        owrite.Close()
        Nwritecount = 1
    Else
        Nwritecount = Nwritecount + 1
    End If

    Suc_eOld = Suc_e
    K_eOld = K_e

```

```

Na_eOld = Na_e
Cl_eOld = Cl_e
Ca_eOld = Ca_e
H_eOld = H_e
AOld = A
RadiusOld = Radius
'ARadiusOld = ARadius
'BRadiusOld = BRadius
Protein_eOld = Protein_e

old0 = oldold
For i = 1 To Nvar 'Store values in case run needs to be restarted.
    Y0(i) = Y(i)
Next
TIME = TIME0 + DT
DT = DTNew
If DT > DTMax Then
    DT = DTMax
End If
KINC = KINC + 1
If TIME > TMax Or KINC > KMax Then
    bRun = False
    strMessage = "Run successfully completed"
End If
Else
    KREJ = KREJ + 1

    pH_i = (pH_i0 - (Y0(1) - H_i0 * Vol_0) / Y0(4) * 1 / (bufferval))
    'pH_i = Y0(15)
    Suc_i = Y0(2) / Y0(4) '* 10 ^ 6
    K_i = Y0(8) / Y0(4) '* 10 ^ 6
    Na_i = Y0(9) / Y0(4) '* 10 ^ 6
    Cl_i = Y0(10) / Y0(4) '* 10 ^ 6
    Ca_i = Y0(11) / Y0(4) '* 10 ^ 6
    H_i = Y0(1) / Y0(4)
    H_si = (Y0(18) + Y0(17) + Y0(16) + Y0(19)) / Y0(4)

    Suc_e = Suc_eOld
    K_e = K_eOld
    Na_e = Na_eOld
    Cl_e = Cl_eOld
    Ca_e = Ca_eOld
    H_e = H_eOld
    A = AOld
    Radius = RadiusOld
    Protein_e = Protein_eOld

    oldold = old0

    pStat = pStatOld
    pDyn = pDynOld

    v = Y0(3)
    Vol = Y0(4)
    n_ATP = Y0(5)
    n_ADP = n0_ADP + n0_ATP - Y0(5)
    n_P = n0_P + n0_ATP - Y0(5)
    TIME = TIME0
    DT = DT / 2
    For i = 1 To Nvar
        Y(i) = Y0(i)
    Next
    If KREJ > RMax Then
        Call ErrorHandler(2, strMessage)
        bRun = False
    End If
    If DT < DTMin Then
        Call ErrorHandler(3, strMessage)
        bRun = False
    End If

```

```
        End If
        'Restart
    End If
End While

'Final Steps
oWrite.Close()

End Sub
Public Sub ErrorHandle(ByVal iCase As Integer, ByRef strMessage As String)
    Select Case (iCase)
        Case 1
            strMessage = "File does not exist. Create file or check location - run terminated."
        Case 2
            strMessage = "Maximum reiterations exceeded - run terminated."
        Case 3
            strMessage = "Recommended timestep below minimum - run terminated."
        Case 4
    End Select
End Sub
End Module
```

APPENDIX C

WATER PURIFICATION CODE

Module Solvers

```
Public Sub Simulation(ByRef strMessage As String, ByVal locSim As String, ByVal locTime As String,  
ByVal locOut As String, ByVal bHN As Boolean, ByVal bHP As Boolean)
```

NOTE: REMOVED MAJORITY OF DIMENSION LINES FOR BREVITY

```
'***** WATER PURIFICATION VARS*****
```

```
Dim v_Ph0 As Double  
Dim v_Nit As Double  
Dim v_OH As Double  
Dim OH_i As Double = 0.1  
Dim Nit_i As Double = 0.001  
Dim Nit_e As Double = 0.16  
Dim Pho_e As Double = 0.0025 'in mM  
Dim Pho_i As Double = Nit_i / Nit_e * Pho_e  
Dim OH_e As Double = 0.1  
Dim Ca_i As Double = 0.0001  
Dim Ca_e As Double = 0.05  
'in mM  
  
Dim iHPHo As Double = 0  
Dim iHNit As Double = 0  
Dim iHOH As Double = 0  
Dim Nit_iold As Double = Nit_i  
Dim Pho_iold As Double = Pho_i  
Dim HPhotGen As Double = 0.005 '(current in pA)  
Dim kHPHo As Double = 0.005  
Dim kHNit As Double = 0.005  
Dim kHATPase As Double = 0.005  
Dim ATP_i As Double = 0.0001  
Dim ADP_i As Double = 0.0001  
Dim v_ATP As Double
```

```
'*****
```

```
If IO.File.Exists(locOut) = True Then  
IO.File.Delete(locOut)  
End If  
oWrite = IO.File.CreateText(locOut)
```

```
Vol = Vol_0  
A = A0  
AOld = A
```

```

Cap = 10 * CapS * 10 ^ -2

n_ATP = n0_ATP
n_ADP = n0_ADP
DATP = DATP0
'convert to mV
v_Nit = (k * Temp) / (-e) * System.Math.Log(Nit_e / Nit_i)
v_Ph0 = (k * Temp) / (-e) * System.Math.Log(Pho_e / Pho_i)
v_0 = 0 'Grabe Oster Calibration

v = v_0

Rho = Rho_0 'This is currently constant
DT = DT0

Temp = Temp_0

'Assign Initial Values
'Determine internal H+ concentration
Vol = 0.001
A = 0.05
pH_i = 6.9
H_i = 10 ^ -(pH_i) * 10 ^ 3
H_e = 10 ^ -(pH_i) * 10 ^ 3
Y(1) = H_i * Vol 'convert pH to ion concentration (mM)
Y(2) = 0
Y(3) = Vol
Y(4) = Nit_i * Vol ' * 10 ^ -6 'Concentrations are in mM or mol/m3
Y(5) = Pho_i * Vol ' * 10 ^ -6
Y(6) = Ca_i * Vol
Y(7) = 0
Y(8) = 0
Y(9) = ATP_i * Vol 'ATP
Y(10) = ADP_i * Vol
vATP0 = (1 / F) * (-28000.0 + R * Temp * System.Math.Log((Vol * Y(5) * Y(10)) / (Vol ^ 2 * Y(9))))
'Write Initial Data
TIME = 0
TIME0 = TIME
dPi0 = R * (10 ^ -3) * Temp * 0.73 * ((H_i - H_ef) + (Nit_i - Nit_e) + (Pho_i - Pho_e))

oWrite.WriteLine("INC TIME(s) pH_i ATP_i H_i OH_i Nit_i Pho_i Ca_i DATP v(mV) iPhoto iHNit iHPho
iHOH iHDiff NitChar PhoChar") 'Header Information
oWrite.WriteLine(KINC & " " & TIME & " " & pH_i & " " & ATP_i & " " & H_i & " " & OH_i & " " &
Nit_i & " " & Pho_i & " " & Ca_i & " " & DATP & " " & Y(2) & " " & HPhotGen & " " & iHNit & " " & iHPho &
" " & iHOH & " " & iHDiff & " " & Nit_i & " " & Pho_i)
oWrite.Close()
'Start Loop
KINC = 1
For i = 1 To Nvar 'Store initial values in case run needs to be restarted.
Y0(i) = Y(i)
Next
kHATPase = e * 5.0929581279 * 10 ^ 14 * A * 100 * 10 ^ 12 * 500 '* 100000.0 '100 = rate constant

Dim iCaChann As Double

kHNit = kHATPase / 2
kHPho = kHATPase / 2
CapS = 3798
'CapS = 6686046
'CapS = 40
kChar = 0 '0.0000001
CapS = 0.6 * 10 ^ -6 / (10 ^ -4) 'from Sarles info
Cap = CapS * A * 10 ^ 9 'CapS is in F/m2, convert to pF
While bRun = True
'Store old time
TIME0 = TIME
For i = 1 To 7

H_i = Y(1) / Y(3)

```

```

Nit_i = Y(4) / Y(3)
Pho_i = Y(5) / Y(3)
Ca_i = Y(6) / Y(3)
v = Y(2)

'Nernst Equilibrium
Dim kuptake As Double = 0.5
Dim Nit_ifree As Double
Dim masschar As Double = 0.1 '(kg char)

Dim q As Double = 5.3448
'Calculate Sponge Uptake
Nit_ifree = (Nit_i * Vol * 62004.5) / (q * masschar / (Vol * 10 ^ 3) + 1)
Nit_ifree = Nit_ifree / (62004.5 * Vol)

v_Nit = (k * Temp) / (-e) * System.Math.Log(Nit_e / Nit_ifree)
v_Ph = (k * Temp) / (-e) * System.Math.Log(Pho_e / Pho_i)
v_H = (k * Temp) / (e) * System.Math.Log(H_e / H_i)
v_Ca = (k * Temp) / (2 * e) * System.Math.Log(Ca_e / Ca_i)

Dim pmf As Double = 200 'proton motive force, mV

iPump = 4 * A * 10 ^ 6 * 40 * (H_i * H_e) ^ (1 / 2) * 1 / H_e * System.Math.Tanh(0.5 * (e *
* (v + pmf - v_H) / (k * Temp))) '* 100000.0

If bHN = True Then
    iHNit = kHNit * (H_i * H_e * Nit_i * Nit_e) ^ (1 / 2) * System.Math.Sinh(0.5 * (e *
(v_H + (-1) * v_Nit) / (k * Temp)))
    If iHNit < 0 Then
        'iHNit = 0
    End If
End If
If bHP = True Then
    iHPho = kHPho * (H_i * H_e * Pho_e * Pho_i) ^ (1 / 2) * System.Math.Sinh(0.5 * (e *
(v_H + (-1) * v_Ph) / (k * Temp)))
    If iHPho < 0 Then
        'iHPho = 0
    End If
End If

'Calcium channels

'Set gating coefficient to 60 mV
Dim XAct As Double
Dim kCCa As Double = kHPho
XAct = 1 / 2 * (1 - System.Math.Tanh(2 * e * (Y(2) + 60) / (k * Temp)))
iCaChann = kCCa * XAct * System.Math.Sqrt(Ca_i * Ca_e) * System.Math.Sinh(e * (v - v_Ca) /
(k * Temp))

If (1 - System.Math.Exp(-1 * F * Y(2) / (R * Temp))) <> 0 Then
    iHDiff = -HDiff * A * F * (F * Y(2) + 0) / (R * Temp) * (H_i - H_e * System.Math.Exp(-
1 * F * Y(2) / (R * Temp))) / (1 - System.Math.Exp(-1 * F * Y(2) / (R * Temp))) * 10 ^ 12
Else
    iHDiff = HDiff * A * F * (H_e - H_i) * 10 ^ 12
End If
iHDiff = 0

D(1) = (-iPump / F + iHDiff / F + iHPho / F + iHNit / F) * 10 ^ -12
D(2) = (-iPump + iHDiff - iCaChann * 2) / Cap
D(3) = 0 'Volume change, set at zero for now
D(4) = iHNit / (F) * 10 ^ -12
D(5) = iHPho / F * 10 ^ -12
D(6) = -iCaChann / (2 * F) * 10 ^ -12

Select Case i
Case 1
    For j = 1 To Nvar
        K1(j) = D(j)
    Next

```

```

Case 2
  For j = 1 To Nvar
    K2(j) = D(j)
  Next
Case 3
  For j = 1 To Nvar
    K3(j) = D(j)
  Next
Case 4
  For j = 1 To Nvar
    K4(j) = D(j)
  Next
Case 5
  For j = 1 To Nvar
    K5(j) = D(j)
  Next
Case 6
  For j = 1 To Nvar
    K2(j) = D(j)
  Next
Case 7
  For j = 1 To Nvar
    K3(j) = D(j)
  Next
End Select

'Every step innocent until proven guilty
bAccept = True

'Calculate next step dependent on current step - integration.
Select Case i
  Case 1
    For j = 1 To Nvar
      Y1(j) = Y0(j) + DT * 0.2 * K1(j)
    Next
    If Y1(1) < 0 Or Y1(4) < 0 Or Y1(5) < 0 Or Y1(9) < 0 Or Y1(10) < 0 Then
      bAccept = False
      i = 8
    End If
    TIME = TIME0 + 0.2 * DT
  Case 2
    For j = 1 To Nvar
      Y1(j) = Y0(j) + DT * (CDec(3 / 40) * K1(j) + CDec(9 / 40) * K1(j))
    Next
    If Y1(1) < 0 Or Y1(4) < 0 Or Y1(5) < 0 Or Y1(9) < 0 Or Y1(10) < 0 Then
      bAccept = False
      i = 8
    End If
    TIME = TIME0 + 0.3 * DT
  Case 3
    For j = 1 To Nvar
      Y1(j) = Y0(j) + DT * (CDec(44 / 45) * K1(j) - CDec(56 / 15) * K2(j) + CDec(32
/ 9) * K3(j))
    Next
    If Y1(1) < 0 Or Y1(4) < 0 Or Y1(5) < 0 Or Y1(9) < 0 Or Y1(10) < 0 Then
      bAccept = False
      i = 8
    End If
    TIME = TIME0 + 0.8 * DT
  Case 4
    For j = 1 To Nvar
      Y1(j) = Y0(j) + DT * (CDec(19372 / 6561) * K1(j) - CDec(25360 / 2187) * K2(j)
+ CDec(64448 / 6561) * K3(j) - (212 / 729) * K4(j))
    Next
    If Y1(1) < 0 Or Y1(4) < 0 Or Y1(5) < 0 Or Y1(9) < 0 Or Y1(10) < 0 Then
      bAccept = False
      i = 8
    End If
    TIME = TIME0 + 0.8 / 0.9 * DT

```

```

        Case 5
            For j = 1 To Nvar
                Y1(j) = Y0(j) + DT * (CDec(9017 / 3168) * K1(j) - CDec(355 / 33) * K2(j) +
CDec(46732 / 5247) * K3(j) + CDec(49 / 176) * K4(j) - CDec(5103 / 18656) * K5(j))
            Next
            If Y1(1) < 0 Or Y1(4) < 0 Or Y1(5) < 0 Or Y1(9) < 0 Or Y1(10) < 0 Then
                bAccept = False
                i = 8
            End If
            TIME = TIME0 + DT
        Case 6
            For j = 1 To Nvar
                Y1(j) = Y0(j) + DT * (CDec(35 / 384) * K1(j) + CDec(500 / 1113) * K3(j) +
CDec(125 / 192) * K4(j) - CDec(2187 / 6784) * K5(j) + CDec(11 / 84) * K2(j))
            Next
            For j = 1 To Nvar
                K2(j) = CDec(71 / 57600) * K1(j) - CDec(71 / 16695) * K3(j) + CDec(71 / 1920)
* K4(j) - CDec(17253 / 339200) * K5(j) + CDec(22 / 525) * K2(j)
            Next
        Case 7
            For j = 1 To Nvar
                'K4(j) = (K2(j) - (1 / 40) * K3(j)) * DT
                K4(j) = DT * K2(j) - CDec(1 / 40) * K3(j) * DT
            Next
        End Select
ERR:
    If bAccept = True Then
        'Shift forwards
        For j = 1 To Nvar
            Y(j) = Y1(j)
        Next
    End If
Next
CheckErr:
    'Check error
    Dim Err As Double
    Dim Denom As Double
    Dim storeval As Double
    Dim EPS As Double = 0.001
    Dim DTNew As Double
    If bAccept = True Then 'If the step hasn't been rejected yet, check for errors
        Err = 0
        For i = 1 To Nvar
            storeval = System.Math.Max(System.Math.Abs(Y1(i)), System.Math.Abs(Y0(i)))
            Denom = System.Math.Max(EPS, storeval)
            Err = Err + (K4(i) / Denom) ^ 2
        Next
        Err = System.Math.Sqrt(Err / Nvar)
        DTNew = DT * System.Math.Min(5, System.Math.Max(0.1, (EPS / Err) ^ (1 / 5) * 0.85))
        If Double.IsNaN(DTNew) = True Then
            DTNew = DT * 0.5
        End If

        If System.Math.Abs(Err) > EPS Or Double.IsNaN(Err) = True Or Double.IsInfinity(Err) = True
Then
            bAccept = False
        End If
    End If
End If

'Check for criteria for each step
If bAccept = True Then
    KREJ = 0
    For i = 0 To (Nvar - 1)
        Y(i) = Y1(i)
        K1(i) = K3(i)
    Next
    Vol = Y(3)

```

```

v = Y(2)

Nit_i = Y(4) / Y(3)
Pho_i = Y(5) / Y(3)
H_i = Y(1) / Y(3)
Ca_i = Y(6) / Y(3)
ATP_i = Y(9) / Y(3)

'Write information to the output file
If Nwritecount >= Nwrite Then
    oWrite = IO.File.AppendText(locOut)
    oWrite.WriteLine(KINC & " " & TIME & " " & pH_i & " " & ATP_i & " " & H_i & " " & OH_i
& " " & Nit_i & " " & Pho_i & " " & Ca_i & " " & DATP & " " & Y(2) & " " & iPump & " " & iHNit & " " &
iHPho & " " & iHOH & " " & iHDiff & " " & Y(7) / Y(3) & " " & Y(8) / Y(3))
    oWrite.Close()
    Nwritecount = 1
Else
    Nwritecount = Nwritecount + 1
End If

For i = 1 To Nvar 'Store values in case run needs to be restarted.
    Y0(i) = Y(i)
Next
TIME = TIME0 + DT
DT = DTNew
If DT > DTMax Then
    DT = DTMax
End If
KINC = KINC + 1
If TIME > TMax Or KINC > KMax Then
    bRun = False
    strMessage = "Run successfully completed"
End If
Else
    KREJ = KREJ + 1
End If
'pH_i = Y0(15)

Nit_i = Y0(4) / Y0(3)
Pho_i = Y0(5) / Y0(3)
H_i = Y0(1) / Y0(3)
Ca_i = Y0(6) / Y0(3)
ATP_i = Y0(9) / Y0(3)
v = Y0(2)
Vol = Y0(3)

TIME = TIME0
DT = DT / 2
For i = 1 To Nvar
    Y(i) = Y0(i)
Next
If KREJ > RMax Then
    Call ErrorHandler(2, strMessage)
    bRun = False
End If
If DT < DTMin Then
    Call ErrorHandler(3, strMessage)
    bRun = False
End If
'Restart
End If
End While

'Final Steps
oWrite.Close()
End Sub
Public Sub ErrorHandler(ByVal iCase As Integer, ByRef strMessage As String)
    Select Case (iCase)

```

```
Case 1
  strMessage = "File does not exist. Create file or check location - run terminated."
Case 2
  strMessage = "Maximum reiterations exceeded - run terminated."
Case 3
  strMessage = "Recommended timestep below minimum - run terminated."
Case 4
End Select
End Sub
End Module
```

APPENDIX D

OSMOTIC ACTUATION CODE

Module Solvers

```
Public Sub Simulation(ByRef strMessage As String, ByVal locSim As String, ByVal locTime As String,
ByVal locOut As String, ByVal locBessel As String, ByVal bATP As Boolean, ByVal bBuffer As Boolean, ByVal
bP As Boolean, ByVal bDamp As Boolean, ByVal bHydro As Boolean, ByVal bPump As Boolean, ByVal bCT As
Boolean, ByVal bDiff As Boolean, ByVal bChann As Boolean, ByVal bIon As Boolean, ByVal bSuc As Boolean,
ByVal bCl As Boolean, ByVal bCa As Boolean, ByVal bK As Boolean, ByVal bNa As Boolean, ByVal bEx As
Boolean, ByVal bNaK As Boolean, ByVal bSponge As Boolean, ByVal bSpongeVar As Boolean)
```

NOTE: REMOVED MAJORITY OF DIMENSION LINES FOR BREVITY

```
K_e = K_ef
K_eOld = K_e
Vol_0 = 4 / 3 * System.Math.PI * ARadius ^ 3 * 10 ^ -18 'keep in m3
A0 = 4 * System.Math.PI * ARadius ^ 2 * 10 ^ -12 'keep in m2
Vol = Vol_0
A = A0
AOld = A
n_ATP = n0_ATP
n_ADP = n0_ADP
DATP = DATP0
n_P = n0_P
VM = 0
HoopStress = 0
'convert to mV
v_K = (k * Temp) / (e) * System.Math.Log(K_e / K_i)
v = v_0
Rho = Rho_0 'This is currently constant
DT = DT0
Temp = Temp_0

'DECLARE INITIAL VARIABLES HERE
pH_e = 5.0
pH_i0 = 5.0
pH_i = pH_i0
K_e = 100
Dim K_e0 As Double = K_e
K_i = K_e
K_i0 = K_e
```

```

Ca_e = 5
Ca_i = Ca_e
Ca_i0 = Ca_e

Radius0 = 0.000001
Radius = Radius0

Vol_0 = System.Math.PI * 4 / 3 * Radius ^ 3
Vol = Vol_0

A0 = 4 * System.Math.PI * Radius ^ 2
A = A0

Dim ChanScale As Double
ChanScale = 61971118040
CapS = 0.01
'Diaphragm characteristics
Dim ModGeom As Double = 1
YMod = 1000000.0 'Lower val for rubber
YMod = 10000000.0 'Use upper value instead
Poissons = 0.5
diat = 0.00002 * ModGeom 'meters, values taken from Homison
Rdia = 0.00025 * ModGeom
Dim height As Double
height = 0.001 * ModGeom

Vol = Rdia ^ 2 * System.Math.PI * height 'meters cubed
Vol_0 = Vol

'K Transport Membrane Characteristics
Dim KMA As Double = 0.5 * Rdia ^ 2 * System.Math.PI 'Surface area of transport membrane is
50% of total area
delta = 0.000001 'Thickness
kPump = 50000 * e * 1 * 10 ^ 12
kEX = kPump
u_K = KMA * ChanScale * 2
Dim KAct As Double = 50
Dim P_OS As Double = 0.03 'Water membrane permeability (assume constant for all membranes)
Cap = KMA * CapS

SCALE = Cap * 100000000.0
'Cap = 6714706 * 1 * 10 ^ -9
'Ca Transport Membrane Characteristics
KDiff = 0.000000016
Dim iKDiff1e, iKDiff2e, iKDiffii

Dim CaMA As Double = KMA
Dim CaAct As Double = 40
Dim VolExt As Double = Vol
Dim VolExt0 As Double = VolExt
u_Ca = CaMA * ChanScale * 2
CapExt = CaMA * CapS

Cap = (KMA) * CapS 'Consider both surface areas for the cells

Dim C As Double = 1 'Membrane Potential Creation

'Driving Force
Dim Amp As Double = 500
Dim Wave As Double = 2
DATP = -1.0E-20
n_H = 1
HDiff = HDiff
Dim xChan As Integer = 0
Dim Ca_ee As Double 'Other side of voltage membrane
Dim Ca_e0 As Double = Ca_e

Dim dpi2 As Double = 0
'secondary osmotic pressure

```

```

H_e = 0.01
H_eOld = 0.01
H_ef = 0.01
H_i0 = 0.01
H_i = 0.1
H_si = 0
Y(1) = H_i0 * Vol_0 'convert pH to ion concentration (mM)
Y(2) = Suc_i * Vol_0 ' * 10 ^ -6
Y(3) = v 'Primary Voltage
Y(4) = Vol_0
Y(5) = n_ATP
Y(6) = 0 'Secondary Voltage
Y(7) = Ca_i * VolExt0 'Ca_e1
Y(8) = K_e * VolExt0 '* 10 ^ -6 'Concentrations are in mM or mol/m3
Y(9) = K_i * Vol_0
Y(10) = H_e * VolExt0
Y(11) = Ca_i * Vol_0 'Ca_e2
Y(12) = 1 / 2 * (1 - System.Math.Tanh(2 * e * (Y(6) + CaAct) / (k * Temp))) 'Calcium Out
Y(13) = 1 / 2 * (1 - System.Math.Tanh(2 * e * (Y(3) + KAct) / (k * Temp))) 'Potassium Out
Y(14) = 1 / 2 * (1 + System.Math.Tanh(2 * e * (Y(6) - CaAct) / (k * Temp))) 'Calcium

Channels
Y(15) = 1 / 2 * (1 + System.Math.Tanh(2 * e * (Y(3) - KAct) / (k * Temp))) 'Potassium
Channels will be slightly open at v = 0 initially
Y(16) = 1 / 2 * (1 - System.Math.Tanh(2 * e * (Y(3) + KAct) / (k * Temp)))
Y(17) = 1 / 2 * (1 + System.Math.Tanh(2 * e * (Y(3) - KAct) / (k * Temp)))
Y(18) = Vol_0 'Secondary Volume
Y(19) = K_e * Vol
Y(20) = K_i * Vol_0

bRun = True

'Write Initial Data
TIME = 0
TIME0 = TIME
iChannelH = 0
iCT = 0
iHDiff = 0
iClDiff = 0
iPump = 0
iChannelH = 0
dPi0 = R * (10 ^ -3) * Temp * 0.73 * ((K_e - K_i) + (Ca_e - Ca_i))

VolInt1 = Y(4)
VolInt2 = Y(18)
VolInt1 = VolExt1
VolInt2 = VolExt2
VolInt10 = VolInt1
VolInt20 = VolInt2
VolTot = VolInt1 + VolExt1
VolInt1 = Y(4)
VolInt2 = Y(18)

'Assume incompressible
VolExt1 = VolExt0 - (VolInt1 - Vol_0)
VolExt2 = VolExt0 - (VolInt2 - Vol_0)

'VolExt = VolTot - Y(4) 'Assume volume conservation, total volume remains unchanged (or
at least total volume of water remains unchanged)
'Set external volume to be constant
H_i = Y(1) / VolInt1 '* 10 ^ 6
H_e = Y(10) / VolExt1

K_e1 = Y(8) / VolExt1
K_e2 = Y(19) / VolExt2
K_i1 = Y(9) / VolInt1
K_i2 = Y(20) / VolInt2

Ca_i1 = Y(7) / VolInt1

```

```

Ca_e1 = Ca_i0 * VolExt0 / VolExt1 'Only changes with volume
Ca_i2 = Y(11) / (VolInt2)
Ca_e2 = Ca_i0 * VolExt0 / VolExt2

'Use instantaneous gating
X2C = 1 / 2 * (1 + System.Math.Tanh(2 * e * (v2 - CaAct) / (k * Temp)))
X1C = 1 / 2 * (1 + System.Math.Tanh(2 * e * (v1 - CaAct) / (k * Temp)))

X1KI = 1 / 2 * (1 - System.Math.Tanh(2 * e * (v1 + KAct) / (k * Temp)))
X1KO = 1 / 2 * (1 + System.Math.Tanh(2 * e * (v1 - KAct) / (k * Temp)))
X2KO = 1 / 2 * (1 + System.Math.Tanh(2 * e * (v2 - KAct) / (k * Temp)))
X2KI = 1 / 2 * (1 - System.Math.Tanh(2 * e * (v2 + KAct) / (k * Temp)))

oWrite.WriteLine("INC TIME(s) K_i1 K_e1 K_i2 K_e2 Ca_i1 Ca_e1 Ca_i2 Ca_e2 v1(mV) v2(mV)
vdrive(mV) VolInt1(um3) W01(um) P1 dPi1 VolInt2(um3) W02(um) P2 dPi2 iChannK1 X1KI X1KO iChannK2 X2KI X2KO
iChannCa1 iChannCa2 X1C X2C") 'Header Information

oWrite.WriteLine(KINC & " " & TIME & " " & K_i1 & " " & K_e1 & " " & K_i2 & " " & K_e2 & " " &
Ca_i1 & " " & Ca_e1 & " " & Ca_i2 & " " & Ca_e2 & " " & v1 & " " & v2 & " " & vdrive & " " & VolInt1 * 10
^ 18 & " " & W01 * 10 ^ 6 & " " & pstat1 & " " & dpi1 & " " & VolInt2 * 10 ^ 18 & " " & W02 * 10 ^ 6 & " "
& pstat2 & " " & dpi2 & " " & iChannelK1 & " " & X1KI & " " & X1KO & " " & iChannelK2 & " " & X2KI & " " &
X2KO & " " & iChannelCa1 & " " & iChannelCa2 & " " & X1C & " " & X2C)
oWrite.Close()
'Start Loop
KINC = 1
For i = 1 To Nvar 'Store initial values in case run needs to be restarted.
Y0(i) = Y(i)
Next
bRun = True
bflag = False
While bRun = True
'Store old time
TIME0 = TIME
For i = 1 To 7

VolInt1 = Y(4)
VolInt2 = Y(18)

'Assume incompressible
VolExt1 = VolExt0 - (VolInt1 - Vol_0)
VolExt2 = VolExt0 - (VolInt2 - Vol_0)

'VolExt = VolTot - Y(4) 'Assume volume conservation, total volume remains
unchanged (or at least total volume of water remains unchanged)
'Set external volume to be constant
H_i = Y(1) / VolInt1 * 10 ^ 6
H_e = Y(10) / VolExt1

K_e1 = Y(8) / VolExt1
K_e2 = Y(19) / VolExt2
K_i1 = Y(9) / VolInt1
K_i2 = Y(20) / VolInt2

Ca_i1 = Y(7) / VolInt1
Ca_e1 = Ca_i0 * VolExt0 / VolExt1 'Only changes with volume
Ca_i2 = Y(11) / (VolInt2)
Ca_e2 = Ca_i0 * VolExt0 / VolExt2

dpi1 = R * (10 ^ -3) * Temp * 0.73 * ((K_i1 - K_e1) + (Ca_i1 - Ca_e1))
dpi1 = dpi1 - dPi0
dpi2 = R * (10 ^ -3) * Temp * 0.73 * ((K_i2 - K_e2) + (Ca_i2 - Ca_e2))
dpi2 = dpi2 - dPi0
dpi3 = R * (10 ^ -3) * Temp * 0.73 * ((K_i1 - K_i2) + (Ca_i1 - Ca_i2))
dpi3 = dpi3 - dPi0

'Nernst Equilibrium
'Units are in mV - CHECKED
v_H = (k * Temp) / (e) * System.Math.Log(H_e / H_i)
v_K1 = (k * Temp) / (e) * System.Math.Log(K_e1 / K_i1)

```

```

v_K2 = (k * Temp) / e * System.Math.Log(K_e2 / K_i2)
v_Ca1 = (k * Temp) / (2 * e) * System.Math.Log(Ca_i2 / Ca_i1)
v_Ca2 = (k * Temp) / (2 * e) * System.Math.Log(Ca_i1 / Ca_i2)

If bflag = False Then
    vdrive = -Amp * System.Math.Sin(TIME * 2 * System.Math.PI / (Wave * TMax))
    If TIME < 0.5 * TMax Then
        vdrive = Amp
    End If
    If TIME > 0.5 * TMax Then
        vdrive = 0
    End If
    vdrive = Amp
Else
    vdrive = 0
End If

v1 = Y(3) '+ (F / Cap * VolExt * 2 * (Ca_i - Ca_e)) * C * 10 ^ 3
v2 = Y(6) '+ (F / CapExt * VolExt * 2 * (K_e - K_e0)) * C * 10 ^ 3

'Exchanger Calculations
If bEx = True Then
    iEX = kEX * System.Math.Sinh(0.5 * (e * (-2 * v + v_H + v_K) / (k * Temp)))
Else
    iEX = 0
End If
'Determine energy release from ATP Hydrolysis
If bATP = True Then
    V_ATP = Vol_0
    V_ADP = Vol_0
    V_P = Vol_0
    n_ADP = n0_ADP
    n_P = n0_P
    n_ADP = n0_ADP
Else
    n_ADP = n0_ADP + n0_ATP - Y(5)
    n_P = n0_P + n0_ATP - Y(5)
    V_ATP = Y(4)
    V_ADP = Y(4)
    V_P = Y(4)
End If

'Pump current
If bPump = True Then
    iPump = kPump * System.Math.Tanh((e * (v - DATP - v_H) / (2 * k * Temp)))
Else
    iPump = 0
End If

'Diffusion
If bDiff = True Then

    '1 to the outside
    If (1 - System.Math.Exp((-F * v1) / (R * Temp))) <> 0 Then
        iKDiff1e = -KDiff * KMA * F * (F * v1 + 0) / (R * Temp) * (K_i1 - K_e1 *
System.Math.Exp(-1 * F * v1 / (R * Temp))) / (1 - System.Math.Exp(-1 * F * v1 / (R * Temp))) * 10 ^ 12
    Else
        'iHDiff1 = HDiff * KMA * (H_e - H_i) * 10 ^ 12
        iKDiff1e = KDiff * KMA * (K_e1 - K_i1) * 10 ^ 12
    End If

    '2 to the outside
    If (1 - System.Math.Exp((-F * v2) / (R * Temp))) <> 0 Then
        iKDiff2e = -KDiff * KMA * F * (F * v2 + 0) / (R * Temp) * (K_i2 - K_e2 *
System.Math.Exp(-1 * F * v2 / (R * Temp))) / (1 - System.Math.Exp(-1 * F * v2 / (R * Temp))) * 10 ^ 12
    Else
        'iHDiff1 = HDiff * KMA * (H_e - H_i) * 10 ^ 12
        iKDiff2e = KDiff * KMA * (K_e2 - K_i2) * 10 ^ 12
    End If

```

```

End If

'1 to 2
If (1 - System.Math.Exp((-F * (v1 - v2 + vdrive)) / (R * Temp))) <> 0 Then
    iKDiffii = -KDiff * CaMA * F * (F * (v1 - v2 + vdrive) + 0) / (R * Temp) *
(K_i1 - K_i2 * System.Math.Exp(-1 * F * (v1 - v2 + vdrive) / (R * Temp))) / (1 - System.Math.Exp(-1 * F *
(v1 - v2 + vdrive) / (R * Temp))) * 10 ^ 12
Else
    'iHDiff1 = HDiff * KMA * (H_e - H_i) * 10 ^ 12
    iKDiffii = KDiff * CaMA * (K_i2 - K_i1) * 10 ^ 12
End If
Else
    iHDiff1 = 0
    iHDiff2 = 0
    iKDiff1e = 0
    iKDiff2e = 0
    iKDiffii = 0

End If

If bChann = True Then

    'Make sure that all channel opening and closing are between 0 and 1
    For j = 12 To 17
        If Y(j) < 0 Then
            Y(j) = 0
        ElseIf Y(j) > 1 Then
            Y(j) = 0
        End If
    Next

    'Use instantaneous gating
    X2C = 1 / 2 * (1 + System.Math.Tanh(2 * e * (v2 - v1 + vdrive - CaAct) / (k *
Temp)))
    X1C = 1 / 2 * (1 + System.Math.Tanh(2 * e * (v1 - v2 - vdrive - CaAct) / (k *
Temp)))

    X1KI = 1 / 2 * (1 - System.Math.Tanh(2 * e * (v1 + KAct) / (k * Temp)))
    X1KO = 1 / 2 * (1 + System.Math.Tanh(2 * e * (v1 - KAct) / (k * Temp)))
    X2KO = 1 / 2 * (1 + System.Math.Tanh(2 * e * (v2 - KAct) / (k * Temp)))
    X2KI = 1 / 2 * (1 - System.Math.Tanh(2 * e * (v2 + KAct) / (k * Temp)))
    If bK = True Then
        If (v1 - v_K1) > 0 Then
            kCk = u_K * X1KO
            iChannelK1 = kCk * System.Math.Sqrt(K_e1 * K_i1) * System.Math.Sinh(e *
(v1 - v_K1) / (2 * k * Temp))
        Else
            kCk = u_K * X1KI
            iChannelK1 = kCk * System.Math.Sqrt(K_e1 * K_i1) * System.Math.Sinh(e *
(v1 - v_K1) / (2 * k * Temp))
        End If
        If (v2 - v_K2) > 0 Then
            kCk2 = u_K * X2KO
            iChannelK2 = kCk * System.Math.Sqrt(K_e2 * K_i2) * System.Math.Sinh(e *
(v2 - v_K2) / (2 * k * Temp))
        Else
            kCk2 = u_K * X2KI
            iChannelK2 = kCk * System.Math.Sqrt(K_e2 * K_i2) * System.Math.Sinh(e *
(v2 - v_K2) / (2 * k * Temp))
        End If
    Else
        iChannelK1 = 0
        iChannelK2 = 0
    End If
    If bCa = True Then
        kCCa = u_Ca * X1C
        iChannelCa1 = kCCa * System.Math.Sqrt(Ca_i1 * Ca_i2) * System.Math.Sinh(e
* (v1 - v2 - v_Ca1 + vdrive) / (k * Temp))

```

```

        kCCa = u_Ca * X2C
        iChannelCa2 = kCCa * System.Math.Sqrt(Ca_i1 * Ca_i2) * System.Math.Sinh(e *
(v2 - v1 - v_Ca2 - vdrive) / (k * Temp))
    Else
        iChannelCa = 0
    End If

    Else 'All channels are disabled. Set flows to zero.
        iChannelK = 0

    End If

Poissons = 0.3

If bP = False Then

    'first we must determine a proper B
    pstat1 = 16 * YMod * diat ^ 3 * (VolInt1 - Vol_0) / (System.Math.PI * Rdia ^ 6 *
(1 - Poissons ^ 2))
    W01 = pstat1 * Rdia ^ 4 / (64 * (YMod * diat ^ 3 / (12 * (1 - Poissons ^ 2))))
    pstat2 = 16 * YMod * diat ^ 3 * (VolInt2 - Vol_0) / (System.Math.PI * Rdia ^ 6 *
(1 - Poissons ^ 2))
    W02 = pstat2 * Rdia ^ 4 / (64 * (YMod * diat ^ 3 / (12 * (1 - Poissons ^ 2))))

    Else
        pStat = 0
    End If
    DV1 = (P_OS * V_bar_H20) / (R * 10 ^ -3 * Temp) * KMA * (sigma * dpi1 - (pstat1))
    DV2 = (P_OS * V_bar_H20) / (R * 10 ^ -3 * Temp) * KMA * (sigma * dpi2 - (pstat2))

    iHDiff = 0
    D(1) = ((-iPump + iHDiff + iEX) / (F)) * 10 ^ -12 'Proton Conc (ignore)
    D(2) = 0
    D(3) = (1 / Cap) * (-iChannelK1 - iChannelCa1 + iChannelCa2 + iKDiff1e + iKDiffii) *
10 ^ -9 'change in v1
    D(4) = DV1 'change in
    volume 1
    D(5) = 0
    D(6) = (1 / Cap) * (-iChannelK2 - iChannelCa2 + iChannelCa1 + iKDiff2e - iKDiffii) *
10 ^ -9 'change in v2
    D(7) = (-iChannelCa1 + iChannelCa2) / (2 * F) * 10 ^ -12 'Ca2i
    D(8) = (iChannelK1 - iKDiff1e) / F * 10 ^ -12 'K1e
    D(9) = (-iChannelK1 + iKDiff1e + iKDiffii) / F * 10 ^ -12 'K1i
    D(10) = -D(1) 'change in H_e
    (ignore)
    D(11) = (-iChannelCa2 + iChannelCa1) / (2 * F) * 10 ^ -12 'Ca2i
    '12 - 17 are channels
    D(18) = DV2
    D(19) = (iChannelK2 - iKDiff2e) / F * 10 ^ -12 'K2e
    D(20) = (-iChannelK2 + iKDiff2e - iKDiffii) / F * 10 ^ -12 'K2i

    'ATP used in the ATPases
    If bATP = False Then 'Not constant ATP
        D(5) = (-System.Math.Abs(iPump + iEX)) / (F * Y(4)) ' * 10 ^ 3
    Else
        D(5) = 0
    End If

    Select Case i
        Case 1
            For j = 1 To Nvar
                K1(j) = D(j)
            Next
        Case 2
            For j = 1 To Nvar
                K2(j) = D(j)
            Next
    End Select

```

```

Case 3
  For j = 1 To Nvar
    K3(j) = D(j)
  Next
Case 4
  For j = 1 To Nvar
    K4(j) = D(j)
  Next
Case 5
  For j = 1 To Nvar
    K5(j) = D(j)
  Next
Case 6
  For j = 1 To Nvar
    K2(j) = D(j)
  Next
Case 7
  For j = 1 To Nvar
    K3(j) = D(j)
  Next
End Select

'Every step innocent until proven guilty
bAccept = True

'Calculate next step dependent on current step - integration.
Select Case i
  Case 1
    For j = 1 To Nvar
      Y1(j) = Y0(j) + DT * 0.2 * K1(j)
    Next
    If Y1(2) < 0 Or Y1(4) < 0 Or Y1(5) < 0 Then
      bAccept = False
      i = 8
    End If
    TIME = TIME0 + 0.2 * DT
  Case 2
    For j = 1 To Nvar
      Y1(j) = Y0(j) + DT * (CDec(3 / 40) * K1(j) + CDec(9 / 40) * K1(j))
    Next
    If Y1(2) < 0 Or Y1(4) < 0 Or Y1(5) < 0 Then
      bAccept = False
      i = 8
    End If
    TIME = TIME0 + 0.3 * DT
  Case 3
    For j = 1 To Nvar
      Y1(j) = Y0(j) + DT * (CDec(44 / 45) * K1(j) - CDec(56 / 15) * K2(j) +
CDec(32 / 9) * K3(j))
    Next
    If Y1(2) < 0 Or Y1(4) < 0 Or Y1(5) < 0 Then
      bAccept = False
      i = 8
    End If
    TIME = TIME0 + 0.8 * DT
  Case 4
    For j = 1 To Nvar
      Y1(j) = Y0(j) + DT * (CDec(19372 / 6561) * K1(j) - CDec(25360 / 2187) *
K2(j) + CDec(64448 / 6561) * K3(j) - (212 / 729) * K4(j))
    Next
    If Y1(2) < 0 Or Y1(4) < 0 Or Y1(5) < 0 Then
      bAccept = False
      i = 8
    End If
    TIME = TIME0 + 0.8 / 0.9 * DT
  Case 5
    For j = 1 To Nvar
      Y1(j) = Y0(j) + DT * (CDec(9017 / 3168) * K1(j) - CDec(355 / 33) * K2(j) +
CDec(46732 / 5247) * K3(j) + CDec(49 / 176) * K4(j) - CDec(5103 / 18656) * K5(j))

```

```

        Next
        If Y1(2) < 0 Or Y1(4) < 0 Or Y1(5) < 0 Then
            bAccept = False
            i = 8
        End If
        TIME = TIME0 + DT
    Case 6
        For j = 1 To Nvar
            Y1(j) = Y0(j) + DT * (CDec(35 / 384) * K1(j) + CDec(500 / 1113) * K3(j) +
CDec(125 / 192) * K4(j) - CDec(2187 / 6784) * K5(j) + CDec(11 / 84) * K2(j))
        Next
        For j = 1 To Nvar
            K2(j) = CDec(71 / 57600) * K1(j) - CDec(71 / 16695) * K3(j) + CDec(71 /
1920) * K4(j) - CDec(17253 / 339200) * K5(j) + CDec(22 / 525) * K2(j)
        Next
    Case 7
        For j = 1 To Nvar
            'K4(j) = (K2(j) - (1 / 40) * K3(j)) * DT
            K4(j) = DT * K2(j) - CDec(1 / 40) * K3(j) * DT
        Next
    End Select
ERR:
    If bAccept = True Then
        'Shift forwards
        For j = 1 To Nvar
            Y(j) = Y1(j)
        Next
    End If
Next
CheckErr:

'Check error
Dim Err As Double
Dim Denom As Double
Dim storeval As Double
Dim EPS As Double = 0.000005
Dim DTNew As Double
If bAccept = True Then 'If the step hasn't been rejected yet, check for errors
    Err = 0
    j = 0
    For i = 1 To Nvar

        storeval = System.Math.Max(System.Math.Abs(Y1(i)), System.Math.Abs(Y0(i)))
        Denom = System.Math.Max(EPS, storeval)
        Err = Err + (K4(i) / Denom) ^ 2

        If Err = 0 Then
            j = j + 1
        End If

    Next
    If (Nvar - j) = 0 Then
        Err = 0
    Else
        Err = System.Math.Sqrt(Err / (Nvar - j))
    End If
    Dim DTScale As Double
    DTScale = System.Math.Min(5, System.Math.Max(0.1, (EPS / Err) ^ (1 / 5) * 0.85))
    DTNew = DT * DTScale
    If Double.IsNaN(DTNew) = True Then
        DTNew = DT * 0.5
    End If

    'Check for negative concentrations
    If Y1(7) < 0 Or Y1(8) < 0 Or Y1(9) < 0 Or Y1(11) < 0 Or Y(1) < 0 Or Y1(19) < 0 Or
Y1(20) < 0 Then
        bAccept = False
    End If

```

```

True Then
    If System.Math.Abs(Err) > EPS Or Double.IsNaN(Err) = True Or Double.IsInfinity(Err) =
        bAccept = False
    End If
End If

'Check for criteria for each step
If bAccept = True Then
    KREJ = 0
    For i = 0 To (Nvar - 1)
        Y(i) = Y1(i)
        K1(i) = K3(i)
    Next

    VolInt1 = Y(4)
    VolInt2 = Y(18)

    'Assume incompressible
    VolExt1 = VolExt0 - (VolInt1 - Vol_0)
    VolExt2 = VolExt0 - (VolInt2 - Vol_0)

    'Set external volume to be constant
    H_i = Y(1) / VolInt1 '* 10 ^ 6
    H_e = Y(10) / VolExt1

    K_e1 = Y(8) / VolExt1
    K_e2 = Y(19) / VolExt2
    K_i1 = Y(9) / VolInt1
    K_i2 = Y(20) / VolInt2

    Ca_i1 = Y(7) / VolInt1
    Ca_e1 = Ca_i0 * VolExt0 / VolExt1 'Only changes with volume
    Ca_i2 = Y(11) / (VolInt2)
    Ca_e2 = Ca_i0 * VolExt0 / VolExt2

    v1 = Y(3)
    v2 = Y(6)

    X2C = 1 / 2 * (1 + System.Math.Tanh(2 * e * (v1 - v2 + vdrive - CaAct) / (k * Temp)))
    X1C = 1 / 2 * (1 + System.Math.Tanh(2 * e * (v2 - v1 - vdrive - CaAct) / (k * Temp)))

    X1KI = 1 / 2 * (1 - System.Math.Tanh(2 * e * (v1 + KAct) / (k * Temp)))
    X1KO = 1 / 2 * (1 + System.Math.Tanh(2 * e * (v1 - KAct) / (k * Temp)))
    X2KO = 1 / 2 * (1 + System.Math.Tanh(2 * e * (v2 - KAct) / (k * Temp)))
    X2KI = 1 / 2 * (1 - System.Math.Tanh(2 * e * (v2 + KAct) / (k * Temp)))

    'Write information to the output file
    If Nwritecount >= Nwrite Then
        oWrite.WriteLine(KINC & " " & TIME & " " & K_i1 & " " & K_e1 & " " & K_i2 & " " &
            K_e2 & " " & Ca_i1 & " " & Ca_e1 & " " & Ca_i2 & " " & Ca_e2 & " " & v1 & " " & v2 & " " & vdrive & " " &
            VolInt1 * 10 ^ 18 & " " & W01 * 10 ^ 6 & " " & pstat1 & " " & dpi1 & " " & VolInt2 * 10 ^ 18 & " " & W02 *
            10 ^ 6 & " " & pstat2 & " " & dpi2 & " " & iChannelK1 & " " & X1KI & " " & X1KO & " " & iChannelK2 & " " &
            X2KI & " " & X2KO & " " & iChannelCa1 & " " & iChannelCa2 & " " & X1C & " " & X2C)

        Nwritecount = 1
    Else
        Nwritecount = Nwritecount + 1
    End If

    For i = 1 To Nvar 'Store values in case run needs to be restarted.
        Y0(i) = Y(i)
    Next
    TIME = TIME0 + DT

    DT = DTNew
    If DT > DTMax Then
        DT = DTMax

```

```

End If
KINC = KINC + 1
If TIME > TMax Or KINC > KMax Then
    bRun = False
    strMessage = "Run successfully completed"
    oWrite.Close()
End If
Else
    KREJ = KREJ + 1

    VolInt1 = Y0(4)
    VolInt2 = Y0(18)

    'Assume incompressible
    VolExt1 = VolExt0 - (VolInt1 - Vol_0)
    VolExt2 = VolExt0 - (VolInt2 - Vol_0)

    'VolExt = VolTot - Y(4)          'Assume volume conservation, total volume remains
unchanged (or at least total volume of water remains unchanged)
    'Set external volume to be constant
    H_i = Y0(1) / VolInt1 '* 10 ^ 6
    H_e = Y0(10) / VolExt1

    K_e1 = Y0(8) / VolExt1
    K_e2 = Y0(19) / VolExt2
    K_i1 = Y0(9) / VolInt1
    K_i2 = Y0(20) / VolInt2

    Ca_i1 = Y0(7) / VolInt1
    Ca_e1 = Ca_i0 * VolExt0 / VolExt1 'Only changes with volume
    Ca_i2 = Y0(11) / (VolInt2)
    Ca_e2 = Ca_i0 * VolExt0 / VolExt2

    v1 = Y0(3)
    v2 = Y0(6)

    n_ATP = Y0(5)
    n_ADP = n0_ADP + n0_ATP - Y0(5)
    n_P = n0_P + n0_ATP - Y0(5)
    TIME = TIME0
    DT = DT / 2

    For i = 1 To Nvar
        Y(i) = Y0(i)
    Next
    If KREJ > RMax Then
        Call ErrorHandler(2, strMessage)
        bRun = False
    End If
    If DT < DTMin Then
        Call ErrorHandler(3, strMessage)
        bRun = False
    End If
    'Restart
End If
End While

'Final Steps
oWrite.Close()
End Sub
Public Sub ErrorHandler(ByVal iCase As Integer, ByRef strMessage As String)
    Select Case (iCase)
        Case 1
            strMessage = "File does not exist. Create file or check location - run terminated."
        Case 2
            strMessage = "Maximum reiterations exceeded - run terminated."
        Case 3
            strMessage = "Recommended timestep below minimum - run terminated."
        Case 4

```

```
    End Select  
  End Sub  
End Module
```

BIBLIOGRAPHY

- [1] SA Sarles and DJ Leo, "Membrane-based biomolecular smart materials," *Smart Mater Struct*, vol. 20, pp. 1-12, 2011.
- [2] E Tzima et al., "A mechanosensory complex that mediates the endothelial cell response to fluid shear stress," *Nature*, vol. 437, pp. 426-431, 2005.
- [3] YW Lin, CM Cheng, PR LeDuc, and CC Chen, "Understanding Sensory Nerve Mechanotransduction through Localized Elastomeric Matrix Control," *PLoS ONE*, vol. 4, pp. 1-9, 2009.
- [4] CM Cheng et al., "Probing localized neural mechanotransduction through surface-modified elastomeric matrices and electrophysiology," *Nature Protocols*, vol. 5, pp. 714-724, 2010.
- [5] SA Sarles, JDW Madden, and DJ Leo, "Hair cell inspired mechanotransduction with a gel-supported, artificial lipid membrane," *Soft Matter*, vol. 7, pp. 4644-4653, 2011.
- [6] VB Sundaresan and DJ Leo, "Chemolectrical Energy Conversion of Adenosine Triphosphate using ATPases," *Journal of Intelligent Material Systems and Structures*, vol. 10, pp. 201-212, 2010.
- [7] CH Nielsen, "Biomimetic membranes for sensor and separation applications," *Anal Bioanal Chem*, vol. 395, pp. 697-718, 2009.
- [8] AW Feinberg et al., "Muscular Thin Films for Building Actuators and Powering Devices," *SCIENCE*, vol. 317, pp. 1366-1370, 2007.
- [9] I van Uitert, S Le Gac, and A van den Berg, "The influence of different membrane components on the electrical stability of bilayer lipid membranes," *Biochimica et Biophysica Acta*, vol. 1798, pp. 21-31, 2009.

- [10] R DeVita and IW Stewart, "Nonlinearities in tilt and layer displacements of planar lipid bilayers," *The European Physical Journal*, vol. 32, pp. 319-326, 2010.
- [11] D Hopkinson, *Measurements and Modeling of the Failure Pressure of Bilayer Lipid Membranes*, 2007.
- [12] D Needham and RS Dunn, "Elastic deformation and failure of lipid bilayer membranes containing cholesterol," *Biophys. J.*, vol. 58, pp. 997-1009, 1990.
- [13] R Northcutt, VB Sundaresan, S Salinas, and H Zhang, "Polypyrrole Bridge As a Support for Alamethicin-Reconstituted Planar Bilayer Lipid Membranes," in *SMASIS*, Scottsdale AZ, 2011.
- [14] M De Rosa and A Gambacorta, "The lipids of archaebacteria," *Prog Lipid Res*, vol. 27, pp. 153-175, 1988.
- [15] W Febo-Ayala, SL Morera-Felix, CA Hrycyna, and DH Thompson, "Functional reconstitution of the integral membrane enzyme, isoprenylcysteine carboxyl methyltransferase, in synthetic bolalipid membrane vesicles," *Biochemistry*, vol. 45, pp. 14683-14694, 2006.
- [16] Y Kaufman, A Berman, and V Freger, "The use of NF membranes as substrates for supported phospholipid bilayers," in *International Congress on Membranes and Membrane Processes*, Honolulu, Hawaii, 2008.
- [17] LP Endresen, K Hall, JS Hoye, and J Myrheim, "A theory for the membrane potential of living cells," *European Biophysical Journal*, vol. 29, pp. 90-103, 2000.
- [18] RL Fournier, *Basic Transport Phenomena In Biomedical Engineering*. New York, NY: Taylor and Francis, 2007.
- [19] AG Lee, "How lipids and proteins interact in a membrane: a molecular approach.," *Mol Biosyst*, vol. 1, pp. 203-212, 2005.
- [20] MA Creasy, *Bilayer Network Modeling*, 2011.
- [21] AL Hodgkin, AF Huxley, and B Katz, "Measurement of Current-Voltage Relations in the Membrane of the Giant Axon of Loligo," *J. Physiol*, vol. 116, pp. 424 - 448, 1952.
- [22] KA Scott et al., "Coarse-Grained MD Simulations of Membrane Protein-Bilayer Self Assembly," *Structure*, vol. 16, pp. 621-630, 2008.

- [23] VB Sundareshan and DJ Leo, "Chemo-mechanical Model for Actuation Based on Biological Membranes," *Journal of Intelligent Material Systems and Structures*, vol. 17, pp. 863-871, 2006.
- [24] VB Sundareshan and DJ Leo, "Modeling and characterization of a chemomechanical actuator using protein transporters," *Sensors and Actuators B*, vol. 131, pp. 383-393, 2008.
- [25] L Matthews, VB Sundareshan, V Giurgitiu, and DJ Leo, "Bioenergetics and mechanical actuation analysis with membrane transport experiments for use in biomimetic nastic structures," *J Mater Res*, vol. 21, pp. 2058 - 2066, 2006.
- [26] VB Sundareshan and H Zhang, Coupled Ion Transport-electron Transfer Processes in a Bioderived Ionic Transistor for Energy Harvesting, September 21, 2011.
- [27] E Freeman, Applications of Biologically Inspired Membranes, 2009.
- [28] JI Schroder and S Hagiwara, "Cytosolic calcium regulates ion channels in the plasma membrane of *Vicia faba* guard cells," *Letters to Nature*, vol. 338, pp. 427-430, 1989.
- [29] MG Palmgren, "Plant Plasma Membrane H⁺ -ATPases: Powerhouses for Nutrient Uptake," *Annu Rev Plant Physiol. Mol Biol.*, vol. 52, pp. 817-845, 2001.
- [30] W Nernst, Zur Kinetik der in Losung befindlichen Korper, 1888.
- [31] M Grabe and G Oster, "Regulation of Organelle Acidity," *J Gen Physiol*, vol. 73, pp. 329-343, 2001.
- [32] LJ Mullins, *Ion transport in heart*. New York: Raven Press, 1981.
- [33] AA Markov, "Extension de la loi de grands nombres aux evenements dependants les uns de autres," *Bul Soc Phys-Math Kasan*, vol. 15, pp. 135-136, 1906.
- [34] G Ehrenstein and H Lecar, "Electrically gated ionic channels in lipid bilayers," *Q Rev Biophys*, vol. 10, pp. 1-34, 1977.
- [35] L Boltzmann, "Studien uber das Gleichgewicht der lebendigen Kraft zwischen bewegten materiellen Punkten," *Akad Wiss Berlin, Gottingen, Leipzig, Munchen Wien*, vol. 58, pp. 517-560, 1868.

- [36] SG Schultz, *Basic Principles of Membrane Transport*. New York: Cambridge University Press, 1980.
- [37] H Disalvo, FA Siddiqi, and H T Tien, "Membrane Transport with Emphasis on Water and Nonelectrolytes in Experimental Lipid Bilayers and Biomembranes," in *Water Transport in Biological Membranes, Vol 1*, G Benga, Ed. Boca Raton, FL: CRC Press Inc, 1989, pp. 41-75.
- [38] SL Bonting and JJHMH de Pont, *New Comprehensive Biochemistry Volume 2 - Membrane Transport*. New York: Elsevier, 1981.
- [39] DE Goldman, "Potential, Impedance, and Rectification in Membranes," *Journal of General Physiology*, pp. 37-60, 1943.
- [40] B Hille, *Ionic Channels of Excitable Membranes, 2nd Ed.* Sunderland, MA: Houghton Mifflin Company, 1992.
- [41] MF Beatty, "Topics in Finite Elasticity: Hyperelasticity of Rubber, Elastomers, and Biological Tissues - With Examples," *Applied Mech Rev*, vol. 40, pp. 1699-1735, 1987.
- [42] S Timoshenko and S Woinowsky-Krieger, *Theory of Plates and Shells*. New York, NY: McGraw-Hill, 1959.
- [43] KJ Laidler, JH Meiser, and BC Sanctuary, *Physical Chemistry, 4th Ed.* Boston, MA: Houghton Mifflin Company, 2003.
- [44] Y Su, L Lin, and A Pisano, "A Water-Powered Osmotic Microactuator," *J. Microelectromechanical Systems*, vol. 11, pp. 736-742, 2002.
- [45] HD Price and TE Thompson, "Properties of Liquid Bilayer Membranes separating Two Aqueous Phases: Temperature Dependence of Water Permeability," *J Mol Biol*, vol. 41, pp. 443-457, 1969.
- [46] C Homison, *Coupled Transport/Hyperelastic Model for High Energy Density Nastic Materials*, 2006.
- [47] A Ishihara, N Hashitsume, and M Tatibana, "Statistical theory of rubber-like elasticity, IV. Two dimensional stretching," *J Chem Phys*, vol. 19, p. 1508, 1951.
- [48] KT Wan, S Guo, and DA Dillard, "A theoretical and numerical study of a thin clamped circular film under an external load in the presence of a tensile residual stress," *Thin Solid Films*, vol. 425, pp. 150-162, 2003.

- [49] LP Endresen, "Runge-Kutta formulas for cardiac oscillators," *Institutt for fysikk*, 2000.
- [50] E Hairer, SP Norsett, and G Wanner, *Solving ordinary differential equations I*. New York: Springer-Verlag, 1987.
- [51] JS Shieh et al., "Non-toxic phototriggered gene transfection by PAMAM-porphyrin conjugates," *Journal of Controlled Release*, vol. 219, pp. 200-206, 2008.
- [52] D Lechadeur, AS Verkman, and GL Lukacs, "Intracellular routing of plasmid DNA during non-viral gene transfer," *Advanced Drug Delivery Reviews*, vol. 57, pp. 755-767, 2005.
- [53] HY Nam et al., "Biodegradable PAMAM ester for enhanced transfection efficiency with low cytotoxicity," *Biomaterials*, vol. 30, pp. 665-673, 2009.
- [54] JP Behr, "The Proton Sponge: a Trick to Enter Cells the Viruses Did Not Exploit," *ILMAC*, vol. 97, 1997.
- [55] R Fuchs, P Male, and I Mellman, "Acidification and Ion Permeabilities of Highly Purified Rat Liver Endosomes," *The Journal of Biological Chemistry*, vol. 226, pp. 2212-2220, 1988.
- [56] S Schmidt, R Fuchs, M Kielian, A Helenius, and I Mellman, "Acidification of Endosome Subpopulations in Wild-Type Chinese Hamster Ovary Cells and Temperature-Sensitive, Acidification-Defective Mutants," *The Journal of Cell Biology*, vol. 108, pp. 1291-1300, 1989.
- [57] C Pichon, C Goncalves, and M Patrick, "Histidine-rich peptides and polymers for nucleic acids delivery," *Adv Drug Deliv Rev*, vol. 53, pp. 75-94, 2001.
- [58] D Yamashiro, SR Fluss, and F Maxfield, "Acidification of Endocytic Vesicles by an ATP-dependent Proton Pump," *J Cell Biology*, vol. 97, pp. 929-934, 1983.
- [59] SL Rybak, F Lanni, and RF Murphy, "Theoretical Considerations on the Role of Membrane Potential in the Regulation of Endosomal pH," *Biophysical Journal*, vol. 73, pp. 674-687, 1997.
- [60] MS Ladinsky, DN Mastrorarde, JR McIntosh, KE Howell, and LA Staehelin, "Golgi structure in three dimensions: functional insights from the normal rat kidney cell," *J Cell Biol*, vol. 144, pp. 1135-1140, 1999.

- [61] RW Van Dyke and JD Belcher, "Acidification of three types of liver endocytic vesicles; similarities and differences," *Am J Physiol*, vol. 266, pp. C81 - C94, 1994.
- [62] B Alberts et al., *Molecular Biology of the Cell 3rd Ed.* New York, NY: Garland Press, 1994.
- [63] ND Sonawane, F Szoka, and AS Verkman, "Chloride Accumulation and Swelling in Endosome Enhances DNA Transfer by Polyamine-DNA Polyplexes," *The Journal of Biological Chemistry*, vol. 45, pp. 44826-44831, 2003.
- [64] S Henon, G Lenormand, A Richert, and F Gallet, "A new determination of the shear modulus of the human erythrocyte membrane using optical tweezers," *Biophysical Journal*, vol. 76, pp. 1145-1151, 1999.
- [65] WI Lencer, P Weyer, AS Ausiello, DA Verkman, and D Brown, "FITC-dextran as a probe for endosome function and localization in kidney," *Am. J. Physiol*, vol. 258, pp. C309 - C317, 1990.
- [66] L Shi, K Fushimi, H Bae, and AS Verkman, "Heterogeneity on ATP-dependent acidification in endocytic vesicles from kidney proximal tubule," *Biophys J*, vol. 59, pp. 1208-1217, 1991.
- [67] O Boussif et al., "A versatile vector for gene and oligonucleotide transfer into cells in culture and in vivo: Polyethylenimine," *Proc Natl Acad Sci*, vol. 92, pp. 7297 - 7301, 1995.
- [68] S Yang and S May, "Release of cationic polymer-DNA complexes from the endosome: A theoretical investigation of the proton sponge hypothesis," *The Journal of Chemical Physics*, vol. 129, 2008.
- [69] WT Godbey, MA Barry, P Saggau, KK Wu, and AG Mikos, "Poly(ethylenimine)-mediated transfection: A new paradigm for gene delivery," *J Biomed Mater Res*, vol. 51, pp. 321-328, 2000.
- [70] ML Forrest and DW Pack, "Acetylation of polyethylenimine enhances gene delivery via weakened polymer/DNA interactions," *Mol Ther*, vol. 6, pp. 57-66, 2002.
- [71] AM Funhoff et al., "Endosomal Escape of Polymeric Gene Delivery Complexes is Not Always Enhanced by Polymers Buffering at Low pH," *Biomacromolecules*, vol. 5, pp. 32-39, 2004.

- [72] GW Jin et al., "PAMAM dendrimer with a 1,2-diaminoethane surface facilitates endosomal escape for enhanced pDNA delivery," *Polymer*, 2010.
- [73] HN Po and NM Senozan, "The Henderson-Hasselbalch Equation: Its History and Limitations," *Journal of Chemical Education*, vol. 78, pp. 1499-1503, 2001.
- [74] M Borkovec and GJM Koper, "Proton binding by linear, branched, and hyperbranched polyelectrolytes," *Polymer*, vol. 41, pp. 5469-5662, 2010.
- [75] AW Opitz and NJ Wagner, "Structural Investigations of Poly(amido amine) Dendrimers in Methanol Using Molecular Dynamics," *Journal of Polymer Science: Part B; Polymer Physics*, vol. 44, pp. 3062-3077, 2006.
- [76] P Somasundaran, *Encyclopedia of Surface and Colloid Science.*: CRC Press, 2006.
- [77] AL Llamas-Saiz, C Foces-Foces, and J Elguero, "Proton Sponges," *Journal of Molecular Structure*, vol. 328, pp. 292-323, 1994.
- [78] NN Rabalais, ER Turner, and WJ Wiseman, "Gulf of Mexico Hypoxia, aka 'The Dead Zone;,'" *Annual Review of Ecology and Systematics*, vol. 33, pp. 235-263, 2002.
- [79] RJ Diaz and R Rosenberg, "Spreading dead zones and consequences for marine ecosystems," *Science*, vol. 321, pp. 926-929, 2008.
- [80] D Perlman. (2008, Aug.) Scientists alarmed by ocean dead-zone growth. [Online]. <http://www.sfgate.com/cgi-bin/article.cgi?f=/c/a/2008/08/15/MNLD12ADSN.DTL>. Retrieved 2010-08-03
- [81] L Mee, "Reviving Dead Zones," *Scientific American*, vol. 78, p. 78, 2006.
- [82] C Filipe and G Daigger, "Development of a Revised Metabolic Model for the Growth of Phosphorus Accumulating Organisms," *Water Environment Federation*, vol. 70, pp. 67-79, 1998.
- [83] j Pramanik, PL Trelstad, AJ Schuler, D Jenkins, and JD Keasling, "Development and Validation of a Flux-Based Stoichiometric Model for Enhanced Biological Phosphorus Removal Metabolism," *Wat Res*, vol. 33, pp. 462-476, 1998.
- [84] K Chandran, Inventories and Triggers of Biogenic Nitrous Oxide from Biological Wastewater Treatment Plants, September 20th, 2011.

- [85] K Soratana and AE Landis, "Evaluating industrial symbiosis and algae cultivation from a life cycle perspective," *Bioresource Technology*, vol. 102, pp. 6892-6901, 2011.
- [86] K Bradsher and A Martin. (2008, April) New York Times. [Online].
<http://www.nytimes.com/2008/04/30/business/worldbusiness/30fertilizer.html?pagewanted=all>
- [87] RC Antweiler, DA Goolsby, and HE Taylor, "Nutrients in the Mississippi River," 1995.
- [88] C Rausch and M Bucher, "Molecular mechanisms of phosphate transport in plants," *Planta*, vol. 216, pp. 23-37, 2002.
- [89] GS Swamy, "How do Plants Absorb Nutrients from the Soil," *Resonance*, pp. 45-52, 1998.
- [90] PR McClure, LV Kochian, RM Spanswick, and JE Shaff, "Evidence for Cotransport of Nitrate and Protons in Maize Roots," *Plant Physiol*, vol. 93, pp. 290-294, 1990.
- [91] JF Allen, "Photosynthesis of ATP-Electrons, Proton Pumps, Rotors, and Poise," *Cell*, vol. 110, pp. 273-276, August 2002.
- [92] T Kurusu, Y Saskurai, A Miyao, H Hirochika, and K Kuchitsu, "Identification of a Putative Voltage-Gated Ca²⁺ permeable Channel (OsTPCI) Involved in Ca²⁺ Influx and Regulation of Growth and Development in Rice," *Plant Cell Physiol*, vol. 45, pp. 653-702, 2004.
- [93] J Lehmann and S Joseph, *Biochar for Environmental Management Science and Technology*.: Routledge, 2009.
- [94] Y Yao et al., "Biochar derived from anaerobically digested sugar beet tailings: Characterization and phosphate removal potential," *Bioresource Technology*, vol. 102, pp. 6273-6278, 2011.
- [95] H McLaughlin, PS Anderson, FE Shields, and TB Reed, "All Biochars are Not Created Equal, and How to Tell Them Apart," in *North American Biochar Conference*, Boulder, CO, 2009.
- [96] K Kameyama, T Miyamoto, T Shiono, and Y Shinogi, "Influence of Sugarcane Bagasse-derived Biochar Application on Nitrate Leaching in Calcaric Dark Red Soil," *J Environ Qual*, 2011.

- [97] M Banno et al., "Capacity and mechanism of nitrate anion adsorption onto bamboo charcoal," *J Jpn. Soc. Water Environ*, vol. 32, pp. 369-374, 2009.
- [98] GJ Allen and D Sanders, "Two Voltage-Gated, Calcium Release Channels Coreside in the Vacuolar Membranes of Broad Bean Guard Cells," *The Plant Cell*, vol. 6, pp. 685-694, 1994.
- [99] AD Angeli et al., "The nitrate/proton antiporter AtClCa mediates nitrate accumulation in plant vacuoles," *Nature*, vol. 442, pp. 939-942, 2006.
- [100] S Haferkamp, H Winfried, AA Pascal, H van Amerongen, and H Kirchhoff, "Efficient Light Harvesting by Photosystem II Requires an Optimized Protein Packing Density in Grana Thylakoids," *Journal of Biological Chemistry*, vol. 285, pp. 17020-17028, 2010.
- [101] TW Jurik, JA Weber, and DM Gates, "Short-Term Effects of CO₂ on Gas Exchanges of Leaves of Bigtooth Aspen (*Populus grandidentata*) in the Field," *Plant Physiol*, vol. 75, pp. 1022-1026, 1984.
- [102] A Gianguzza, P Ezio, and S Sammartano, *Chemistry of Marine Water and Sediments.:* Springer, 2002.
- [103] B Alberts, A Johnson, and J Lewis, *Molecular Biology of the Cell*. New York: Garland Science, 2002.
- [104] P Gajdanowicz et al., "Potassium (K⁺) gradients serve as a mobile energy source in plant vascular tissue," *PNAS*, vol. 108, pp. 864-869, 2010.
- [105] V Sukhov and V Vodeneey, "A Mathematical Model of Action Potential in Cells of Vascular Plants," *J Membrane Biol*, vol. 232, pp. 59-67, 2009.
- [106] I Dreyer and MR Ballt, "What makes a gate? The ins and outs of Kv-like K⁺ channels in plants," *Trends in Plant Science*, vol. 14, pp. 383-390, 2009.
- [107] Y Cao, M Anderova, NM Craford, and JI Schroeder, "Expression of an Outward-Rectifying Potassium Channel from Maize mRNA and complementary RNA in *Xenopus* Oocytes," *The Plant Cell*, vol. 4, pp. 961-969, 1992.
- [108] C Maurel, "Aquaporins and Water Permeability of Plant Membranes," *Annu Rev Plant Physiol Plant Mol Biol*, vol. 48, pp. 399-429, 1997.
- [109] JM Skotheim and L Mahadevan, "Physical Limits and Design Principles for Plant and Fungal Movements," *Science*, vol. 308, p. 1308, 2005.

- [110] R Hedrich et al., "Inward rectifier Potassium channels in plants differ from their animal counterparts in response to voltage and channel modulators," *Eur Biophys J*, vol. 24, pp. 107-115, 1995.
- [111] N Moran et al., "Potassium Channels in Motor Cells of *Samanea saman*," *Plant Physiol*, vol. 88, pp. 643-648, 1988.
- [112] U Homann, "Fusion and fission of plasma-membrane material accomodates for osmotically induced changes in the surface area of guard-cell protoplasts," *Planta*, vol. 206, pp. 329-333, 1998.
- [113] DW Keifer and RM Spanswick, "Activity of the Electrogenic Pump in *Chara corallina* as Inferred from Measurements of the Membrane Potential, Conductance, and Potassium Permeability," *Plant Physiol*, vol. 62, pp. 653-661, 1978.
- [114] RA Leigh and RGW Jones, "A Hypothesis Relating Critical Potassium Concentrations for Growth to the Distribution and Functions of this Ion in the Plant Cell," *New Phytol*, vol. 97, pp. 1-13, 1984.
- [115] IG Abidor et al., "Electric Breakdown of Bilayer Lipid Membranes: The Main Experimental Facts and Their Qualitative Discussion," *Bioelectrochemistry and Bioenergetics*, vol. 6, pp. 37-52, 1979.
- [116] A Shmygol, K Noble, and S Wray, "Depletion of membrane cholesterol eliminates the Ca²⁺ activated component of outward potassium current and decreases membrane capacitance in rat uterine myocytes," *J Physiol*, vol. 581, pp. 445-456, 2007.
- [117] SH Heinemann, F Conti, W Stuhmer, and E Neher, "Effects of Hydrostatic Pressure on Membrane Processes," *J Gen Physiol*, vol. 90, pp. 765-778, 1987.
- [118] E Freeman and LM Weiland, "High Energy Density Nastic Materials: Parameters for Tailoring Active Response," *Journal of Intelligent Material Systems and Structures*, vol. 00, pp. 1-11, 2008.
- [119] HW Zhang and J Lv, "Two-Scale Model for Mechanical Analysis of Nastic Materials and Structures," *Journal of Intelligent Material Systems and Structures*, vol. 22, pp. 593 - 609, 2011.
- [120] E Freeman, LM Weiland, and W Meng, "Application of Proteins in Burst Delivery Systems," *Smart Mater Struct*, vol. 19, 2010.

[121] WL Hsieh, WS Pierce, and H Sze, "Calcium-Pumping ATPases in Vesicles from Carrot Cells," *Plant Physiol*, vol. 97, pp. 693-702, 2004.